DENDRIMER-ENCAPSULATED METAL NANOPARTICLES:

SYNTHESIS, CHARACTERIZATION, AND APPLICATIONS TO CATALYSIS

A Dissertation

by

YANHUI NIU

Submitted to the Office of Graduate Studies of
Texas A&M University
in partial fulfillment of the requirements for the degree of

DOCTOR OF PHILOSOPHY

May 2003

Major Subject: Chemistry

DENDRIMER-ENCAPSULATED METAL NANOPARTICLES:

SYNTHESIS, CHARACTERIZATION, AND APPLICATIONS TO CATALYSIS

A Dissertation

by

YANHUI NIU

Submitted to the Office of Graduate Studies of
Texas A&M University
in partial fulfillment of the requirements for the degree of

DOCTOR OF PHILOSOPHY

Approved as to style and content by:

Richard M. Crooks (Chair of Committee)	Victoria J. DeRose (Member)
D. Wayne Goodman (Member)	Roger J. Morgan (Member)
Emile A. Schweikert (Head of Department)	

May 2003

Major Subject: Chemistry

ABSTRACT

Dendrimer-Encapsulated Metal Nanoparticles: Synthesis, Characterization, and Applications to Catalysis. (May 2003)

Yanhui Niu, B.S., Zhengzhou University, Zhengzhou, China;

M.S., The Institute of Chemistry, Chinese Academy of Sciences, Beijing, China;

M.S., The University of Akron

Chair of Advisory Committee: Dr. Richard M. Crooks

The research in this dissertation examines the chemistry and applications of dendrimers in homogeneous catalysis. We examined interactions between dendrimers and charged probe molecules, prepared dendrimer-encapsulated metal nanoparticles in organic solvents, studied size-selectivity of dendrimer-encapsulted catalysts, and designed molecular rulers as *in-situ* probes to measure the location of dendrimer-encapsulted metal nanoparticles.

The intrinsic proton binding constant and a constant that characterizes the strength of electrostatic interactions among occupied binding sites in poly(amidoamine) (PAMAM) dendrimers have been obtained by studying the effect of solution pH on the protonation of the dendrimers. The significant finding is that these two factors are greatly modulated by the unique and hydrophobic microenvironment in the dendrimer interior.

Hydrophilic poly(propylene imine) (PPI) dendrimers were modified with various hydrophobic alkyl chains through an amide linkage and were then used as templates for preparing intradendrimer copper nanoclusters. The main driving force for encapsulating metal-ions was found to be the differences in metal-ion solubility between the solvent and the interior of the dendrimer.

Nanometer-sized metal particles are synthesized and encapsulated into the interior of dendrimers by first mixing together the dendrimer and metal ion solution and then reducing the composite chemically, and the resulting dendrimer-encapsulated metal nanoparticles can then be used as catalysts. By controlling the packing density on the dendrimer periphery using either different dendrimer generations or dendrimer surface functionalities, it is possible to control access of substrates to the encapsulated catalytic nanoparticle.

Molecular rulers consisting of a large molecular "stopper", a reactive probe and a linker were designed as *in-situ* probes for determining the average distance between the surface of dendrimer-encapsulated palladium nanoparticles and the periphery of their fourth-generation, hydroxyl-terminated PAMAM dendrimer hosts. By doing so, we avoid having to make assumptions about the nanoparticle size and shape. The results suggest that the surface of the encapsulated nanoparticle is situated 0.7 ± 0.2 nm from the surface of the dendrimer.

To my parents

Anlin Niu and Weidong Zhang

and my husband

Xu Li

and my son

Jerry J. Li

For their love and support

ACKNOWLEDGEMENTS

First, I would like to thank my research advisor, Dr. Richard M. Crooks, for providing me with guidance, support, and an ideal atmosphere for doing research in this group. He was always there when I needed his advice. He provides a fine example of tremendous work ethic, scientific diligence and integrity, and enthusiasm for chemistry. Without his help the success of this work would not be possible.

Second, I would like to thank those who were directly involved in the projects discussed in this dissertation: Dr. Li Sun, Dr. Lee K. Yeung, Dr. Juio Alvarez, Dr. Sang Keun Oh. Especially I would like to express my deep thanks to Dr. Li Sun for extensive help in chemistry and discussions over the past four years. I would also like to acknowledge other members of Dr. Crooks' group with whom I have been inspired during the past four years: Dr. Buford Lemon, III, Dr. Bill Lackowski, Dr. Wendy Baker, Dr. Lane Baker, Dr. Pradyut Ghosh, Dr. K. Joseph Thomas, Gina Mealey, Brooke Rowan, Greg Perez, Erin Docking, Aldalin Asinas, Wei Zhan, Ding Li, Yong-Gu Kim, Jinseok Heo, Dr. Takashi Ito, Dr. Gi Hun Seong, Heechang Ye, Dr. Jinhui Dai, Dr. Robert Scott, Orla Wilson, and Ronald Henriquez. I would also like to thank Dr. D. Wayne Goodman, Dr. Victoria DeRose, Dr. Roger Morgan, Dr. Cynthia Werner for their willingness to serve on my committee.

I would like to thank my parents and in-laws for their help in taking care of my baby during the past two years. In particular, I thank my husband, Xu Li, for his support and understanding of my hard work.

Financial support of this work was provided by the Office of Naval Research, the National Science Foundation, the Robert A. Welch Foundation, and the American Chemical Society Petroleum Research Foundation.

Transmission Electron Microscopy (TEM) results are based upon research conducted at the Microscopy and Imaging Center, Texas A&M University. I thank Dr. Zhiping Luo and Ms. Ann Ellis for valuable help and discussions on the TEM experiments.

TABLE OF CONTENTS

CHAPTER Page

LIST OF FIGURES

FIGURE Page

FIGURE Page

FIGURE Page

LIST OF TABLES

CHAPTER I

INTRODUCTION

1.1. Motivation/Objectives

The studies reported in this dissertation can be divided into two areas. The first involves the synthesis and characterization of functional dendrimers and dendrimer-encapsulated metal nanoparticles (DEMNs). The second part concerns the applications of dendrimers to the field of catalysis, and particularly to enhancing the selectivity of catalysts by taking advantage of the dendrimer structure.

Derived from the Greek words *dendron* (tree) and *meros* (part), the term dendrimer refers to its characteristic appearance, which is a somewhat hollow, monodisperse, and globular macromolecule having a perfect, or nearly perfect, branched structure. Since the first report of a successful dendrimer synthesis in the late 1970's,[1,2] there has been a rapid increase in interest and publications in these fascinating materials (Figure 1.1). During the first decade, people focused their research on the development of suitable synthetic protocols to prepare new families of dendrimers having novel structures and high generations. In the last few years, however, there has been increasing interest in finding applications for these materials.[3-11] Particularly, because of their unique structural topology and chemical versatility, dendrimers have found many applications that include catalysis,[3,5,8] drug delivery,[12,13] energy transfer,[14-16] and molecular recognition.[6,17] These and other applications have been facilitated by

---

This dissertation follows the style and format of *Accounts of Chemical Research.*

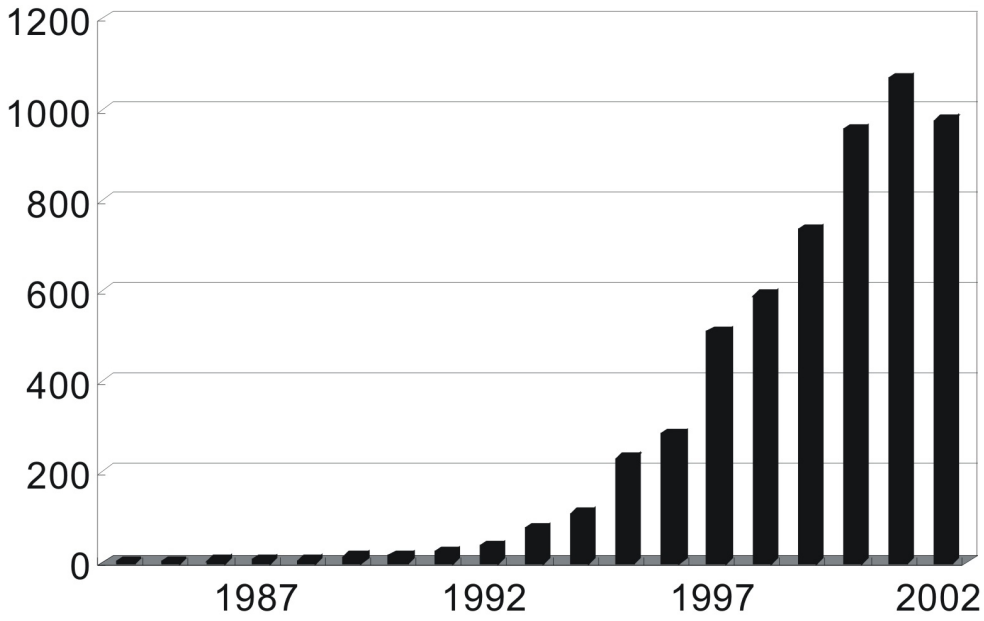

Figure 1.1. Number of publications of dendrimer chemistry based on SciFinder search.

theircommercial availability through Dendritech, Inc. (Midland, MI) and Dutch State Mines (DSM, The Netherlands). My particular research interest is in discovering specific catalytic functions and properties of dendrimers that are a direct consequence of their dendritic architecture.

In many cases, these aforementioned applications strongly depend on the equilibrium between dendrimers and ions, but there have only been a few experimental studies that address this issue.[18-20] A theoretical interpretation of experimentally determined titration data for poly(amidoamine) (PAMAM) dendrimers was studied in Chapter III.[21] Specifically, I used a multi-shell structural model[20] to analyze experimental data from potentiometric pH titrations. The goals are to obtain the intrinsic proton binding constants for amine groups in PAMAM dendrimers, and to estimate the strength of electrostatic repulsion among occupied proton binding sites.

We[5,22-26] and others[27-30] have previously reported the synthesis of dendrimer-encapsulated metal and semiconductor[31] nanoparticles. Nearly monodisperse intradendrimer nanoparticles having sizes in the range of 1-4 nm (depending on the size of the dendrimer) can be easily obtained. Most of the nanoparticles are synthesized in aqueous phase. However, nanoparticles in organic solution may find broader applications. Chapter IV demonstrates the preparation of large DEMNs using organic solvents. The significant new finding is that differences in metal-ion solubility between the solvent and the dendrimer interior can be used to drive the encapsulation process. This approach expands the scope of our previously reported strategy for preparing

DEMNs, which relies on specific interactions between metal ions and intradendrimer functional groups for metal-ion encapsulation.

Some data in our previous reports suggested high levels of selectivity for either a particular substrate or a particular product.[32] Accordingly, Chapter V describes a quantitative study correlating DEC structure to catalytic rate. Using our method,[5] the size of dendrimer-encapsulated Pd(0) nanoparticles can be controlled regardless of the dendrimer generation or dendrimers with different surface steric crowdings. The result demonstrated that by controlling the steric crowding on the dendrimer periphery it is possible to selectively control access of substrates to the encapsulated metal particle. Because selectivity is induced by the dendrimer, rather than by the intrinsically non-selective Pd catalyst, this approach should be generally applicable to any reaction that involves a catalyst that can be placed within the interior of a dendrimer or related nanoporous materials.[33]

A key question raised in these previous studies concerns the size, shape, and location of the encapsulated nanoparticles. Transmission electron microscopy (TEM) and scattering methods to place Au nanoparticles somewhat offset from the center of generation 6 – 9 (G6-G9) PAMAM dendrimers.[28] However, interpretation of data from these methods, and correlation of the results to the conformation of solution-phase dendrimers, is complex and model dependent. Our previous work on activity modulated by the dendrimer generation and size selective catalysis in DEMNs[32,33] inspired us to use a catalytic reaction as an *in-situ* reporter of the particle location within the DEMN composite. Chapter VI describe the synthesis of a series of molecular nanorulers with

different lengths and their application as *in-situ* reporters for the location of catalytic particles confined in the interiors of PAMAM dendrimers.[34]

In summary, the objectives of this dissertation have been to solve basic chemical and technological problems related to dendrimer and transitional-metal-based nanocapsules. With the careful design of each project, these studies provide the information for a better and thorough understanding of dendrimer architecture, and the chemical and structural properties of these materials for catalysis and other applications.

1.2. Dendrimers

Synthesis of Dendrimers. Dendrimers are a type of hyperbranched polymer that contains three anatomical features, namely a core, repetitive branch units, and terminal functional groups.[7,11,35,36] However, unlike other polymers which are synthesized by either chain polymerization or step polymerization, dendrimers are usually synthesized by one of two construction strategies: the divergent or convergent approaches.

The divergent method is an "outside in" method. In this approach, dendrimers are synthesized from the central core outwards toward the periphery. In each repeat cycle *n* reactive groups on the dendrimer surface react with *n* monomer units to add a new layer, or generation to the dendrimer. Figure 1.2a illustrates the overview of this strategy.[37] Thus, the number of coupling reactions increases exponentially with each successive generation. In this way dendrimers can be built up step by step until steric interactions prevent further reactions of the end groups.[1,36,38] However, higher generation dendrimers synthesized by the divergent strategy always contain structural defects

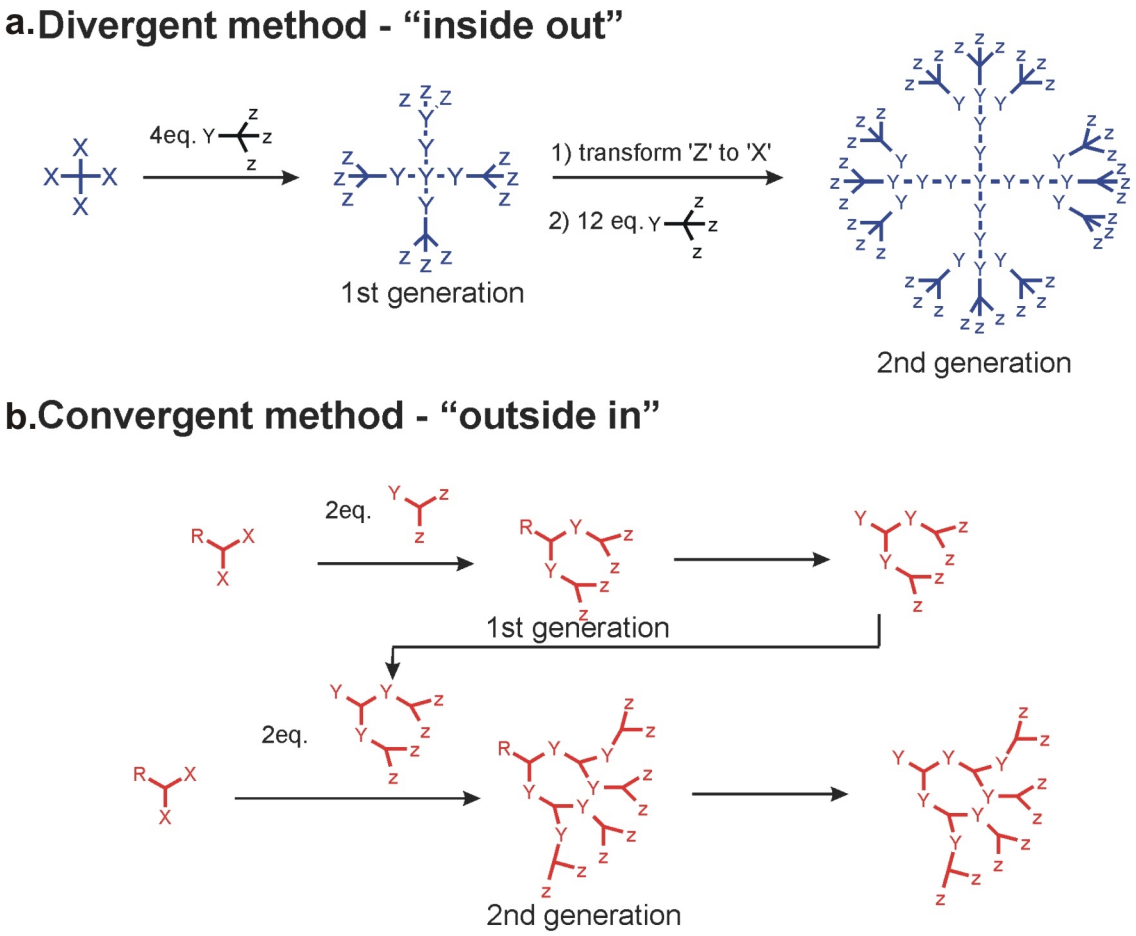

Figure 1.2. Schematics of dendrimer synthesis (adapted from ref. 37).

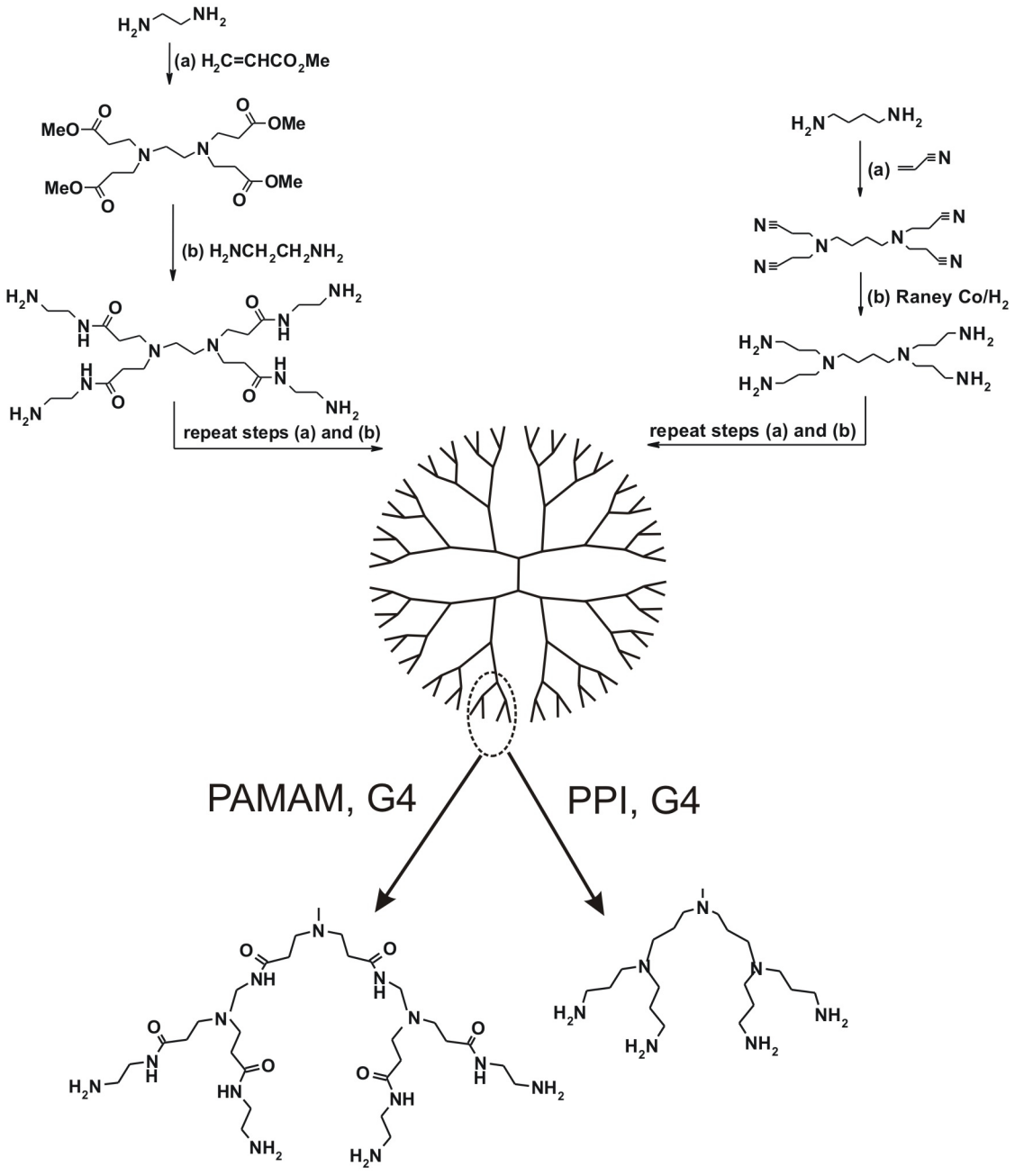

Figure 1.3. Synthesis of PAMAM and PPI dendrimers.

because defects begin to multiply at higher generation as the result of exponential increase of reactions at the congested dendrimer surface

In contrast to the divergent strategy, the convergent method is an "inside out" method. In this method, the dendrimer is constructed from the periphery toward the central core. In this approach, different generations of "wedges" or "dendrons" (individual dendrimer branches, Figure 1.2b) are first synthesized, followed by reactions toward the same central core to give different generations of dendrimers. Compared with dendrimers prepared by the divergent strategy, the convergent approach generally provides more homogeneous and easier to be separated dendrimers. However, it is impossible to prepare higher generation dendrimers by the convergent approach because the reaction efficiency between high-generation dendrons and the core is low. Usually up to generation 10 (G10) dendrimers can be prepared by divergent methods whereas the convergent approach produces dendrimers of generation 8 (G8) and lower. The two commercially available families of dendrimers, PAMAM and poly(propylene imine) (PPI) dendrimers, are both synthesized using the divergent approach. A short review of the synthesis is list below because of their importance in this dissertation.

The synthesis of commercially available amine-terminated PAMAM dendrimers starts from an ethylene diamine core. The synthesis proceeds as a series of two reiterative reactions: a Michael addition reaction of amino groups on ethylene diamine to the double bond of methyl acrylate, followed by amidation of the resulting methyl ester with ethylene diamine (Figure 1.3). The ester-terminated products are denoted as $Gn_{0.5}$, half-generation dendrimers and the full-generation amine-terminated dendrimers are

denoted Gn. Different monomers used for the last step results in different groups appended to the periphery of the dendrimer. For example, if ethanolamine (NH_2-$(CH_2)_2$-OH) is used, hydroxyl-terminated dendrimers (Gn-OH) will be obtained. Up to the 10th generation PAMAM dendrimer has been commercialized.

The synthesis of PPI dendrimers involves a repetitive Michael addition reaction of two equivalents of acrylonitrile to a primary amine group, followed by hydrogenation of the nitrile groups to yield the primary amine groups (Figure 1.3). Because of the small size and large numbers of surface groups on PPI dendrimers, the synthesis of higher generations ($n > 5$) becomes extremely difficult because of the steric crowding on the periphery of the higher generation dendrimers. It has been reported that on average only 23% of the fifth generation PPI dendrimer are perfect.[4] Nevertheless, dendrimer molecules still have a very low polydispersity compared to hyperbranched polymers.

As the dendrimer generation increases, the molecular weight and number of periphery terminal groups increases exponentially. However, the dendrimer size only increases almost linearly. This causes the density of dendrimer terminal groups (normalized to the surface area) to increase nonlinearly – the higher the dendrimer generation, the more densely packed the dendrimer surface. Table 1.1 and Figure 1.4 show the relationship between dendrimer generation, molecular weight, measured diameter, and the number of interior tertiary amines for ideal PAMAM and PPI dendrimers. Another consequence of the exponential growth pattern of dendrimers is a change of shape with generation. Molecular simulation results show that up to G2 dendrimers have an expanded or 'open' configuration, but as the dendrimer grows in size,

Table 1.1. General features of PAMAM and PPI dendrimers.

Gen.	Surface Groups	Tertiary Amines	Molecular Weight[a]		Diameter[b], nm		Surface group/surface area ($1/nm^2$)	
			PAMAM[b]	PPI	PAMAM	PPI	PAMAM	PPI
0	4	2	517	317	1.5	0.9	0.14	0.39
1	8	6	1,430	773	2.2	1.4	0.13	0.32
2	16	14	3,256	1,687	2.9	1.9	0.15	0.35
3	32	32	6,909	3,514	3.6	2.4	0.20	0.44
4	64	62	14,215	7,168	4.5	2.8	0.25	0.65
5	128	126	28,826	14,476	5.4	-	0.35	-
6	256	254	58,048	29,093	6.7	-	0.45	-
7	512	510	116,493	58,326	8.1	-	0.62	-
8	1024	1022	233,383	116,792	9.7	-	0.87	-
9	2048	2046	467,162	235,494	11.4	-	1.25	-
10	4096	4094	934,720	469,359	13.5	-	1.79	-

[a]Molecular weight is based on perfect dendrimers.
[b]For PAMAM dendrimers, the molecular dimensions were determined by size-exclusion chromatography and the dimensions of PPI dendrimers were determined by SANs; data for the high-generation PPI dendrimers are not available.

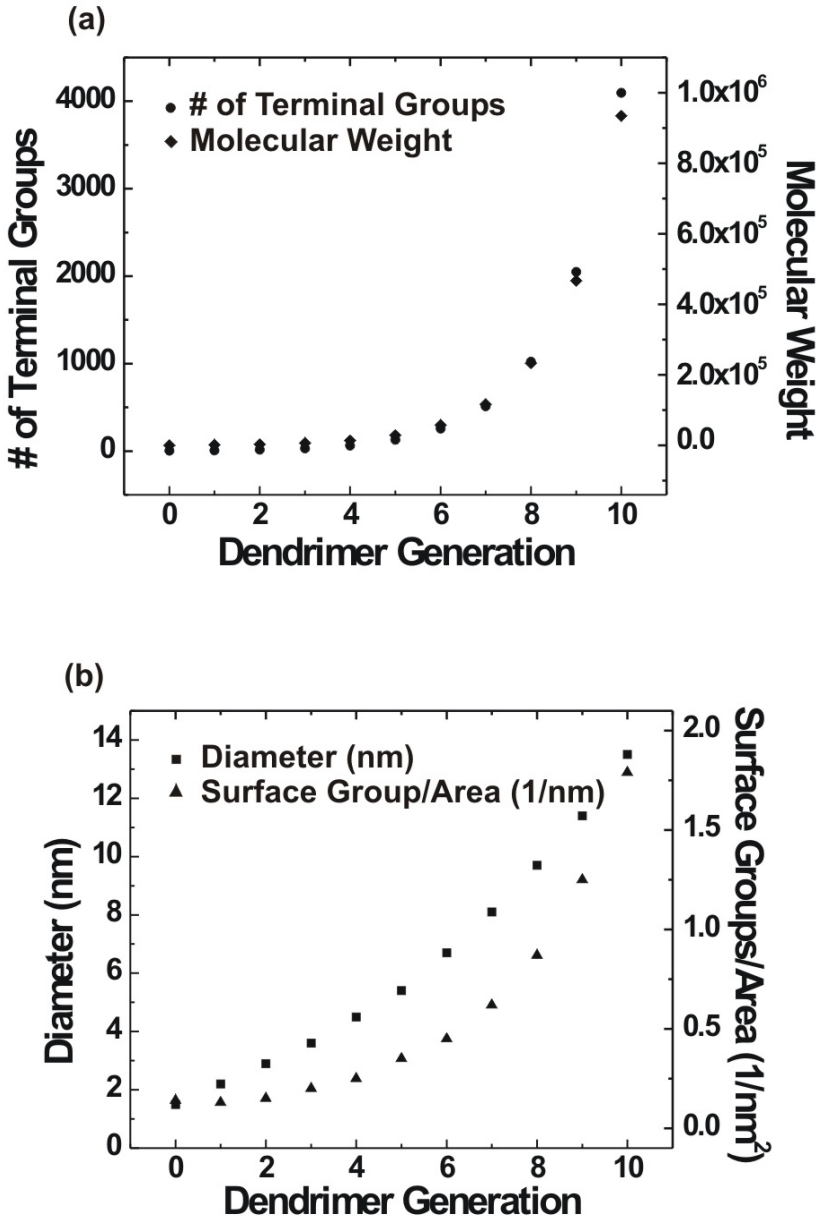

Figure 1.4. Structural dependence of PAMAM dendrimers (a) the number of terminal groups and molecular weight, (b) diameter and surface group per area, *vs.* dendrimer generation.

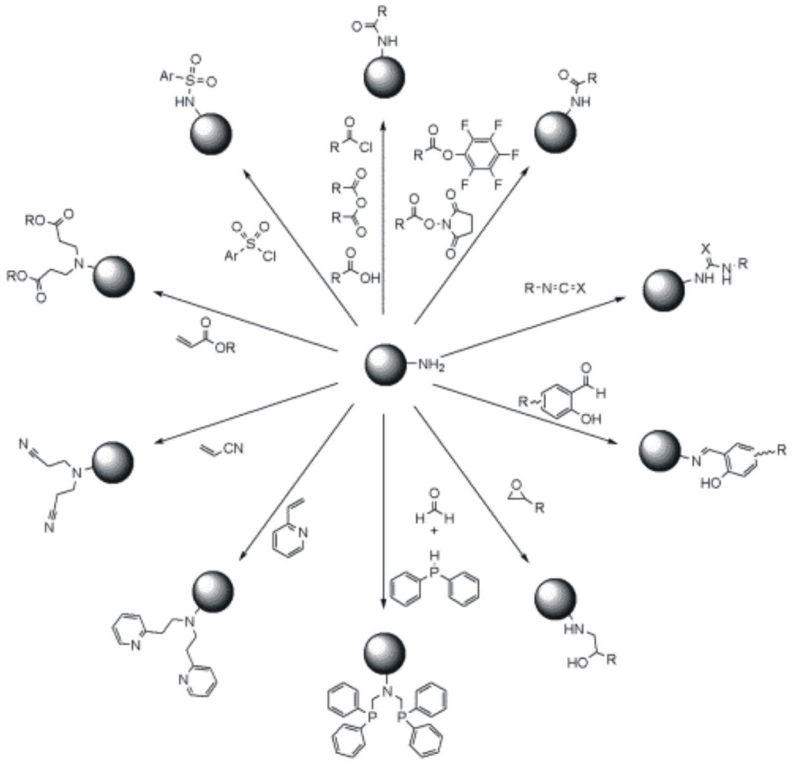

Figure 1.5. Functionalization of PAMAM or PPI dendrimers (taken from ref. 40).

crowding of the surface functional groups causes the dendrimer to adopt a spherical or globular structure.[36,39]

As mentioned above, the commercialization of PAMAM and PPI dendrimers has greatly boosted interest in the applications of these specific materials. This is partly due to the highly branched structure of dendrimers acting as carriers of functional groups - high reactivity of surface amino groups and thus different functional groups can be attached to the surface for other properties. A summary of typical reactions are shown in Figure 1.5.[40] The corresponding polynitrile,[41] polyesters,[42] polyamides,[43-46] perfluorated dendrimers[47] have been studied and attempted to a variety of applications. Moreover, α-aminoalcohol[48] and urea[49] derivatives can be formed by the coupling with epoxides or isocyanates, respectively.

Applications of Dendrimers. The fascinating structural features of dendrimers, such as their nanoscopic sizes, spheroidal shape, and cavernous interiors, have inspired many potential applications. This section provides some recent successful applications of PAMAM and PPI dendrimers.

Applications in Drug Delivery. An ideal drug carrier must be biochemically inert and non-toxic, but still able to protect the drug within the carrier until it reaches the desired site of action, and then release the drug. Many polymeric drug-delivery systems have been developed over the years.[50] The use of dendrimers as carriers, especially PAMAM dendrimers, may use in this application because of their desirable chemical and physical properties, including: uniform size, biocompatibility, water solubility,

modifiable surface functionality, and available internal cavities.[13,51,52] For example, folate-conjugated PAMAM dendrimers can deliver significantly increased amount of metal ions to a target site or area and thus increase the image contrast for magnetic resonance imaging (MRI).[53-55]

Several approaches have been described to improve drug releasing ability of dendrimers. For example, polyethylene glycol (PEG) is usually grafted onto the surface of PAMAM dendrimers to improve their biocompatibility and solubility.[12] The ability of a dendrimer to encapsulate hydrophobic drugs within the dendritic core increases with increasing of dendrimer generation and chain length of grafted PEG. The release of drug molecules from quaternized PPI dendrimers has been found to be pH-sensitive, which suggests that these materials can also be engineered for controlled release applications.[56] Dual functionality on the surface of "Fréchet type" dendrimers has also been achieved by attaching PEG, where slow and sustained *in vitro* drug release characteristics have been found.[57,58]

Because of the inherent interaction between antibodies and antigens, antibodies are very useful in targeted drug therapy. Utilizing this property, an attractive approach to increase drug loading is to attach the antibody to a dendrimer containing drug molecules. For instance, Roberts and coworkers coupled dendrimers with porphyrin where copper ions were chelated.[59] The result showed 90% of the immunoreactivity of the antibody was retained, while 100% of conjugated bound to the heavy chain of antibody was observed, indicating a potential application in cancer imaging and therapy.

Molecular Recognition. Since their introduction, dendrimers have always been considered as interesting candidates for applications in host-guest chemistry[36,60] The driving force for guest encapsulation within dendrimers can be based on electrostatic interactions, van der Waals forces, complexation reactions, sterics, or their combination.

Meijer's group was the first to a "dendritic box" structure to physically entrap small molecules within the dendrimer interior.[61-63] The encapsulation of molecules was performed by reaction of the 5th generation PPI dendrimer with a bulky activated ester in the presence of guest molecules having some affinity for the interior tertiary amines. Excess guest molecules present in solution and on the periphery of the dendrimer were removed by extensive washing and/or dialysis. Molecular mechanics calculations of the dendritic box suggested it had a globular architecture with an estimated radius of 2.3 ± 0.3 nm, where the interior is almost completely shielded by the bulky end groups.[64] The release of guests in the dendritic box was only possible after disruption of the bulky groups on the periphery by hydrolysis of the shell. The potential applications of this method include drug delivery, release of fluorescent markers, and fundamental studies of chemical and physical properties of isolated molecules.

A unimolecular inverted micellar structure soluble in organic solvent can be obtained when the periphery of a relative hydrophilic PPI dendrimer is modified with hydrophobic groups such as palmitoyl chains.[46] As a result, guest molecules, e.g. Rose Bengal can be encapsulated in organic media. More interestingly, several anionic xanthene dyes can be extracted from the aqueous phase to the organic phase by modified dendrimers.[43] In this case, the number of guests per dendrimer is directly related to the

dendrimer generation. Similarly, with hexafluoropropylene oxide on the periphery of PPI dendrimer, methyl orange, which is a supercritical CO_2-insoluble guest, can be extracted from water to the CO_2 phase.[47]

Guest molecule recognition based on hydrophobic interactions is another active area in dendrimer host-guest chemistry. Diederich *et al.* developed "dendrophanes", consist of a cyclophane core modified with pendant poly(ether amide) dendrimer, as models for globular proteins.[65-67] Flat aromatics or steroids can bind to the "dendrophane" acceptor effectively. The excellent inclusion complexation of ferrocene to β–CD has also been used to lure β–cyclodextrin (β–CD) to the periphery of ferrocenyl-functionalized PPI dendrimers .[68]

Light Harvesting and Energy Transfer in Dendrimers. In nature, the light harvesting and energy-transfer processes involve transferring the energy of photons absorbed by a light-absorbing antenna moiety to a nearby secondary energy acceptor species. Thus, artificial light-harvesting systems capable of converting solar radiation into a useful source of energy with similar efficiencies would be extremely beneficial. Recognizing this fact, interest in molecules and molecular assemblies capable of light harvesting and energy transfer has expanded greatly. Two basic characteristics of dendrimers make them promising candidates for light harvesting: (1) exponential growth of the number of peripheral absorbing units with generation number; and (2) the relative short distance between the periphery and the center, where a photochemical sensor or trap can be located.[69,70] Several examples of nanoscale photonic molecular assemblies in which light absorption is followed by nearly quantitative energy transfer have been

reported. These include "hopping" or energy funneling processes through the dendrimer to a core chromophore, using dendrimers as scaffolds, and energy transfer in host-guest systems.

In the hopping process in dendrimers, an energy funnel is created by the monotonic decrease in electronic excitation energy for each generation toward the locus. When the dendrimer is illuminated by light, excitations initially localized at the molecular periphery are influenced by a thermodynamic bias, and preferentially "hop" inward toward the center. "Compact" and "extended" Bethe dendrimers have been synthesized and characterized by Moore *et al*.[16,56,71] The compact dendrimers do not act as energy funnels due to their energetically degenerate nature. With increasing chain length toward the center of the molecules, the extended Bethe dendrimers, however, show very efficient energy transfer due to the energetic bias.

In the associated perylenic derivatives of both compact and extended Bethe dendrimers, perylene acts as an exciton trap that collects absorbed photonic energy at the base of the energetic funnel. The energy gradient inherent in the extended nanostar molecule is sufficiently larger than the entropic hopping bias toward the periphery. Thus rapid and efficient funneling of the absorbed light energy toward the locus occurs with nearly 100% energy transfer efficiencies.

Unlike the hopping process, dendrimers can act as scaffolds for energy transfer.[72,73] Fréchet *et al.* synthesized a series of dye-labeled poly(arylether) dendrimers using the laser dye coumarin 2 as the terminal donor chromophore and coumarin 343 as the focal acceptor dye.[15] The terminal chromophores collectively act as antennae for

light harvesting, while the focal dye plays the role of a fluorescent probe. In these dye-labeled dendrimers, light is absorbed by the numerous peripheral chromophores followed by rapid funneling to a fluorescent core with a remarkably high efficiency. Since the whole transfer process is independent of the dendritic architecture, the role of the dendrimer backbone is a structural rather than functional one. This approach provides exceptional flexibility in that additional features, such as affinity towards a cell, or a drug, can be easily introduced by simply changing the components of the dendrimer.

Meijer and coworkers demonstrated another type of energy transfer—the transfer occurred in host-guest complexes, from the arms of dendrimers to encapsulated dye molecules.[74] Water-soluble anionic dyes can be extracted into organic phases with high efficiency by functionalized PPI dendrimers conjugated to oligo(p-phenylene vinylene) (OPV) groups through an amide linkage. Drop-cast thin films of the host-guest systems show almost complete quenching of the OPV fluorescence with higher than 90% transfer efficiency.

Dendritic Catalysts. Among the potential applications for dendrimers, catalysis may be one of the most promising, because it is relatively easy to tune the structure, size, and location of catalytically active sites,[3] and because dendrimers have the potential to combine the advantages of both heterogeneous and homogeneous catalysts.[8] An enormous variety of catalytic reactions involving composite metal-dendrimer materials have been studied; these include, but are not limited to, hydrogenations, hydroformylation, olefin metathesis, Heck reactions, Suzuki coupling, alkylation, and

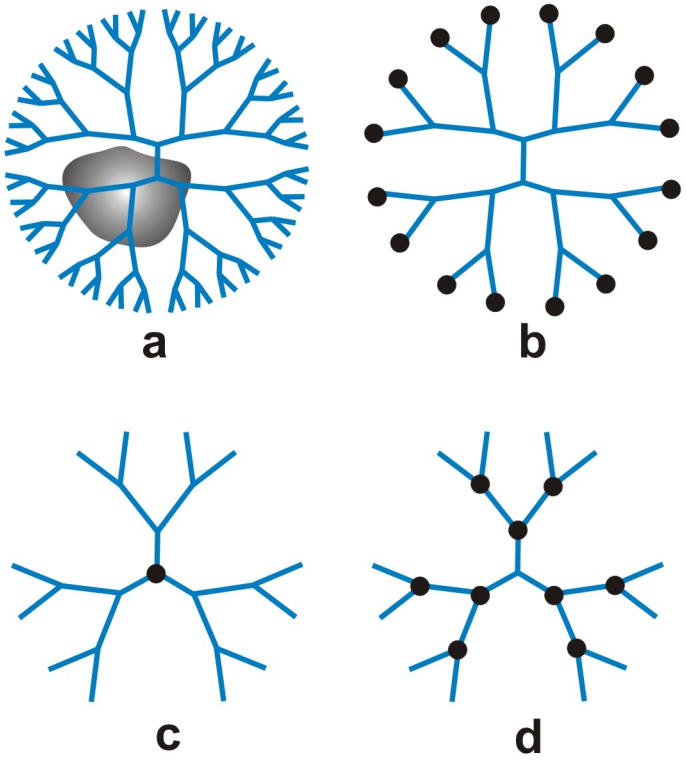

Figure 1.6. Types of metallodendrimer complexations: (a) dendrimer-encapsulated metal nanoparticles, (b) periphery metallodendrimers, (c) core metallodendrimers, (d) focal metallodendrimers (adapted from ref. 3).

oxidations. The properties of dendrimer-based catalysts, such as selectivity, activity, and stability, are dependent on the location and nature of the metal. Figure 1.6 is a schematic illustration of the four most common metallodendrimer configurations. The next section of this chapter focuses mainly on dendrimer-encapsulated metal nanoparticles (Figure 1a), and particularly their catalytic properties.

1.3. Dendritic Catalysts

Types of Metallodendrimers.

Dendrimer-Encapsulated Metal Nanoparticles (DEMNs). We[5,75] and others[27-30] have previously reported the synthesis of dendrimer-encapsulated monometallic, bimetallic,[76] and semiconductor[31] nanoparticles (Figure 1.6(a)). Nearly monodisperse intradendrimer nanoparticles having sizes of less than 4 nm (depending on the size of the dendrimer) can be prepared. As a direct consequence of their three-dimensional structure, dendrimers are particularly attractive hosts for catalytically active metal nanoparticles for the following five reasons: (1) bearing fairly uniform composition and structure, the dendrimer templates themselves yield well-defined nanoparticle replicas; (2) the nanoparticles are stabilized by encapsulation within the dendrimer, and therefore they do not agglomerate during catalytic reactions; (3) the nanoparticles are retained within the dendrimer primarily by steric effects and therefore a substantial fraction of their surface is unpassivated and available to participate in catalytic reactions; (4) the dendrimer branches can be used as selective gates to control the access of small molecules (substrates) to the encapsulated (catalytic) nanoparticles; (5) the dendrimer

periphery can be tailored to control solubility of the hybrid nanocomposite and used a handle for facilitating linking to surfaces and other polymers.

Periphery Metallodendrimers. In contrast to DEMNs, substrates can easily access the active catalytic sites on the surface of the dendrimer support to facilitate high reaction rates comparable with homogeneous systems (Figure 1.6(b)).[77] Moreover, as a consequence to extremely high local catalyst concentrations cooperative effects may play a very important role in overall reaction. For example, Reetz *et al.*[78] modified generation 3 poly(propylene imine) (PPI) dendrimer with diphenylphosphine ligands. The modified dendrimer complexes with various transition-metal groups, which resulted in Figure 1.6(b) type catalysts. Hydroformylation of 1-octene with Rh^{+} dendritic catalyst showed a comparable catalytic rate to that of the monomer. However, the Pd^{2+} complex catalyzed the Heck reaction with a 4-fold increase in turnover number via a bimetallic mechanism[79] compared with the corresponding monomeric analogue. However, because of the high local concentration, deactivation thus reduced activity of the catalyst through a bimetallic mechanism is also possible.[80]

Core (or Focal) Metallodendrimers. A substrate has to enter the core or focal metallodendrimers (Figure 1.6(c) and (d)) prior to the catalytic reaction.[81-83] Thus, the selectivity, activity and solubility of catalyst could be tuned by the dendritic structure similar to DEMNs. Moreover, because the catalysts are isolated from one another a bimetallic deactivation can be avoided in this type of catalyst. However, the reaction rate decreased as the dendritic generation increased, which was attributed to a more difficult mass transport with increasing surface crowding of the dendritic wedges.

Moreover, a bimetallic deactivation can be avoided in this type of catalyst. For instance, a series of diphosphine ligands centered on 1,1'-bis-diphenylphosphinoferrocene-bearing dendritic carbosilane substituents at the para aryl positions were systhesized. Further reactions with $[Pd(MeCN)_2Cl_2]$ afforded the ferrocene-centered chelate complexes, and these metallodendrimers were shown to be efficient in palladium-catalyzed allylic alkylation.[84] The reaction rate decreased as the dendritic generation increased which was due to a more difficult mass transport with increasing surface crowding of the dendritic wedges. Nonetheless, the application of this type catalyst could be limited by much higher costs because of the low catalyst loading per dendrimer and relatively complicated multi-step synthesis.

One significant advantage of DEMNs over the other three types of metallodendrimer catalysts shown in Figure 1.6 is that the necessary PAMAM and PPI dendrimers[85] are commercially available. Solubility of these commercially available materials can be easily tuned by modification of the peripheral functional groups [9] or by using biphasic solvents.

Synthesis and Characterization of DEMNs. Dendrimer/metal-ion composite materials, which are the precursors for DEMNs, are prepared by mixing solutions containing dendrimers and metal ions, such as Pt^{2+}, Pd^{2+}, Au^{3+}, Ag^{+}, Cu^{2+}, Ni^{2+}, Ru^{3+}, Mn^{2+}, and Fe^{3+} (Figure 1.7).[5,27,28,30,86,87] The reaction is usually carried out in water, but as described later organic solvents have also been used. PAMAM dendrimers having non-complexing peripheral functional groups have been used extensively for this purpose, but other types of dendrimers have also been studied.[88,89] In favorable cases the

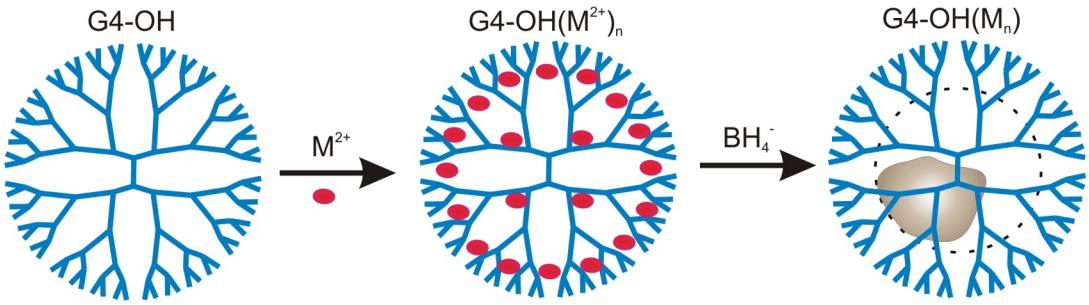

Figure 1.7. Synthesis of dendrimer-encapsulated metal nanoparticles.

metal ions partition into the dendrimer interior where they complex strongly with interior tertiary amine groups. UV-vis, EPR, MALDI-MS, and XPS have been used to characterize dendrimer/metal-ion composites.[26,32,75,86,87,90] In the case of the PAMAM/Cu^{2+} composite,[75] for example, a strong ligand-to-metal charge transfer (LMCT) band at 300 nm and a 210 nm shift of the d-d optical transition signal metal ion complexation by the interior amine groups. The maximum number of Cu^{2+} ions that can be extracted into each dendrimer is related to the dendrimer generation and has been assessed by spectrophotometric titrations.[75]

To successfully extract metal ions into the interior of dendrimers having complexing peripheral groups, such as amine-terminated dendrimers, the solution pH may play an important role. This is because PAMAM dendrimers are polyprotonic bases where the surface primary amines (pK_a = 9.23) are more basic than the internal tertiary amines (pK_a = 6.30), which is demonstrated in Chapter III.[21] Results from calculations based on a multi-shell model provide insight into dendrimer protonation over a broad range of pH.[20,21] Acidic conditions have been shown to be effective for trapping metal ions within the interior of amine-terminated dendrimers while avoiding coordination of metal ions to primary amine groups on the periphery.[91]

Reduction of dendrimer/metal-ion composites with an excess of a chemical reducing agent (usually $NaBH_4$) in water yields nearly monodisperse, zero-valent intradendrimer metal nanoparticles (Figure 1.7). Reduction is apparent from the immediate change in color of the solution. In the case of Cu, for example, the UV-vis spectrum changes from the aforementioned pair of discreet bands prior to reduction to a

monotonically increasing absorbance toward shorter wavelength, indicating the presence of small nanoparticles. The absence of an absorption peak arising from Mie plasmon resonance indicates that the Cu clusters are smaller than 4 nm.[92,93] Consistent with this observation, no precipitation of metal occurs.

High-resolution transmission electron microscopy (HRTEM) is widely used to study the size and size distribution of metal nanoparticles. HRTEM clearly shows that DEMNs are typically in the size range of 1-4 nm.[26,28,32,33,94] The particle size can be controlled by varying the dendrimer/metal-ion ratio. For example, we have shown that a dendrimer/$PdCl_4^{2-}$ ratio of 1:40 yields Pd nanoparticles having a diameter of 1.7 ± 0.2 nm regardless of the dendrimer generation (Gn-OH dendrimers (n = 4, 6, 8))[33] or steric crowding on the dendrimer surface.[95] Note, however, that the size of a spheriodal particle containing 40 close-packed Pd atoms should be ~1.1 nm in diameter. That is, TEM over-estimates the size of small Pd DEMNs contained within low-generation PAMAM dendrimers by more than 50% in some cases.[5,32,94] Consistent with the relatively limited void space within low-generation PAMAM dendrimers, this result might indicate that DEMNs prepared under these conditions have complex shapes. In contrast, the measured size of large Au nanoparticles (2.0 - 4.0 nm) encapsulated within high-generation (G6-G9) PAMAM dendrimers correlates well with the calculated size of spheroidal nanoparticles.[28] Additionally, our group recently showed that when DEMNs are prepared using a magic number[96,97] (or close to a magic number) of metal ions (for example, a dendrimer/$AuCl_4^-$ ratio of 1:140), the size of the resulting nanoparticles (1.6 ± 0.3 nm for a 140 Au-atom particle, Figure 4)[88] matches the theoretical expectation (1.6

nm) very well, even for low-generation dendrimers.[97,98] Moreover, the degree of monodispersity obtained using magic numbers is truly remarkable. Gröhn and co-workers have used TEM staining methods and scattering data to demonstrate that Au DEMNs are encapsulated within high-generation dendrimers and that the location of the nanoparticles are, on average, somewhat offset from the center of PAMAM dendrimers.[28] The shape and location of encapsulated metal nanoparticles will be discussed further in later in this thesis.

DEMNs soluble in nonaqueous solvents have also been synthesized. For example, our group recently demonstrated that Pd particles within water-soluble, amine-terminated PAMAM dendrimers can be transported into an organic phase or a fluorous phase by addition of a fatty acid[91] or a perfluorinated fatty acid, respectively.[99] It is also possible to extract metal ions from an aqueous phase into a nonaqueous phase,[100] and then reduce the ions to the zero-valent metal in the nonaqueous phase. Esumi *et al.* used this approach to prepare dendrimer-encapsulated Au nanoparticles within PAMAM dendrimers carrying hydrophobic groups on their periphery.[101] Our group later showed that this strategy can be used to prepare fluorous-soluble DEMNs.[24] It is also possible to completely avoid the extraction process by preparing DEMNs in the absence of water. This is accomplished by first sorbing the metal ions into the dendrimer interior in a nonaqueous solvent, and then reducing the composite.[102,103] The results in Chapter IV suggest that it is possible to use this approach to encapsulate larger metal nanoparticles within dendrimers, because the main driving force for encapsulation is the difference in metal-ion solubility between the solvent and the interior of the dendrimer.[102] This

approach greatly expands the scope of our previously reported strategy for preparing DEMNs in water.

Homogeneous catalysis using DEMNs. Because the active sites of metal catalysts are on the particle surface, smaller metal particles are, on a per-atom basis, usually more efficient than larger particles (exceptions to this generality exist, particularly for nanoparticles in the 1-3 nm size range).[104,105] However, the high total surface energy of small particles is also a strong driving force for aggregation. This negative consequence of small-sized particles can be avoided by adding stabilizers to the metal-ion solution prior to reduction. The stabilizers sorb to the surface of the growing particles and lower their surface energy, thereby reducing the likelihood of aggregation and precipitation.[106,107] Reduction of the corresponding ions in the presence of monomeric amphiphiles, such as thiols[108,109] or detergents,[110] or polymers,[111,112] results in formation of stabilized nanoparticles. For homogeneous catalysis, however, complete and irreversible adsorption of stabilizers is undesirable, because all active sites on the particle surface are poisoned, which in turn leads to loss of catalytic activity. Clearly, synthesis of highly efficient nanoparticle catalysts requires optimization of both the particle size and the surface protective chemistry.

Because DEMNs are, at least to some extent, sterically retained within dendrimers, a significant fraction of their surface is unpassivated and thus available for catalysis. Furthermore, DEMNs can be used as homogeneous catalysts in almost any solvent, because the host dendrimers can be tailored for specific solvents. For example, hydroxyl-terminated, fourth-generation PAMAM dendrimers containing 40-atom Pd

nanoparticles (G4-OH(Pd_{40})) efficiently catalyze the hydrogenation of both linear and branched alkenes in aqueous solution.[32] DEMNs have also been used to catalyze Suzuki cross-coupling reactions between arylboronic acids and aryl halides in water.[94] In this study G3-OH(Pd_{10}) was shown to be more efficient for coupling phenylboronic acid and iodobenzene than G4-OH(Pd_{10}), but G3-OH(Pd_{10}) was found to be less stable. This is a consequence of the relative openness of the dendritic architecture: more open architectures permit more facile ingress and egress of substrates and products, but they are not as robust for stabilization.

Solvent plays an important role in the rate of DEMN-catalyzed hydrogenation reactions. For example, the TOFs for the hydrogenation of allyl alcohol in water using G4-OH(Pd_{40}), G6-OH(Pd_{40}), and G8-OH(Pd_{40}) catalysts are 220, 200, and 130 mol H_2(mol Pd)$^{-1}$ h^{-1}, respectively.[32,33] In contrast, the maximum TOFs for allyl alcohol hydrogenation in a mixed MeOH-H_2O (4:1, v/v) solvent are greater by about a factor of two for G4-OH(Pd_{40}) and G6-OH(Pd_{40}), but nearly the same for G8-OH(Pd_{40}).[33] It is possible that the increased solubility of hydrogen in methanol,[113,114] changes in the surface chemistry of the encapsulated Pd nanoparticles, structural changes of the dendrimer template driven by differences in solvent polarity, or enhanced partitioning of the substrate into the dendrimer in the mixed solvent[115,116] are responsible for this finding, but a clear understanding awaits a comprehensive study.

In addition to water and mixed water-alcohol phases, our group has also tested the catalytic activities of DEMNs in pure organic solvents. For example, after being extracted from water into toluene as monodisperse inverse micelles by a surfactant

(dodecanoic acid), Pd nanoparticles encapsulated within fourth-generation, amine-terminated (G4-NH_2) PAMAM dendrimers exhibited better hydrogenation activity for allyl alcohol than was observed in water.[91] We attribute this finding to the relatively hydrophilic interior of the PAMAM dendrimer molecule, which may facilitate partitioning of the substrate into the vicinity of the encapsulated nanoparticle.

Supercritical CO_2 ($scCO_2$) is an important solvent, because it has easily tunable solvent properties and because it is nontoxic.[117] Our group recently showed that Pd nanoparticles encapsulated within perfluorinated dendrimers are soluble in $scCO_2$, and that they catalyze Heck coupling. Interestingly, we found that coupling of aryliodides and methacrylate yields the highly unfavorable 2-phenylacrylic acid methyl ester isomer, rather than the preferred trans-cinnimaldehyde.[23] This finding suggests that judicious tuning of solvent conditions, dendrimer structure, and catalyst composition may provide a means for enhancing product selectivity.

Recycling DEMNs. Invention of strategies for recycling homogeneous catalysts is an important challenge. Recently, new methods, such as the use of biphasic solvents,[118,119] supercritical fluids,[117,120,121] and nanofiltration,[122] have been developed for this purpose. A few examples of methods that have been used to recycle DEMNs are summarized next.

Reactions in biphasic fluorous/organic solvents have demonstrated advantages for recycling of soluble homogeneous catalyst.[118] We used this approach for hydrogenation and Heck reactions using DEMNs. Noncovalent ion-pairing interactions between the surfaces of PAMAM dendrimers and perfluoroether groups solubilize Pd

DEMNs in fluorous phases.[99] These fluorous-soluble catalysts were found to have high activity for the hydrogenation of alkenes when the two phases are mixed. Most importantly, the catalyst can be easily recovered by allowing the two phases to separate, and they could be recycled up to 12 times without appreciable loss of catalytic activity.

We were also able to covalently link perfluoroether groups onto the surface of PPI dendrimers and thereafter prepare encapsulated Pd nanoparticles.[24] These DEMNs catalyzed the Heck reaction between iodobenzene and *n*-butyl acrylate in a fluorous/hydrocarbon solvent to yield *n*-butyl trans-formylcinnamate with 100% regioselectivity at 90 ^{o}C. No leaching of metal from the dendrimer was observed, but the original activity of the catalysts was not fully recovered.

Heterogeneous Catalysis. Because of the ease of separating catalysts from substrates and products, heterogeneous catalysts are very commonly used in industrial processes. However, catalysts supported on silica, alumina, or highly cross-linked polymer beads often suffer from diminished activity compared to their homogeneous analogues due to limited accessibility.[123] Thus, immobilization of nanoparticles onto solid supports is a very crucial step in fabrication of practical heterogeneous catalysts.

Because of potential applications of DEMNs as heterogeneous catalysts, we studied the electrocatalytic properties of DEMNs for O_2 reduction. Such studies have potential applications to fuel cells.[26] In the presence of O_2, a G4-OH(Pt_{60})-modified Au electrode reveals a much higher current and a positive shift in the onset potential for oxygen reduction compared to a G4-OH-modified Au electrode lacking the encapsulated Pd nanoparticles. These results are consistent with substantial catalytic activity. Pd

nanoparticles can also be immobilized onto flat surfaces, such as mica and highly orient pyrolytic graphite (HOPG).[124] Surface modification can be accomplished either by direct adsorption of DEMNs, or by first adsorbing the empty dendrimer and then synthesizing the nanoparticle *in situ*. In both cases, it is possible to use the materials as heterogeneous catalysts.

It is also possible to remove the dendrimer template after sorption of DEMNs onto mica or HOPG supports, but in this case aggregation of nanoparticles was observed. The use of different supports, such as silica, would provide a better platform for stabilizing the nanoparticles after removal of the dendrimer template. For example, silica-PAMAM dendrimer hybrids have been prepared by first modifying the dendrimer with 3-(trimethoxysilyl) propyl acrylate, and then reacting this material with partly hydrolyzed tetraethylorthosilicate.[125] Condensation of this material yielded the final composite material, which exhibited a high metal-ion complexation capacity presumably due to the presence of the dendrimer. Although the authors didn't reduce the resulting material, one could easily imagine doing so thereby obtaining DEMNs for catalyst applications.

1.4. Summary and Accomplishments

In Chapter III of this dissertation, I will discuss the effect of solution pH on the protonation of the dendrimers. Specifically, I have correlated a theoretical calculation to experimental spectroscopic pH titrations of G4-OH, G4-NH_2 dendrimers. Such an

analysis yields two binding parameters: the intrinsic proton binding constant and a constant that characterizes the strength of electrostatic interactions among occupied binding sites. The significant finding is that these two factors are greatly modulated by the unique and hydrophobic microenvironment in the dendrimer interior. Specifically, the intrinsic binding constant (or pK) is reduced by more than 1 pK unit and the strength of electrostatic interactions is reduced by nearly an order of magnitude. Both are attributed to specific ion pairing between bound charges and counter ions.

Preparation of metal nanoclusters within amphiphilic dendrimers in organic solution is demonstrated in Chepter IV. Hydrophilic PPI dendrimers were first modified with various hydrophobic alkyl chains through an amide linkage. The modified dendrimers were then used as templates for preparing intradendrimer copper nanoclusters by first sorbing Cu^{2+} into the dendrimer interior and then reducing the composite. The main driving force for encapsulating metal-ions is the differences in metal-ion solubility between the solvent and the interior of the dendrimer. The preparation of dendrimer/Pd nanoparticles by this method and its application to hydrogenation is also demonstrated.

We have demonstrated that nanometer-sized metal particles are synthesized and encapsulated into the interior of dendrimers by first mixing together the dendrimer and metal ion solution and then reducing the composite chemically, and the resulting dendrimer-encapsulated metal nanoparticles can then be used as catalysts. The size selectivity of these dendrimer-encapsulated catalysts will be discussed in Chapter V. Our results indicate that by controlling the packing density on the dendrimer periphery

by using either different dendrimer generations or dendrimer surface functionalities, it is possible to control access of substrates to the encapsulated catalytic nanoparticle.

Chapter VI of the thesis involves a further study of the location of the DEMNs using an *in-situ* method for determining the average distance between the surface of dendrimer-encapsulated palladium nanoparticles and the periphery of their fourth-generation, hydroxyl-terminated PAMAM dendrimer hosts. The advantage of measuring the periphery-to-surface distance *in-situ*, is that we avoid having to make assumptions about the nanoparticle size and shape. The measurements were made using molecular rulers consisting of three parts: a catalytically active probe at the distal terminus that may undergo a hydrogenation reaction upon contact with the encapsulated catalyst; a large molecular "stopper" at the proximal end that is unable to enter the host; and intervening alkyl chains having different lengths that tether the probe to the stopper and which therefore define the maximum extension of the ruler. Three molecular rulers were configured with a monosubstituted β-cyclodextrin (β-CD) stopper, which is too large to penetrate the dendrimer periphery, at one end and an alkene functional group at the other. The time necessary to hydrogenate these molecular rulers was monitored by ^{1}H NMR, and this information was then used to estimate the average location of the encapsulated Pd nanoparticles. The data indicate that the surface of the encapsulated nanoparticle is situated 0.7 ± 0.2 nm from the surface of the dendrimer.

The research in this dissertation is important because dendrimer-encapsulated metal nanoparticle serves as a tool allowing us to gain both fundamental and application-oriented information about dendritic polymers and nanometer-scale materials. The

results in this dissertation lay the groundwork for future studies that address the use of dendrimers for catalysis, chemical sensors, separation membranes, environmental remediation, corrosion passivation, and controlled release.

CHAPTER II

EXPERIMENTAL

2.1. Chemicals

Starburst poly(amidoamine) (PAMAM) dendrimers and poly(propylene imine) (PPI) dendrimers were used in this work. Hydroxyl- and amine-terminated full generation (Gn-OH, Gn-NH_2, n = 0 – 8 is the generation) PAMAM dendrimers having an ethylenediamine core were provided as 10-25% methanol solutions by Dendritech, Inc. (Midland, MI). The dendrimers were vacuum-evaporated to remove methanol before use. Amine-terminated G2, G3, and G4 PPI dendrimers, DAB-$(NH_2)_{16}$, DAB-$(NH_2)_{32}$, DAB-$(NH_2)_{64}$, were purchased from DSM Fine Chemicals (The Netherlands) and used as received. All aqueous solutions were prepared with filtered water (18 MΩ·cm Milli-Q, Millipore).

Other chemicals used in this work are discussed in specific Chapters.

2.2. Substrates

Au substrates were used for ellipsometry and X-ray photoelectron spectroscopy (XPS) experiments. Au-coated substrates were prepared by sputtering 10 nm of Cr followed by 200 nm of Au onto Si(100) wafers (Lance Goddard Assoc., Foster City, CA). Before use, each wafer was rinsed with methanol and chloroform, dried in a flowing stream of N_2 gas, and then cleaned in a low-energy ozone cleaner for 10 min (Boekel Industries, Inc., model 135500) immediately prior to use.

2.3. Techniques

Ultraviolet-Visible Spectroscopy (UV-vis). Analytical UV-vis absorption spectroscopy is described by Beer's Law (equation 2.1), where the absorbance (A) of a molecule is a function of the molar absorptivity (ε), the path length (l), and the concentration (c).

$$A = \varepsilon l c \qquad (2.1)$$

This technique is very powerful for the characterization of the complexation between dendrimers and transition metal ions, the formation of the clusters upon reduction of dendrimer/metal-ion composites, as well as the size and band structure of the clusters. For some metal colloids (diameter > 4 nm), such as Cu, Ag, and Au, the plasma resonance absorption band can be observed in the UV-vis region due to the collective oscillation of freely mobile conduction-band electrons. Because the plasmon resonance absorption has a third power dependence on the particle diameter, as the particle size decreases these absorptions weaken or are not observable due to damping and broadening of the resonance, as a result of interband transitions of electrons from (n-1)d band to ns or np band.[97,126] Therefore, the plasmon absorption is a very powerful tool to determine the size of metal particles. However, because the plasmon peak of Pd or Pt metal nanoclusters appears at very high energy according to Mie theory, only the interband transition adsorption can be observed.[126,127] The particle sizes studied in this dissertation are less than 4 nm.

Absorption spectra were recorded on a Hewlett-Packard HP 8453 UV-vis spectrometer. As discussed in the individual chapters, the optical path length was 0.1 or 1.0 cm and deionized water or a specific organic solvent was used as a reference for all measurements.

High-Resolution Transmission Electron Microscopy (HRTEM). HRTEM is one of the most useful methods for the characterization of nanoparticles.[5,32,33,97] A transmission electron microscope (TEM), has magnification and resolution capabilities that are over a thousand times beyond that offered by the light microscope.[128,129] The ultrastructure of plant or animal cells as well as viruses can be revealed by TEM.

The TEM is a complex viewing system equipped with a set of electromagnetic lenses in order to generate extremely fine structural details by projecting electrons through a very thin slice of tissue (specimen) to produce a two-dimensional image on a phosphorescent screen (Figure 2.1). The brightness of a particular area of the image is proportional to the number of electrons that are transmitted through the specimen. An electron microscope usually consists of an illuminating system, a specimen manipulation system, and an imaging system. The illuminating system consists of the electron gun and condenser lenses that give rise to and control the amount of radiation striking the specimen. A specimen manipulation system, including the specimen stage, specimen holders, and related hardware, is necessary for orienting the thin specimen outside and inside the microscope. The imaging system includes the objective, intermediate, and projector lenses that are involved in forming, focusing, and magnifying the image on the

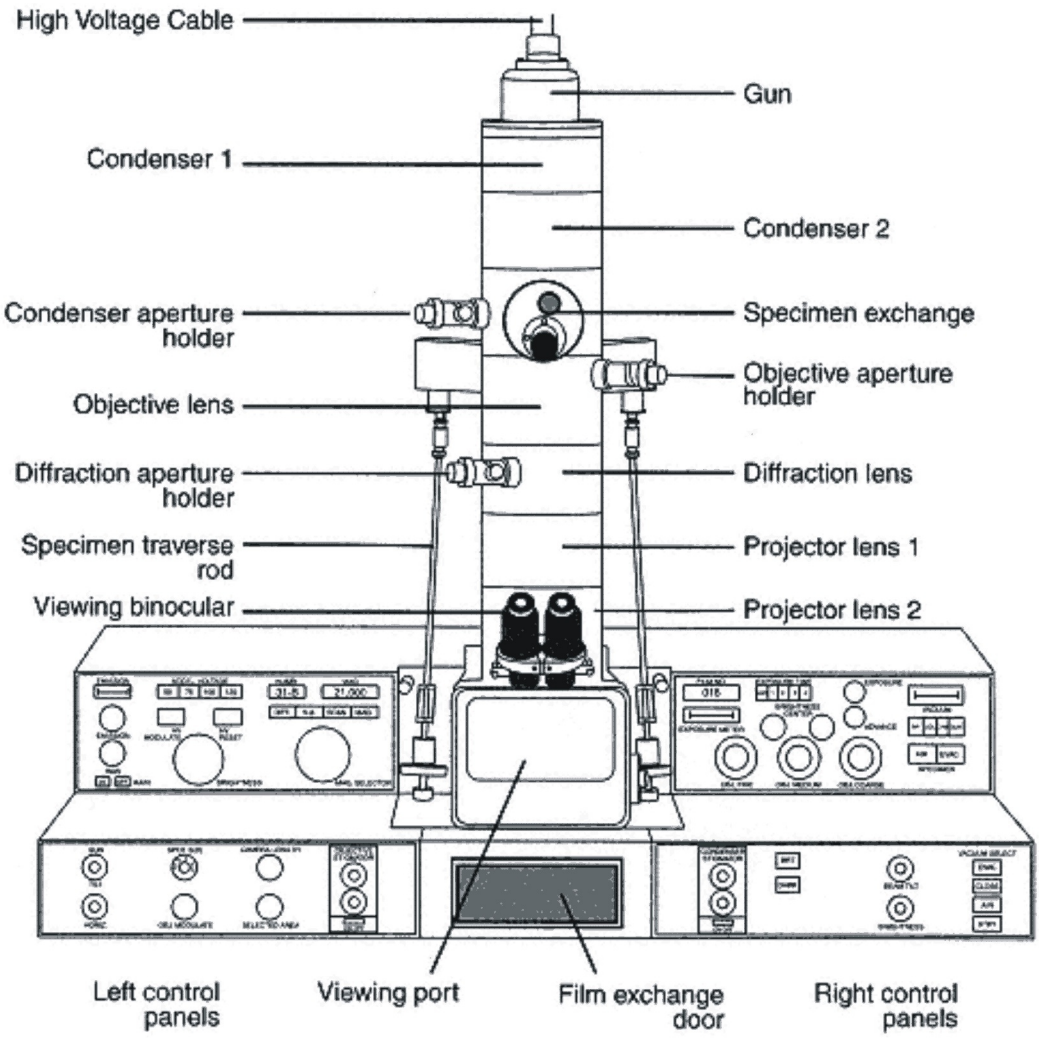

Figure 2.1. Diagrams of a modern transmission electron microscope (taken from ref. 130).

Table 2.1. The components of TEM and their functions.

Component	Function of Components
Illumination System	
Electron Gun	Generates electrons and provides first coherent crossover of electron beam
Condenser Lens 1	Determines smallest illumination spot size on specimen
Condenser Lens 2	Varies amount of illumination on specimen
Condenser Aperture	Reduces spherical aberration, helps control amount of illumination striking specimen
Specimen Manipulation System	
Specimen Exchanger	Chamber and mechanism for inserting specimen holder
Specimen Stage	Mechanism for moving specimen inside column of microscope
Imaging System	
Objective Lens	Forms, magnifies, and focuses first image
Objective Aperture	Controls contrast and spherical aberration
Intermediate Lens	Normally used to help magnify image from objective lens and to focus diffraction pattern
Intermediate Aperture	Selects area to be diffracted
Projector Lens 1	Helps magnify image, possibly used in some diffraction work
Projector Lens 2	Same as Projector Lens 1
Observation and Camera Systems	
Viewing Chamber	Contains viewing screen for final image
Binocular Microscope	Magnifies image on viewing screen for accurate focusing
Camera	Contains film for recording image

viewing screen as well as the camera that is used to record the image. The functions of the major components in TEM are listed in Table 2.1. Very importantly, a vacuum system is necessary to remove interfering air molecules from the column of the electron microscope.

HRTEM can provide information about nanoparticle size and size distribution, because the organic dendrimer can not be observed under microscope. Furthermore, HRTEM also provide compositional information for clusters, even single particles, by combining with other in-column analytical methods such as X-ray energy-dispersive spectroscopy (EDS).

To further reveal if metal nanoparticles synthesized by our method are encapsulated within dendrimers, or stabilized by several dendrimers, heavy metal salts (stains) are used to increase contrast levels in TEM. Two staining techniques[130,131] are usually used in biology: in positive staining, the heavy metal salts attach to various organelles or macromolecules within the specimen to increase their density and thereby increase contrast, while in contrast, the background area surrounding the specimen is made dense by a heavy metal salt by the negative stain so that the specimen appears lighter. Negative staining is more practical for analyzing DEMNs.

In this work, high-resolution transmission electron micrographs (HRTEM) were obtained using a JEOL-2010 transmission electron microscope having a point-to-point resolution of 0.19 nm. Samples were prepared by placing a drop of dilute, aqueous dendrimer solution (0.01 to 0.05 mM) on the grid, which was placed on a paper towel,

and allowing the water to evaporate in air. Holey carbon-coated Cu (200 mesh) or Au (300 mesh) grids (SPI supplies, West Chester, PA) were used throughout.

X-ray Photoelectron Spectroscopy (XPS). XPS, also called electron spectroscopy for chemical analysis (ESCA), is an electron spectroscopic method and a surface-specific technique for solids that uses x-rays to knock electrons out of inner-shell orbitals (Figure 2.2).[132] Normally XPS provides information from the top 1-10 nm of materials, depending on the material studied. The emitted photoelectrons have energies given by

$$KE = h\nu - BE - \phi_s \qquad (2.2)$$

Here, $h\nu$ is the energy of the x-ray photons, BE is the binding energy of the atomic orbital from which the electron originates, and ϕ_s is the spectrometer work function. The binding energy is the energy required to remove the electron from its original atomic orbital to the vacuum level. Core electrons have the potential to provide both quantatitive and qualitative chemical information due to the fact that they have characteristic binding energies. Because the electron binding energies are dependent on the chemical environment of the atom, the binding energies exhibit a chemical shift (1-10 eV) due to interaction of the core electron with valence electrons and surrounding atoms. The intensity of the photoelectron peak is proportional to the number of atoms present. XPS is therefore useful to identify the oxidation state and ligands of an atom. Thus, XPS is used to investigate elemental composition and oxidation state of atoms within DECs.

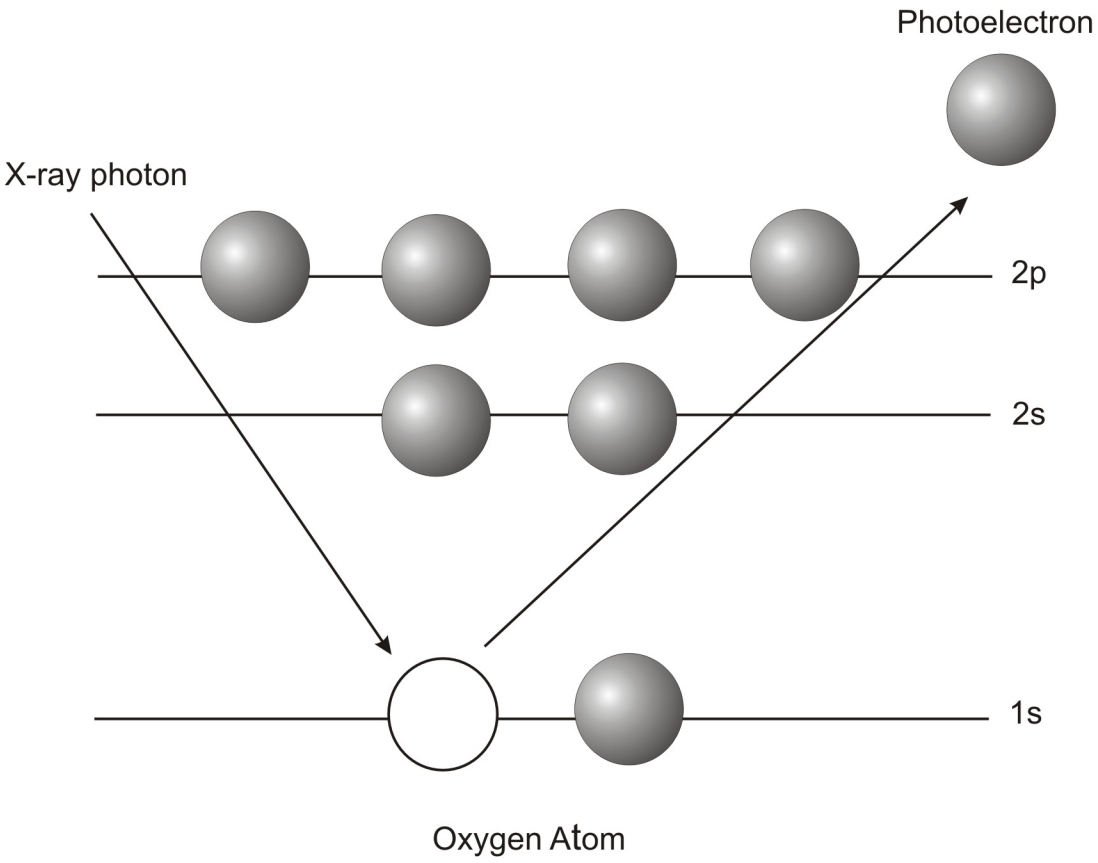

Figure 2.2. Schematic representation of generating a photoelectron from an oxygen atom.

Nuclear Magnetic Resonance Spectroscopy (NMR). Under appropriateconditions in a magnetic field, a sample can absorb electromagnetic radiation in the radio frequency region at frequencies governed by the characteristics of the sample. Aplot of frequencies of the absorption peaks versus peaks intensities constitutes an NMR spectrum. Thus, NMR is a very useful technique in obtaining detailed information about molecular structure.

In this dissertation, NMR is used to identify the formation of specific products of reactions and integrations of peak intensities which are used to track the progress of the hydrogenation reactions. Because in some cases, the concentration of the dendrimer template is below the detection limit of NMR or remains constant, the characterization of reaction products is simplified.

CHAPTER III

INTERACTIONS BETWEEN DENDRIMERS AND CHARGED PROBE MOLECULES: DETERMINATION OF INTRINSIC PROTON BINDING CONSTANTS VIA POTENTIOMETRIC PH TITRATION

3.1. Synopsis

Protonation of fourth-generation poly(amidoamine) dendrimers terminated with hydroxyl and amine functional groups has been studied by potentiometric pH titration. The titration data are analyzed using a multi-shell structural model and a Frumkin adsorption isotherm to approximate proton-dendrimer binding equilibria. Site-to-site correlation is ignored, and counter ions are treated according to the standard Debye-Hückel theory. This analysis yields two binding parameters: the intrinsic proton binding constant and a constant that characterizes the strength of electrostatic interactions among occupied binding sites. For the hydroxyl-terminated dendrimers, the internal tertiary amines have an average binding constant (pK = 6.30) 1 - 2 pH units smaller than the value expected for a single, isolated binding site. This shift in pK is attributed to a hydrophobic microenvironment within the dendrimer interior. In contrast, no significant shift has been observed in the binding constant (pK = 9.23) for the peripheral primary amines in the amine-terminated dendrimer, because the microenvironment around the primary amines is more hydrophilic. The strength of electrostatic interactions obtained from titration data is 3 times (primary amines) and 8 times (tertiary amines) smaller than the calculated values based on the multi-shell model. We hypothesize that the

diminished interaction strength results from ion-pairing between bound protons and counter ions. In addition to the Debye-Hückel contribution from mobile ions, ion-pairing provides extra Coulomb charge screening.

3.2. Introduction

Because of their unique structural topology and chemical versatility, dendrimers have found applications related to catalysis, drug delivery, energy transfer, and molecular recognition.[3,5,6,12,13,15-17,28] In many cases, these applications strongly depend on the equilibrium between dendrimers and ions, but there have only been a few experimental studies that address this issue.[18,20,47] Here, I present a theoretical interpretation of experimentally determined titration data for poly(amidoamine) (PAMAM) dendrimers.

We recently developed a theoretical approach, which we refer to as the 'shell model', to quantify ion-dendrimer binding.[20] Some of the characteristics of this model are summarized here. First, electrostatic interactions are assumed to be the sole source of site-to-site interactions. The total energy is calculated by adopting a multi-shell dendrimer model, and discrete charges within each shell are summed and approximated as a shell of continuous charge. This procedure makes it possible to solve the linearized Poisson-Boltzmann (PB) equation analytically within the limit of the Debye-Hückel approximation (i.e., a dilute electrolyte solution). Second, no distinction is made between binding configurations (or microstates) that have the same set of intra-shell proton binding numbers. Instead, all degenerate configurations are averaged (mean-field

approximation) so that site-to-site correlations need not be considered. In contrast, such a correlation is a key aspect of the Ising model that has been used previously for modeling dendrimer binding equilibria.[133] Borkovec and Koper (B&K) used the Ising model to understand the protonation of poly(propylene imine) (PPI) dendrimers, and their calculated results were found to agree fairly well with experimental NMR results.[19]

In this study, we use the shell model to analyze experimental data from potentiometric pH titrations. Our goals are to obtain the intrinsic proton binding constants for amine groups in poly(amidoamine) (PAMAM) dendrimers, and to estimate the strength of electrostatic repulsion among occupied proton binding sites. The results indicate that interior amine groups have a smaller proton affinity compared to a single isolated amine group in the bulk electrolyte. In addition, electrostatic repulsion between occupied proton sites is weaker than that predicted by the standard electrolyte theory. Clearly, the unique microenvironment within the dendrimer interior is responsible for both of these results.

3.3. Experimental

Chemicals. Potassium hydrogen phthalate (KHP, Fisher Scientific), Na_2CO_3, $NaHCO_3$, NaOH, concentrated HCl (EM Science), and $NaClO_4$ (Aldrich) were used as received.

Potentiometric pH Titration. A custom-built microtitrator permitted titrations to be carried out within a 1 cm cuvette of the type used for UV-vis spectroscopic measurements. The cuvette was capped with a PDMS block fitted with a pH

microelectrode (U-05991-61, Cole-Parmer, Vernon Hills, IL) and tubing (0.3 mm ID, Teflon) for titrant addition and for mixing via a gently bubbling N_2 stream. To minimize solution evaporation, the N_2 stream was pre-saturated with water vapor by passing it through a NaCl solution having an ionic strength similar to that of the sample solution being titrated. The temperature was maintained at 25 ^{o}C using a cuvette holder (8453A, Agilent Technologies, Palo Alto, CA) thermostatted by an external water circulator (F12, Julabo, Allentown, PA). In a typical titration experiment, 600 μL of a 1.00 mM G4-OH or G4-NH_2 stock solution was fully protonated with excess HCl (47.6 or 95.2 μmol, respectively). Enough $NaClO_4$ (0.00, 30.0, 60.0, 150.0, or 300.0 μmol) was added to the solution to increase the ionic strength by 0, 10, 20, 50, or 100 mM, respectively. The ionic strengths of acidified G4-OH and G4-NH_2 dendrimers prior to adding $NaClO_4$ were 15 mM and 29 mM, respectively.[134] The total solution volume was adjusted to 3.00 mL with water at the start of titration. NaOH titrant was added using a syringe pump (M365, Thermo Orion, Beverly, MA) at a constant rate of 0.203 μL/s, and the pH was recorded (pH213, Hanna Instruments, Woonsocket, RI) continuously via an RS232 interface. The pH meter was calibrated daily using standard solutions (pH 4.008, 50.0 mM KHP; pH 10.012, 25.0 mM Na_2CO_3 plus 25.0 mM $NaHCO_3$).[135] NaOH (186 mM, stored under N_2) and HCl (238 mM) stock solutions were standardized against KHP. The precision of the titrations was consistently better than 0.5%.

Dendrimer Structural Parameters Used for Simulation. A multi-shell dendrimer structural model was used for the simulations.[20] Equilibrium shell diameters for G4-OH and G4-NH_2 dendrimers were assumed to be the same as the dendrimer

diameters of the relevant generations.[136] Thus, the outermost shell of 64 terminal groups was assumed to have a diameter of 4.5 nm, identical to the diameter of a fourth-generation PAMAM dendrimer. The diameters and the number of tertiary amine groups (numbers in parentheses) for the inner shells were assumed to be 3.6 nm (32), 2.9 nm (16), 2.2 nm (8) and 1.5 nm (4). The two core nitrogen sites were combined with those in the innermost shell, but the error due to this approximation was not quantified since it was probably very small. Other important simulation conditions are noted in the appropriate location in the text.

3.4. Results and Discussion

Brief Review of Proton-Dendrimer Binding Equilibria. We have previously shown that proton-dendrimer binding can be analyzed using a simple isotherm method, which yields simulation results equivalent to those derived from more rigorous (and complex) statistical methods.[20] In the isotherm method, only a representative or averaged binding site is considered (eq 3.1).

$$A + H \rightleftharpoons HA \tag{3.1}$$

Here, A denotes the averaged proton binding site and H is a proton with its charge omitted for simplicity and generality. The proton binding constant β_A' for site A in the above equilibrium specifies a Frumkin adsorption isotherm (eq 3.2).

$$\frac{\bar{h}}{h_0 - \bar{h}} = \beta_A'[H] = 10^{pK-pH}10^{-\bar{\delta}} \tag{3.2}$$

Here, $\bar{h}$ is the average proton binding number per dendrimer; h_0 is the total number of binding sites; [*H*] is the equilibrium concentration of proton; and *pK* specifies the intrinsic proton binding constant. A unitless parameter, $\bar{\delta}$, characterizes the increase in binding free energy per unit bound charge arising from site-to-site interactions, averaged over all the binding sites. Note that a list of symbols is provided at the end of the text.

Determination of Binding Parameters from Potentiometric pH Titrations. In the shell model, the proton binding number for each shell can be calculated. The sum of these binding numbers, or the average proton binding number per dendrimer, can then be compared to the experimental value. Generally, it is not possible to determine the proton binding constant for each shell, because in this case the total number of adjustable parameters would exceed the number of independent parameters extractable from titration data.

Under some special conditions, however, this problem can be avoided. For example, in the case of a G4-OH multi-shell dendrimer, we can decrease the total number of adjustable parameters by assuming that all the internal tertiary amine sites have the same intrinsic proton binding constant (*pK*) and will experience the same free energy increase caused by site-to-site interactions ($\bar{\delta}$). With this assumption (*vide infra*), titration data can be linked to adjustable parameters in a very direct and transparent way. Specifically, our previous results showed that $\bar{\delta}$ varies approximately

linearly with respect to the total charge Q,[20] or in this work, $\bar{h}$ (eq 3.3).

$$\bar{\delta} = \bar{w}Q = \bar{w}\bar{h} \tag{3.3}$$

Here, $\bar{w}$ can be thought of as the contribution of each protonated site to $\bar{\delta}$. Substituting eq 3.3 into eq 3.2 and rearranging, we obtain eq 3.4.

$$G(\bar{h}) = pH + \log\frac{\bar{h}}{h_0 - \bar{h}} = pK - \bar{w}\bar{h} \tag{3.4}$$

A plot of $G(\bar{h})$ vs. $\bar{h}$ is a straight line with an intercept of pK and a slope of $-\bar{w}$.[137,138] The function $G(\bar{h})$ is experimentally accessible, because solution pH can be measured directly and $\bar{h}$ can be obtained from eq 3.5, which is the material balance equation for proton.

$$H_0 - B_0 - [H] + \beta_w[H]^{-1} - \bar{h}L_0 = 0 \tag{3.5}$$

Here, L_0, H_0, and B_0 are the total concentrations for dendrimer ligand L (totally deprotonated state), the strong acid added initially, and the strong base (titrant) added, respectively. $[H]$ and $[OH]$ are linked to each other by β_w, the auto-dissociation constant of water. In a typical experiment, excess acid (that is, a constant H_0) is added initially, and then titration with a strong base yields a string of data pairs consisting of B_0

and [*H*] (or *pH*). Using eq 3.5, we can calculate $\bar{h}$ at every point along the titration curve. The validity of this approach can be tested by plotting $\bar{h}$ against $(B_0/L_0) - (H_0 - h_0L_0)/L_0$. The horizontal axis of this plot can be understood as a corrected NaOH/dendrimer molar ratio. The correction term, $(H_0 - h_0L_0)$, is the amount of strong acid in excess of the stoichiometric amount needed to titrate a completely deprotonated dendrimer. The plot should be a straight line with a slope of –1 when both [*H*] and [*OH*] are small compared to the amount of bound proton ($\bar{h}\,L_0$). Figure 3.1 shows that this is indeed the case. The intercepts of the straight line on both axes are the same (62.0) and equal to h_0, or the total number of amine groups per dendrimer molecule (also 62).

Protonation of G4-OH PAMAM Dendrimer. Figure 3.2 shows the pH titation curves of G4-OH PAMAM dendrimer are different ionic strengths. Proton binding to tertiary amine sites will be influenced by two factors: the inherent affinity of the site toward proton and the electrostatic repulsion between protonated sites. These two factors can be quantified by *pK* and $\overline{w}$, respectively (eq 3.4). Figure 3.3A shows that experimental $G(\bar{h})$ functions are linear over a wide range of $\bar{h}$, except when $\bar{h}$ approaches 0 or h_0, where the $\log[\bar{h}/h_0 - \bar{h})]$ term in eq 3.4 diverges quickly. This linearity provides strong support for our earlier assumption that the intrinsic proton binding constants for all tertiary amine sites are roughly the same (*vide supra*).

pK and $\overline{w}$ are independent parameters that allow us to gain some insight into the binding chemistry and structure of the G4-OH dendrimer. Eq 3.3 indicates that $\overline{w}$ can also be evaluated from the calculated $\bar{\delta}(\bar{h})$ (Figure 3.3B), a function averaged over Λ

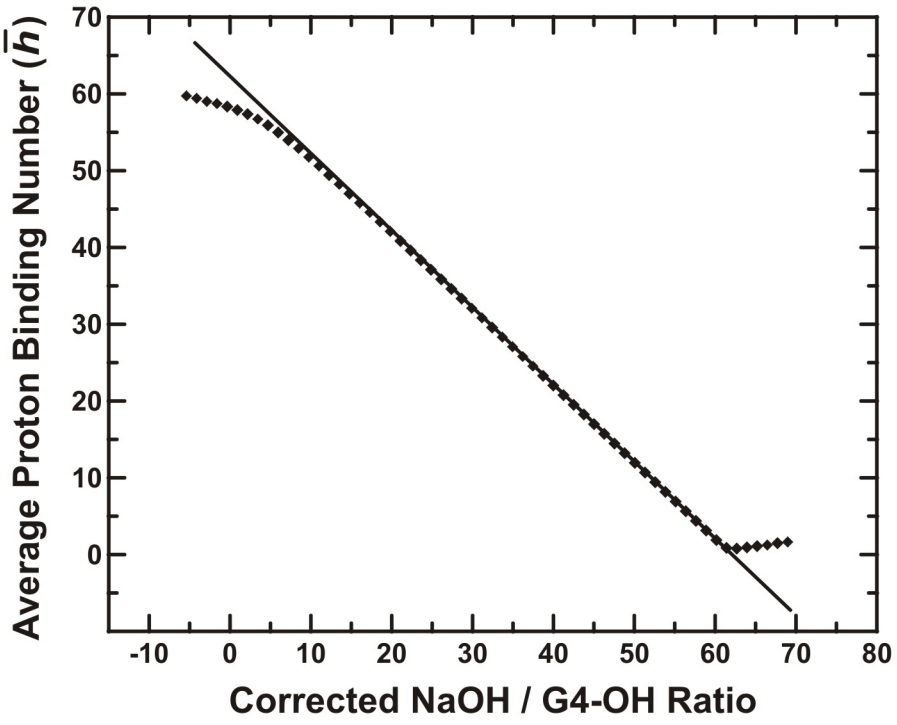

Figure 3.1. Average proton binding number, $\bar{h}$, as a function of the corrected NaOH/dendrimer molar ratio, or $(B_0/L_0) - (H_0 - h_0L_0)/L_0$. The points represented by diamonds are experimental data for the G4-OH dendrimer, and the solid line is the least-squares linear fit to the middle portion of the data. The intercepts on the horizontal and vertical axes are both 62.0.

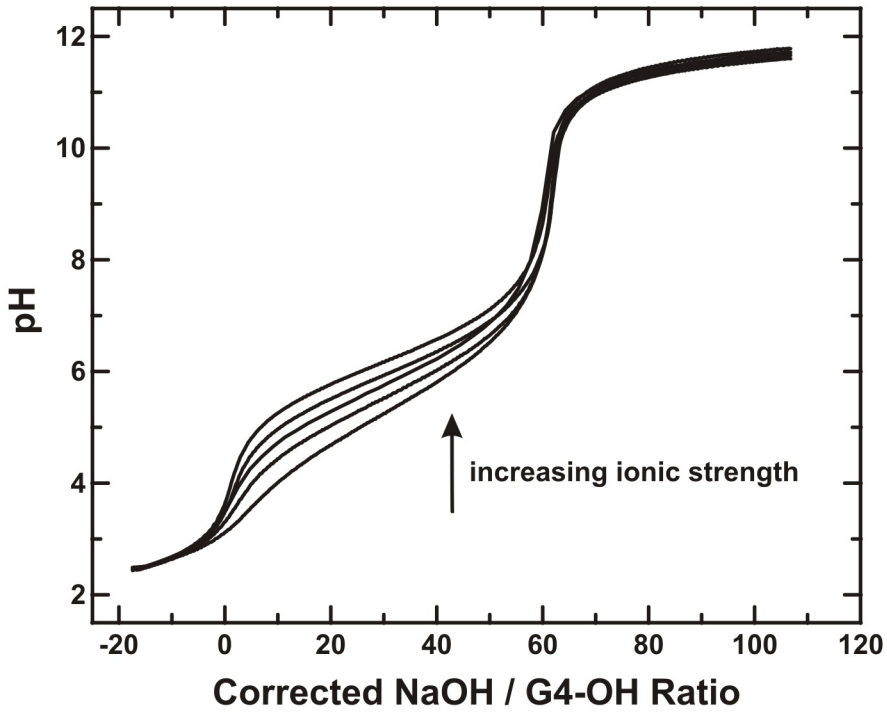

Figure 3.2. Potentiometric pH titration curves for G4-OH at ionic strength of 15 mM, 25 mM, 35 mM, 65 mM, and 115 mM, respectively.

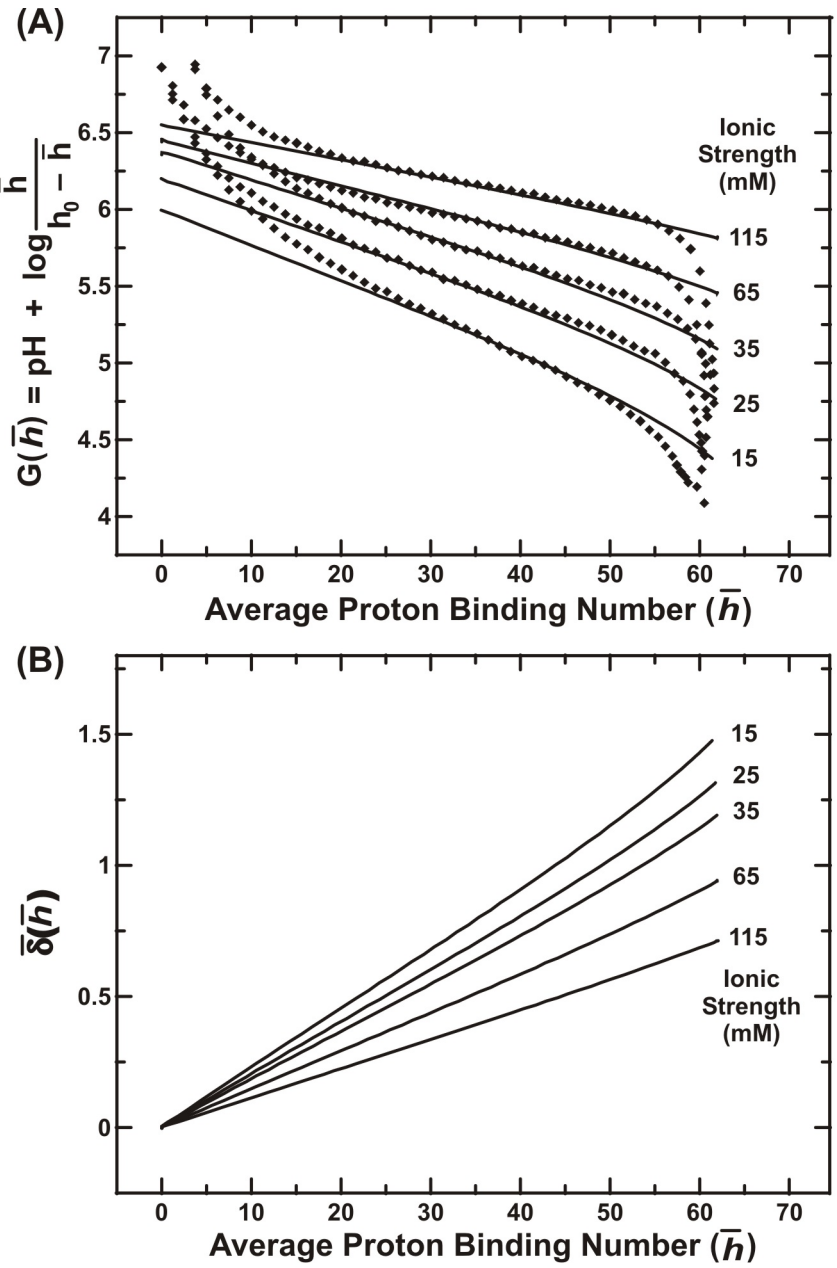

Figure 3.3. (A) $G(\bar{h})$ (eq 3.4) as a function of average proton binding number ($\bar{h}$) for the G4-OH dendrimer at the indicated ionic strengths. The datapoints were determined experimentally, and the solid lines are the best fits from theory. The intercepts (slopes) of these fits are 6.04 (-2.36×10^{-2}), 6.20 (-2.09×10^{-2}), 6.38 (-1.89×10^{-2}), 6.45 (-1.50×10^{-2}), and 6.55 (-1.14×10^{-2}), respectively, from ionic strength 15 mM to 115 mM. The scaling factor (f_0) for bound charge is 0.12 for all curves. (B) The best fits in (A) recast in terms of the function $\bar{\delta}(\bar{h})$, which is the average interaction energy per bound charge.

charged shells as shown in eq 3.6.

$$\bar{\delta}(\bar{h}) = \frac{f_0 e^2}{k_B T \ln(10)} \sum_{\lambda=1}^{\Lambda} \phi_\lambda \tag{3.6}$$

Here T is the absolute temperature, k_B is the Boltzmann constant, e is the charge on an electron, and f_0 is a linear scaling factor (its meaning will become apparent shortly). ϕ_λ consists of a linear combination of shell charges, q_λ, and the linear coefficients depend on many variables including the average proton binding number per dendrimer ($\bar{h}$), the ionic strength (I), the dielectric constant of the electrolyte solution (ε_0) and that of the dendrimer interior (ε), the fraction of the dendrimer volume occupied by the electrolyte solution (α), and the dendrimer dimensions (that is, the diameters of all the shells). Many of these variables are not well understood; for example, ε and α are difficult to estimate. Pistolis *et al.* have studied the dielectric properties of PAMAM dendrimer interiors using a fluorescent pyrene probe, and an estimated value of $\varepsilon = 23$ can be inferred from their data.[139,140] Based on a report by Tomalia *et al.*, we conclude that α is roughly 0.5 for G4 PAMAM dendrimers.[36,141]

Using the best estimates we have for various structural parameters, we can fit ($\overline{w}$) values calculated from $\bar{\delta}(\bar{h})$ to the titration data. Figure 3.3A shows that a good fit over ionic strengths ranging from 15 mM to 115 mM can be obtained, but it requires setting f_0 to 0.12. Note, f_0 is an arbitrary scaling factor included in eq 6 for the

convenience of comparing experimental and theoretical $\overline{w}$ values. If our theoretical model of the dendrimer is satisfactory, then f_0 should have a value of 1. Because $\overline{w}$ specifies the strength of electrostatic interactions, a f_0 value of less than 1 can be interpreted as the observed electrostatic interactions between protonated sites being weaker than those expected from theory. However, this interpretation of f_0 depends on the assumption that the theoretical model itself is valid. That is, the calculated value of $\overline{w}$ should not change significantly when the adjustable parameters used for the simulation are varied over physically reasonable ranges.[36,139-141] In addition, we have ignored the possibility of pH-responsive changes in dendrimer size,[18,142,143] although this behavior can be easily incorporated into our algorithm. For PAMAM dendrimers, diameters will increase as pH decreases, or as electrostatic repulsion increases. An expanded dendrimer would reduce the calculated value of $\overline{w}$, which would partially account for f_0 being smaller than the ideal value of 1.

Despite less than perfect knowledge of the aforementioned factors, it is still not possible to fully account for the observed large deviation in f_0 from 1. To illustrate this point, it is instructive to compare the scaling factors for a dendrimer and for a simple diamine separated by a linear alkyl spacer. As previously described,[20] the linearity of $\overline{\delta}(\overline{h})$ with respect to $\overline{h}$ is equivalent to B&K's mean-field approximation.[133] More specifically, $\overline{w}$ used in our model is algebraically equivalent to $\varepsilon^{(mf)}$, a nearest-neighbor pair-wise interaction parameter used by B&K. For a PAMAM dendrimer, $\overline{w}$ is expected to be comparable to $\varepsilon^{(mf)}$ for hexamethylene diamine (HMDA), because

nearest-neighbor proton binding sites are separated by six atoms or seven covalent bonds in both cases. A $\varepsilon^{(mf)}$ value of 0.28 can be obtained from experimental proton binding constants (pK_1= 10.95 and pK_2 = 10.07 at an ionic strength of 0.1 M)[144] and eq 3.7.[133]

$$\varepsilon^{(mf)} = pK_1 - pK_2 - \log 4 \tag{3.7}$$

Alternatively, an estimated $\varepsilon^{(mf)}$ value of 0.19 can be derived from theory alone (eq 3.8).[138,145]

$$\varepsilon^{(mf)} = \frac{e^2}{k_B T \ln(10)} \frac{\exp(-r_{AVG}\kappa_0)}{\varepsilon_0 r_{AVG}} \tag{3.8}$$

Here, r_{AVG} is the average distance between the two terminal amine sites, and κ_0^{-1} is the Debye length. The agreement between the experimental and calculated $\varepsilon^{(mf)}$ is remarkable, because eq 3.8 represents a very crude approximation.[145,146] As expected, these $\varepsilon^{(mf)}$ values for HMDA are comparable to $\overline{w}$ for the dendrimer (0.100 at 0.1 M ionic strength) calculated from $\overline{\delta}(\overline{h})$ using eq 3.6. In contrast, the experimental $\overline{w}$ (0.0114 at 0.1 M ionic strength determined using the data in Figure 3.3A) is about an order of magnitude smaller; that is, a f_0 value of approximately 0.1 is needed in order to fit calculated $\overline{w}$ to experimental $\overline{w}$.

The results in the previous paragraph indicate that electrostatic interactions for a simple diamine molecule can be described by the standard Debye-Hückel theory, but

such a description for a multi-shell dendrimer overestimates the strength of electrostatic interactions between charge sites. To explore further the physical meaning of the f_0 factor, we focus our attention on eq 3.6. Since ϕ_λ is a linear combination of q_λ,[20] we may think of f_0 as a scaling factor for the bound charges. A small f_0, as we have seen here for G4-OH, means that the effective charges on the tertiary amine sites are smaller than expected. One possible explanation for this is that, in addition to screening by mobile ions, bound charges experience extra Coulomb screening from less-mobile counter ions due to ion pairing. This hypothesis is consistent with the following information. First, the interior of a dendrimer molecule is more hydrophobic and has a smaller dielectric constant than the surrounding bulk electrolyte,[110,140] and both of these factors favor the formation of ion pairs.[147,148] Second, ion pairing only reduces the effective bound charges but does not modify the relative distribution of mobile ions (the Debye length is independent of the magnitude of the bound charges). It follows that, if we correct the effects of ion-pairing by choosing an appropriate f_0 factor, then the simulation results should follow the predictions of the standard Debye-Hückel theory. One such prediction is that as the ionic strength increases, the Coulomb screening by counter ions will increase, resulting in a decrease in electrostatic repulsion between bound charges. Indeed, when a single scaling factor is used, calculated $\overline{w}$ values at different ionic strengths agree quantitatively with the trend predicted by theory (Figure 3.3A). Finally, ion pairing or "specific" ion binding has also been noticed by Huang *et al.*, who measured the effective electrokinetic charge of a carboxylic acid-terminated dendrimer using capillary electrophoresis.[149]

In addition to $\overline{w}$, the experimental data shown in Figure 3.3A also allow us to obtain the intrinsic proton binding constant of interior tertiary amines. As the ionic strength *I* increases, *pK* systematically increases from 6.00 at *I* = 15 mM to 6.65 at *I* = 115 mM. This slight increase in *pK* is anticipated because eq 3.4 has been derived with the implicit assumption that the activity coefficients for *A* and *HA* in eq 3.1 are neglected.[150] Compared with the *pK* (8.07) for a monomeric tertiary amine in a structurally similar compound,[151] the intrinsic *pK* for binding sites inside a dendrimer is 1 - 2 pH units smaller. This shift in *pK* is probably due to the same factors that shift the *pK* of a titratable residue localized within the hydrophobic pocket of some proteins.[152] That is, a hydrophobic microenvironment significantly increases the energy penalty for adding a charge to a neutral functional group.

Of particular interest to chemists is the ability to predict the degree of protonation of a dendrimer as a function of pH. Such a binding curve is essentially a plot of $\overline{h}$ *vs. pH* (Figure 3.4A). Here, the experimental data agree with theoretical fits over a range of ionic strengths from 15 mM to 115 mM. Generally, the slope at 50% binding increases as the ionic strength increases. When interactions between binding sites are absent, the binding curve approaches the limiting shape for an isolated single binding site. Unlike the titration data, results of calculations based on a multi-shell model can provide additional insight into dendrimer protonation. For example, Figure 3.4B shows that the pH at 50% binding for an outer shell is higher than that for an inner shell. This result is consistent with intuition, because an inner-shell binding site experiences a higher degree of electrostatic interactions than an outer-shell site.[20]

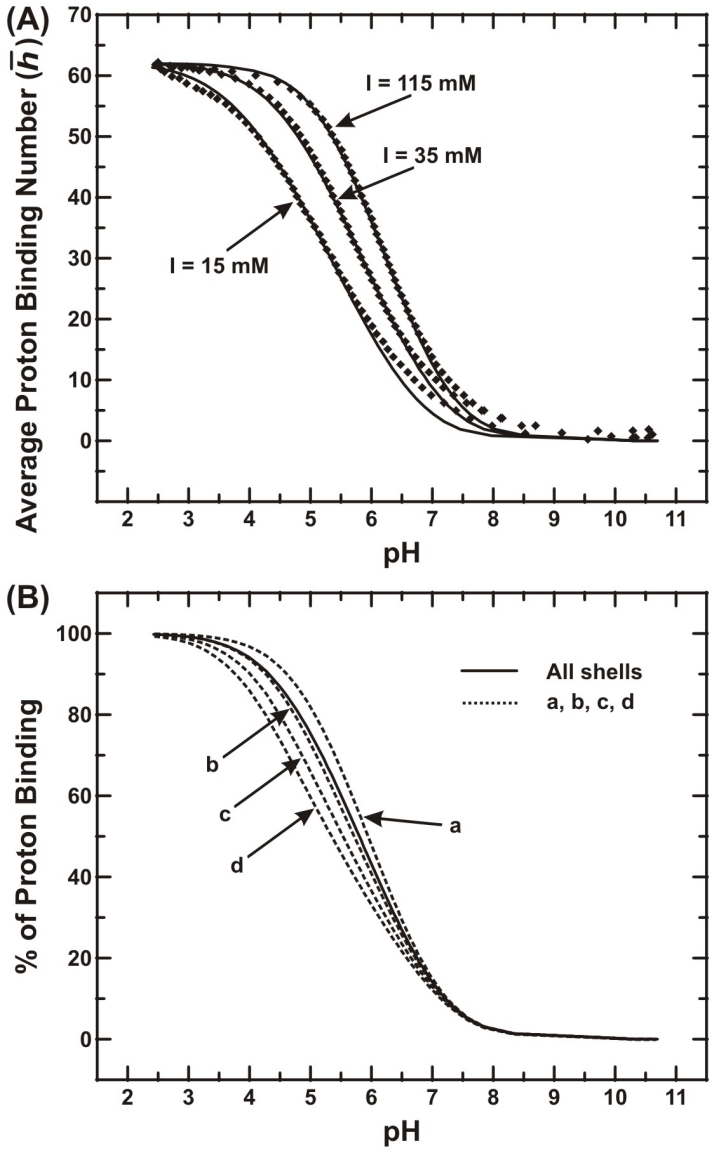

Figure 3.4. Alternative presentation of the data shown in Figure 3.3. (A) Proton binding curve for the G4-OH dendrimer, plotted as the average proton binding number vs. pH, at the indicated ionic strengths. The datapoints are experimental data and the solid lines are the best fits from theory. (B) Shell-level proton binding curves, plotted as the percentage of proton binding vs. pH, at an ionic strength of 35 mM. The solid line represents overall binding, and the dashed lines correspond to binding at shells containing (a) 32, (b) 16, (c) 8, and (d) 6 (which includes 2 core sites) binding sites.

Protonation of G4-NH_2 PAMAM Dendrimers. Results of the analysis described in the previous section for G4-OH provide a starting point for modeling protonation of the structurally related G4-NH_2 dendrimer. For example, we may assume that structural and binding parameters for all the tertiary amines in G4-NH_2 are the same as those found for G4-OH. This will leave two adjustable parameters to be determined for the peripheral primary amines: *pK*, the intrinsic proton binding constant, and f_0, the scaling factor for charge.[153] Again, using the titration data (Figure 3.5 and Figure 3.6) over a range of ionic strengths, we find that *pK* for the primary amines varies from 9.15 at I = 29 mM to 9.30 at I = 129 mM. These values do not differ significantly from the *pK* (9.28) of a monomeric analogue.[154] In addition, the best f_0 for primary amines, 0.35, is larger than that for the tertiary amines, indicating reduced specific ion pairing around the peripheral primary amines. The above results are well within intuitive expectations, because a primary amine site is in close proximity with the surrounding bulk electrolyte and thus its average microenvironment is certainly more hydrophilic than the dendrimer interior.

Because the intrinsic *pKs* for tertiary and primary amines differ by almost 3 pH units, we would expect the titration curve for G4-NH_2 to exhibit two endpoints corresponding to stepwise protonation of two different kinds of amine groups. The data in Figure 3.5 confirm this expectation. This result can be observed more clearly in binding curves ($\bar{h}$ vs. *pH*), which include both experimental and simulation data. Figure 3.7 shows that at a pH of about 7.0, most primary, but few tertiary, amines are protonated. This type of information highlights the usefulness of theoretical modeling,

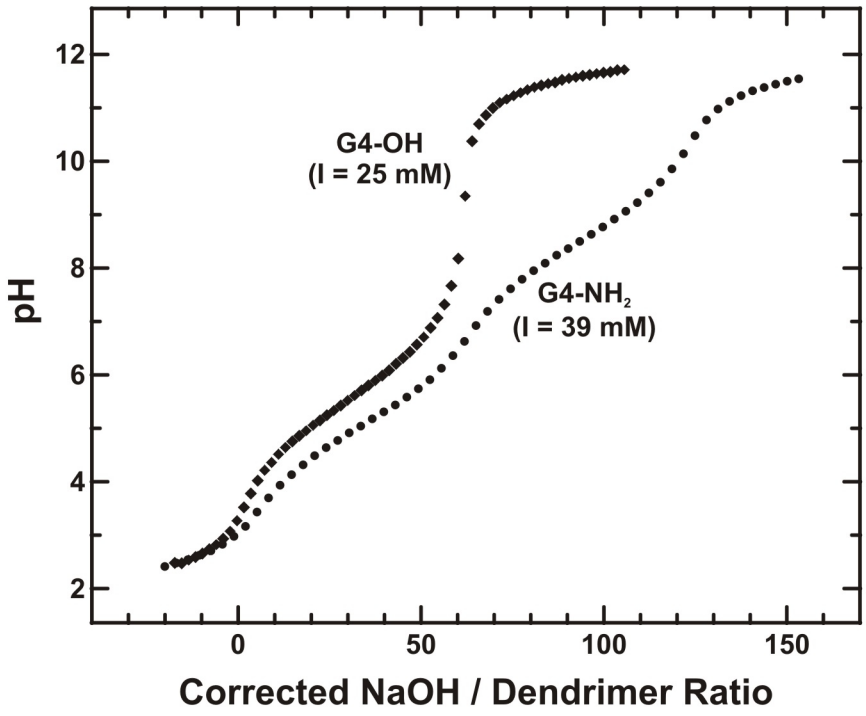

Figure 3.5. Potentiometric pH titration curves for G4-OH and G4-NH_2 at the indicated ionic strengths (I). The G4-OH curve exhibits only one endpoint at a molar ratio of about 62, while G4-NH_2 exhibits two endpoint transitions at molar ratios of about 62 and 126. The horizontal axis is calculated the same way as in Figure 3.1.

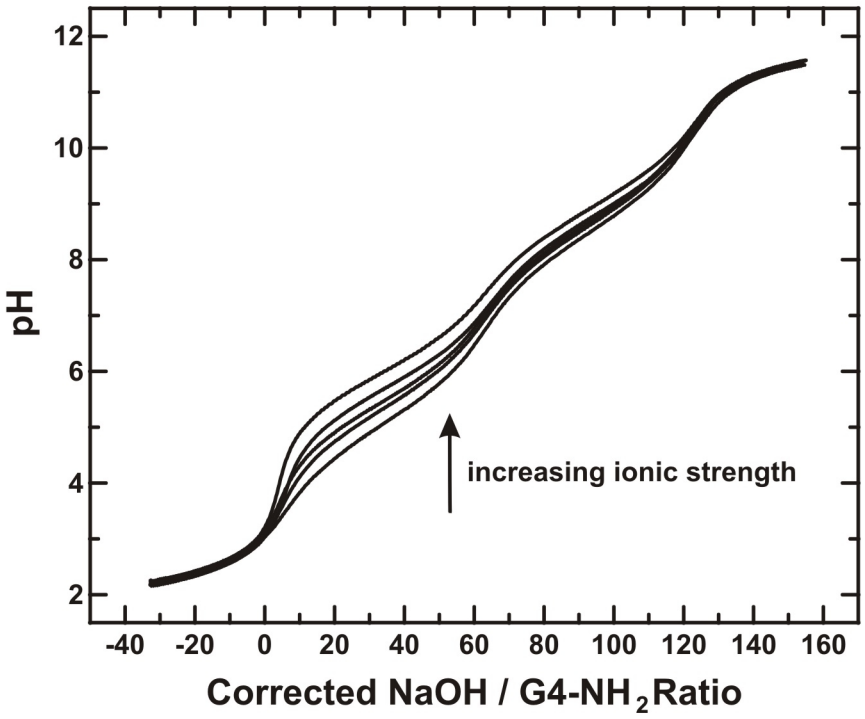

Figure 3.6. Potentiometric pH titration curves for G4-NH_2 at ionic strength of 29 mM, 39 mM, 49 mM, 69 mM, and 129 mM, respectively.

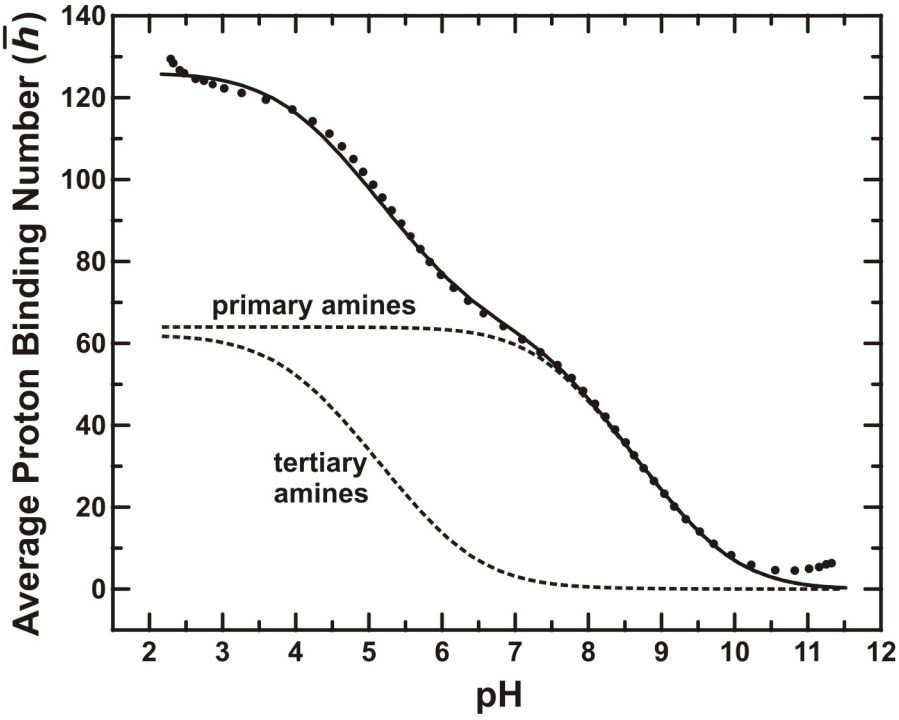

Figure 3.7. Proton binding curve for the G4-NH_2 dendrimer, plotted as the average proton binding number vs. pH, at an ionic strength of 39 mM. The circles represent experimental data, the solid line is the best theoretical fit to the experimental data, and the dashed lines are shell-level binding curves for the outermost shell of 64 primary amine sites, and all the inner shells containing a total of 62 tertiary amine sites. The scaling factor (f_0) is 0.35 for the primary amines and 0.12 for the tertiary amines.

because such information is difficult to obtain from titration data alone.

It is interesting to compare the pH-dependent proton binding properties of PAMAM and PPI dendrimers. Like G4-NH_2, a PPI dendrimer terminated with primary amines yields a titration curve with two endpoints. However, based on NMR data, Koper *et al.* concluded that these steps result from site-to-site correlation, which becomes significant only when electrostatic interactions between two neighboring groups are very strong.[19] Specifically, to avoid strong interactions, even-numbered dendrimer shells protonate at a different pH than odd-numbered shells, resulting in the observed two titration endpoints. It should be emphasized that this correlation mechanism assumes nearly identical intrinsic *pK* values for tertiary and primary amines; therefore, it is significantly different than the assumption underpinning the approach described here. If the correlation mechanism is operative for PAMAM dendrimers, then the titration curve for G4-OH would also reveal two endpoints. Because only one endpoint is actually observed, we can conclude that the correlation mechanism does not have to be considered for PAMAM dendrimers. This is understandable because the distance between two neighboring binding sites in PAMAM dendrimers is much larger than it is for PPI dendrimers, hence weaker nearest-neighbor interactions are expected for PAMAM dendrimers. In addition, ion-pairing further diminishes these nearest-neighbor interactions. Ignoring the correlation mechanism is important for us, because the isotherm method used here is algebraically equivalent to adopting a mean-field approximation which, by definition, does not include site-to-site correlation. It is not possible to use titration data alone to distinguish between the two possible protonation

mechanisms for PPI dendrimers, because both predict a two-endpoint titration curve. However, this question could be answered if PPI dendrimers containing only internal tertiary amines were available for titration studies.

3.5. Summary and Conclusions

We have studied protonation of G4-OH and G4-NH_2 PAMAM dendrimers using both experimental and theoretical methods. Data from potentiometric pH titrations were analyzed using a multi-shell structural model and an isotherm binding equilibrium. Binding between protons and dendrimers is controlled by two factors: the intrinsic proton binding constant and electrostatic interactions between occupied binding sites. We found that these two factors are significantly modulated by the hydrophobic microenvironment within the dendrimer interior. Specifically, the intrinsic proton binding constant (or pK) is reduced by 1 – 2 pH units and the strength of electrostatic interactions is reduced by nearly an order of magnitude compared to a structurally similar monomeric analogue. In other words, a tertiary amine site within the dendrimer interior has a lower proton affinity than a similar site outside the dendrimer. In addition, counter ions accompany the proton into the dendrimer interior, which reduces both the effective charge of bound protons and the interactions between them. Thus, an important conclusion of this study is that negatively charged counter ions easily penetrate PAMAM dendrimers and reside therein.

The theoretical method used in this study is applicable to more complicated systems involving binding between metal ions and dendrimers. However, such an

investigation requires a detailed understanding about dendrimer protonation, and therefore the results described here will be very useful for future studies of metal-dendrimer equilibria.[8]

3.6. List of Symbols

α: fraction of the dendrimer volume occupied by the electrolyte solution

β_A': proton binding constant for an averaged binding site

β_w: auto-dissociation constant of water

$\bar{\delta}$: increase in binding free energy per unit bound charge, averaged over all the binding sites

ε_0: dielectric constant of the electrolyte solution

ε: dielectric constant of the dendrimer interior

$\varepsilon^{(mf)}$: nearest-neighbor pair-wise interaction parameter used by B&K

κ_0^{-1}: Debye length

B_0: concentration of the strong base (titrant) added

e: charge on an electron

f_0: arbitrary scaling factor

h_0: total number of binding sites

$\bar{h}$: average proton binding number per dendrimer

H_0: concentration of the strong acid added initially

[H]: equilibrium concentration of proton

I: ionic strength

k_B Boltzmann constant

L_0: total concentration for dendrimer ligand *L*

pK: logarithm of the intrinsic proton binding constant

Q: total bound charge per dendrimer molecule

q_λ : charges on each shell

r_{AVG}: average distance between the two terminal amine sites in a simple diamine molecule

T: absolute temperature

$\overline{w}$: slope of a plot of $\overline{\delta}$ versus $\overline{h}$

CHAPTER IV

PREPARATION OF DENDRIMER-ENCAPSULATED METAL NANOPARTICLES USING ORGANIC SOLVENTS

4.1. Synopsis

Preparation of dendrimer-encapsulated metal nanoparticles (DEMNs) within amphiphilic dendrimers in an organic solvent is reported. The important new result is that metal ion encapsulation is driven by solubility differences between the metal salt in solution and within the dendrimer interior. This contrasts with previous studies, which have relied on specific interactions between metal ions and ligands within the dendrimer interior to drive encapsulation. This new approach makes it possible to prepare relatively large DEMNs. Both Cu and Pd DEMNs have been prepared, and the latter are shown to be catalytically active for hydrogenation reactions.

4.2. Introduction

We wish to report a new method for preparing dendrimer-encapsulated metal nanoparticles (DEMNs). The significant new finding is that differences in metal-ion solubility between the solvent and the dendrimer interior can be used to drive metal ion encapsulation. Subsequent chemical reduction of the dendrimer/metal ion composite results in formation of DEMNs. This approach contrasts with our previously reported strategy for preparing DEMNs,[75] which relies on specific interactions between metal ions and intradendrimer functional groups for metal-ion encapsulation.[5,22] Because

reliance on specific metal/ligand interactions are relaxed, this new approach provides a means for increasing both the type and size of nanoparticles that can be encapsulated within dendrimers.

Dendrimers are polymers that can be highly monodisperse in size, shape, and chemical composition.[4,155,156] We[5,75] and others,[27-30,89] have shown that poly(amido amine) (PAMAM) and poly(propylene imine) (PPI) dendrimers can be used as templates for preparing nearly monodisperse intradendrimer metal nanoparticles using a "ship-in-a-bottle" approach: first the metal ions are loaded into the dendrimeric template, and then chemical reduction results in formation of DEMNs. Transition metal ions, such as Cu^{2+}, Pt^{2+}, Pd^{2+}, Au^{3+}, Ru^{3+}, and Ni^{2+}, partition into dendrimers from aqueous solutions and complex irreversibly with internal tertiary amine groups. Because the dendrimeric template can be monodisperse in structure, each dendrimer molecule contains about the same number of interior functional groups.[5,75] Accordingly, the same number of metal ions should reside in each dendrimer, and therefore the intradendrimer nanoparticles that result from reduction should all contain nearly the same number of atoms.

DEMNs are retained within the dendrimer host primarily by steric considerations, but chemical interactions between the dendrimer and metal particle are also probably important. We have previously shown that DEMNs can be rendered soluble in essentially any solvent by controlling the chemistry of their periphery,[5] that the dendrimeric host can impart selectivity to intrinsically nonselective encapsulated catalytic metal nanoparticles,[32,33] and that this same synthetic approach can be used to prepare dendrimer-encapsulated semiconductor quantum dots.[31]

Nanoparticles soluble in organic solvents can be synthesized by reduction of the corresponding ions in the presence of monomeric amphiphiles such as thiols,[108,109] micelles,[110] polymers,[112,157] or by ligand-exchange reactions.[158,159] Dendrimers can also be used to solubilize nanoparticles in nonaqueous solvents. For example, we recently demonstrated that metal particles within water-soluble, amine-terminated PAMAM dendrimers can be transported into an organic phase by addition of a fatty acid.[91] It is also possible to extract metal ions from an aqueous phase into a nonaqueous phase,[100] and then reduce the ions to zero-valent metal particles in the nonaqueous phase. Esumi *et al.*[101] were the first to use this approach by preparing Au dendrimer-encapsulated nanoparticles within PAMAM dendrimers carrying hydrophobic groups on their periphery. We later showed that this strategy could also be used to prepare fluorous-soluble DEMNs.[24] However, the extraction processes was slow and several washing and extraction iterations were required.

Esumi has also demonstrated that it is possible to completely avoid the extraction process and prepare Pt nanoparticles in the complete absence of water.[103] This was accomplished by reduction of $PtCl_6^-$ in ethyl acetate using dimethylamineborane in the presence of methyl ester-terminated PAMAM dendrimers. This is the approach followed in the present study. Specifically, we modified the periphery of amine-terminated PPI dendrimers with hexanoyl or palmitoyl groups to render them soluble in organic solvents. Next, Cu^{2+} was introduced into the dendrimer by mixing solutions containing $CuCl_2$ and the dendrimer in a $CHCl_3$-MeOH mixed solvent. Finally, DEMNs were obtained by reducing the dendrimer/Cu^{2+} composite with $NaBH_4$.

In prior studies it was demonstrated that Cu^{2+} does not complex with functional groups inside PPI dendrimers.[88,89] However, encapsulation of Cu^{2+} is a necessary condition for DEMN formation, and therefore we infer that in our case the metal ions are driven into the dendrimer by differential solubility.

4.3. Experimental

Materials. Poly(propylene imine) dendrimers were purchased from DSM (Geleen, The Netherlands) and were dried under vacuum in a Schlenk flask at 23 ± 2 ^{o}C to remove residual H_2O and low molecular weight impurities. Palmitoyl chloride, hexanoyl chloride, chloroform (HPLC grade), methanol (HPLC grade), deuterated chloroform, $CuCl_2$-$2H_2O$, $NaBH_4$, and 1-hexene were used as received from the Aldrich Chemical Co. (Milwaukee, WI). Dichloromethane was purchased from Aldrich and distilled over CaH_2 before used. Triethyl amine was dried over KOH prior to use. $Pd(CH_3CO_2)_2$ was purchased from Strem Chemicals, Inc. (Newburyport, MA) and used without further purification.

Characterization. ^{1}H and ^{13}C NMR spectra were recorded on a Unity p300 spectrometer at 300 MHz (75 MHz for ^{13}C). High-resolution transmission electron micrographs (HRTEM) were obtained with a JEOL-2010 TEM having a point-to-point resolution of 0.19 nm. Samples were prepared by placing a drop of solution on a holey-carbon-coated Au TEM grid and allowing the solvent to evaporate in air. Absorption spectra were recorded on a Hewlett-Packard HP 8453 UV-vis spectrometer. The optical

path length was 1.0 cm or 0.1 cm and the mixed solvent ($CHCl_3$-MeOH) was used as reference for all measurements.

Procedure for the Preparation of Hexanoyl or Palmitoyl-Modified Poly(propylene imine) Dendrimers. The procedure used to functionalize the periphery of PPI dendrimers was similar to that reported by Stevelmans *et al.*[160] and Liu *et al.*[161] with minor modifications. For example, a fifth-generation poly(propylene imine) dendrimer having 64 terminal amine groups (D64) was functionalized with palmitoyl (D64P64) as follows. To a solution of 44.9 mg of D64 under N_2 in 20 mL dry CH_2Cl_2, 2.5 mL triethylamine was added, followed by addition of 0.13 mL palmitoyl chloride (1.1 equiv. per terminal amino group). After stirring for 15 h at room temperature, the solvent was evaporated. The remaining solid was heated under reflux with 50 mL of diethyl ether for 30 min to remove the excess palmitoyl chloride. The mixture was then refluxed with saturated aqueous Na_2CO_3 for 6 h followed by extraction with CH_2Cl_2. The organic layer was separated and dried *in vacuo* at 23 ± 2 ^{o}C to yield a white/yellow solid. Characterization of this material was in accord with results reported by Stevelmans *et al*.[160] Similar procedures were used to prepare the other generations of palmitoyl-functionalized dendrimers (DnPn) and hexanoyl-functionalized dendrimers (DnHn). NMR results for DnHn are given below.

D16H16. ^{1}H NMR (300 MHz, $CDCl_3$): δ 0.84 (t, CH_3, 48H), 1.01-1.69(m, $CH_3(C\underline{H}_2)_3$, $NCH_2C\underline{H}_2CH_2N$, $NCH_2C\underline{H}_2C\underline{H}_2CH_2N$, $NCH_2C\underline{H}_2CH_2NHCO$, 156H), 2.14 (t, $NHCOC\underline{H}_2$, 32H), 2.34 (m, $NC\underline{H}_2CH_2CH_2C\underline{H}_2N$, $NC\underline{H}_2CH_2C\underline{H}_2N$, $C\underline{H}_2CH_2CH_2NHCO$, 84H), 3.22 (q, $C\underline{H}_2NHCO$, 32H), 7.16 (br, NHCO, 16H). ^{13}C NMR

(75 MHz, $CDCl_3$): δ 14.2, 22.6, 24.9, 25.8, 27.2, 29.9, 31.7, 36.8, 38.0, 51.7, 52.3, 54.4, 174.0.

D32H32. ^{1}H NMR (300 MHz, $CDCl_3$): δ 0.85 (t, CH_3, 96H), 1.16-1.68 (m, $CH_3(C\underline{H}_2)_3$, $NCH_2C\underline{H}_2CH_2N$, $NCH_2C\underline{H}_2C\underline{H}_2CH_2N$, $NCH_2C\underline{H}_2CH_2NHCO$, 316H), 2.15 (t, $NHCOC\underline{H}_2$, 64H), 2.35 (m, $NC\underline{H}_2CH_2CH_2C\underline{H}_2N$, $NC\underline{H}_2CH_2C\underline{H}_2N$, $NC\underline{H}_2CH_2CH_2NHCO$, 180H), 3.22 (q, $C\underline{H}_2NHCO$, 64H), 7.34 (br, NHCO, 32H). ^{13}C NMR (75 MHz, $CDCl_3$): δ 14.2, 22.7, 24.9, 25.8, 27.3, 29.8, 31.8, 36.8, 38.0, 51.7, 52.4, 174.0.

D64H64. ^{1}H NMR (300 MHz, $CDCl_3$): δ 0.86(t, CH_3, 192H), 1.19-1.70 (m, $CH_3(C\underline{H}_2)_3$, $NCH_2C\underline{H}_2CH_2N$, $NCH_2C\underline{H}_2C\underline{H}_2CH_2N$, $NCH_2C\underline{H}_2CH_2NHCO$, 444H), 2.17 (t, $NHCOC\underline{H}_2$, 128H), 2.37 (m, $NC\underline{H}_2CH_2CH_2C\underline{H}_2N$, $NC\underline{H}_2CH_2C\underline{H}_2N$, $NC\underline{H}_2CH_2CH_2NHCO$, 372H), 3.23 (q, $C\underline{H}_2NHCO$, 128H),7.55 (br, NHCO, 64H). ^{13}C NMR (75 MHz, $CDCl_3$): δ 14.2, 22.6, 24.9, 25.8, 27.2, 29.8, 31.7, 36.8, 38.0, 51.7, 52.3, 174.0.

Procedure for UV-vis Titration of Hexanoyl- or Palmitoyl-Modified PPI Dendrimers with $CuCl_2$. UV-vis titrations of the modified dendrimers with Cu^{2+} were carried out to assess the average maximum number of Cu^{2+} ions that can be encapsulated within each dendrimer generation. The titration of D32P32(Cu^{2+}) in $CHCl_3$:MeOH (4:1, v/v) is described as an example. 1 mL of 1×10^{-4} M D32P32 dendrimer $CHCl_3$ solution was prepared from dry D32P32 and added to a cuvette (optical path = 1 cm) with a cap on the top and a stirring bar at the bottom. 0.6 mL $CHCl_3$ and 0.4 mL of MeOH was then added and mixed well to make the $CHCl_3$:MeOH (4:1, v/v) mixed solvent. 40 mM

$CuCl_2$ in $CHCl_3$:MeOH (4:1, v/v) was added to the stirred dendrimer solution within the cuvette using a micropipette. After addition of an aliquot of the Cu^{2+} solution, the cap was placed on the cuvette to prevent solvent evaporation and then a UV-vis absorption spectrum was obtained.

Preparation of dendrimer/Cu^{2+} Complexes and Cu DEMNs. These procedures are described using D32P32(Cu_{40}) in $CHCl_3$:MeOH (4:1, v/v) as an example. A reaction vial containing a stirring bar was filled with 1 mL of a 1×10^{-4} M DnPn $CHCl_3$ solution. 0.6 mL CHCl3 and 0.4 mL of MeOH was then added and mixed well to make the $CHCl_3$:MeOH (4:1, v/v) mixed solvent. 100 μL of 40 mM $CuCl_2$ in $CHCl_3$:MeOH (4:1, v/v) was added to the stirred reaction vial and a yellow solution was obtained. 20 equiv. (mol) $NaBH_4$ in $CHCl_3$:MeOH (4:1, v/v) was dissolved in 80 μL MeOH followed by addition of 320 μL $CHCl_3$. This solution was then added to the stirred vial to reduce Cu^{2+} to Cu^0. The color of the solution turned to golden brown. A cap was placed on the container to prevent solvent evaporation. The color of the solution slowly turned yellow in the presence of atmospheric O_2, but when O_2 was excluded it remained golden brown.

Preparation of Dendrimer/Pd^{2+} Complexes and Pd DEMNs. These procedures are described using preparation of D32P32(Pd^{2+})$_{20}$ and D32P32(Pd)$_{20}$ as an example. 300 μL of a 1×10^{-4} M D32P32 solution in $CHCl_3$:MeOH (2:1, v/v) was placed in a reaction vial. 1640 μL $CHCl_3$ and 955 μL of MeOH was then added and mixed well to make the $CHCl_3$:MeOH (2:1, v/v) mixed solvent. With vigorous stirring, 15 μL of 40 mM $Pd(OAc)_2$ in MeOH was added. A cap was placed on top of the vial to

prevent solvent evaporation. After stirring for 30 min, 20 equiv. of $NaBH_4$ in $CHCl_3$:MeOH (2:1, v/v) were added dropwise to the vial to yield golden brown $D32P32(Pd)_{20}$.

Hydrogenation Reactions. The hydrogenation apparatus was the same as that described in reference 33. To a 25 mL Schlenk flask, 300 μL of a 1×10^{-4} M D32P32 solution in $CHCl_3$:MeOH (2:1, v/v), 1640 μL $CHCl_3$, and 955 μL of MeOH were added and mixed well followed by 15 μL of 40 mM $Pd(OAc)_2$ in MeOH under vigorous stirring. A light yellow solution was obtained immediately. After stirring for 30 min, 90 μL of a 133 mM $NaBH_4$ $CHCl_3$:MeOH (2:1, v/v) solution was added, which changed the color of the solution to golden brown. All the joints of the apparatus were sealed with silicone grease and checked for leaks before adding the substrate. The system was purged with H_2 for 15 min with continuous addition of $CHCl_3$:MeOH (2:1, v/v) to maintain the volume. To verify that H_2 was not consumed in the absence of substrate, the catalyst was stirred in solution over a known volume of H_2. The H_2 volume did not change over a period of hours. Experiments were carried out by adding 0.6 mmol of 1-hexene by syringe under vigorous stirring conditions. The rate of stirring was maintained high and constant throughout all hydrogenation reactions.

4.4. Results and Dicussion

General Approach. We[5,75] and others[27-30] have previously shown that reduction of metal ions specifically coordinated to ligand sites within dendrimers present in aqueous solutions leads to formation of dendrimer-encapsulated metal nanoparticles.[5,22]

While this synthetic approach is broadly applicable, we sought to further generalize it. The approach is to use solubility differences between the solvent and the dendrimer interior to drive the encapsulation process, rather than relying exclusively on fixed stoichiometries between metal ions and ligands. This new approach eliminates the size limitation imposed on DEMNs by the finite number of ligand sites within dendrimers. We wish to emphasize that Esumi *et al.* have previously used methyl ester-terminated dendrimers to prepare Pt DEMNs using ethyl acetate as the solvent. However, the role played by differential solubility was not examined in that study.[103]

To test this new synthetic approach we synthesized and characterized hydrophobic PPI dendrimers terminated on their periphery with both palmitoyl (C16) (DnPn, n = 16, 32, and 64) and hexanoyl (C6) (DnHn, n = 16, 32, 64) functional groups.[160,161] Longer (C16) and shorter (C6) alkyl chain-lengths were used to determine if the hydrocarbon periphery plays a role in controlling nanoparticle size. $CHCl_3$-MeOH is a miscible mixed-solvent system in which both dendrimers and metals ions are soluble. This is a convenience that avoids the extra step of a biphasic extraction of the metal into the dendrimers. This mixed solvent also makes it possible to use $CuCl_2$ rather than more hydrophobic salts, such as $Cu(OAc)_2$, which have less desirable spectroscopic properties.[162]

Dendrimer-Encapsulated Cu Nanoparticles. Encapsulated Cu nanoparticles were synthesized by first sorbing Cu^{2+} into the dendrimer interior and then chemically reducing the resulting nanocomposite.[5,75] To characterize each stage of the synthesis leading up to formation of the DEMNs we monitored the relevant solutions by UV-vis

absorption spectroscopy (Figure 4.1). In the absence of Cu^{2+}, dendrimer D32P32 does not absorb light in the range of 350-1000 nm, while Cu^{2+} alone in the mixed solvent reveals a broad absorption centered around 900 nm and corresponding to the d-d transition of Cu^{2+}. In the presence of both Cu^{2+} and D32P32 ($[Cu^{2+}]/[D32P32] = 40$) the solution turns yellow, the absorption onset shifts to 835 nm, and the extinction coefficient at 835 nm increases by 40% (spectrum c, Figure 4.1). In contrast, aqueous or methanolic solutions of dendrimer/Cu^{2+} nanocomposites are usually blue and exhibit a d-d transition around 600 nm[75] or 620 nm.[88]

$NaBH_4$ is not very soluble in $CHCl_3$. However, by first dissolving $NaBH_4$ in MeOH and then adding $CHCl_3$, it is possible to prepare a 200 mM solution of $NaBH_4$ in $CHCl_3$:MeOH (4:1, v/v). Upon the addition of $NaBH_4$, the dendrimer-containing solution turns brown and the discrete d-d transition resulting from Cu^{2+} is replaced by a monotonically increasing absorption to shorter wavelength (spectrum d, Figure 4.1). This indicates conversion of Cu^{2+} into zerovalent Cu nanoparticles.[126] When the same experiment is carried out in the absence of dendrimer, Cu^0 precipitates as soon as $NaBH_4$ is introduced. This indicates stabilization of the nanoparticle by the hydrophobic dendrimer. If the D32P32-encapsulated Cu^0 composite is exposed to atmospheric O_2 for 4 h, then the Cu^0 nanoparticles start to reoxidize and the solution changes in color from golden brown back to yellow. This reduction-oxidation cycle can be repeated many times.

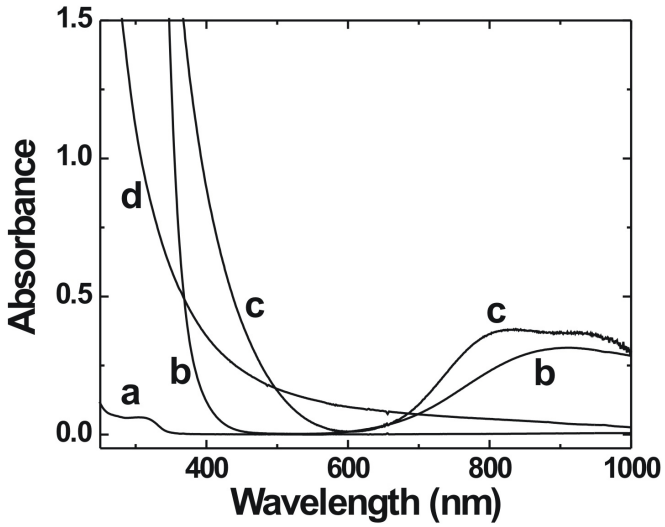

Figure 4.1. Absorption spectra of $CHCl_3$:MeOH (4:1, v/v) solutions containing: (a) 0.050 mM D32P32; (b) 2 mM $CuCl_2$; (c) 0.050 mM D32P32 and 2.0 mM $CuCl_2$; (d) D32P32(Cu_{40}). The optical path length was 1 cm, and temperature was 25 ± 2°C.

Determination of the maximum Cu^{2+} loading of DnPn dendrimers. Figure 4.2 shows the results of a titration of D32P32 dendrimers with a 40 mM $CuCl_2$ solution in $CHCl_3$:MeOH (4:1, v/v). The titrations were carried out by mixing discreet ratios of DnPn with Cu^{2+}, adjusting the total volume of the solution, and measuring the absorbance at λ_{max} = 835 nm. We have previously shown that titrations carried out in this way using hydroxyl-terminated PAMAM dendrimers lead to plots having two distinct linear regions.[75] We previously associated the point defined by extrapolation of these two linear regions as an estimate of the maximum number of Cu^{2+} ions residing within the dendrimers. In the present case, this analysis suggests maximum ratios of $[Cu^{2+}]/[DnPn]$ of 20 ± 2, 40 ± 3, and 75 ± 3 for D16P16, D32P32, and D64P64, respectively. The initial slope of the titrations shown in Figure 4.2 indicate that the extinction coefficients for Cu^{2+} complexed with DnPn is $\varepsilon_1 \sim 180\ M^{-1}\ cm^{-1}$. The slope after the threshold ($\varepsilon_2 \sim 90\ M^{-1}\ cm^{-1}$) is significantly smaller. The titrations were terminated at a ratio of Cu^{2+} to dendrimer about twice that of the threshold value, because in preliminary studies no further change in slope was observed.

The threshold numbers determined here are substantially higher than the corresponding maximum complexation numbers for both PPI/Cu^{2+} and PAMAM/Cu^{2+} composites, which arise exclusively from specific interactions between N ligands and Cu^{2+} in methanolic or aqueous solutions, respectively.[75,88,89] In the PPI/Cu^{2+} case, Bosman *et al.*[88] and Floriano *et al.*[89] demonstrated that Cu^{2+} only coordinates with peripheral primary amines and the outermost tertiary amines but not interior tertiary amines. In our experiment, after functionalization of the surface of PPI dendrimer with

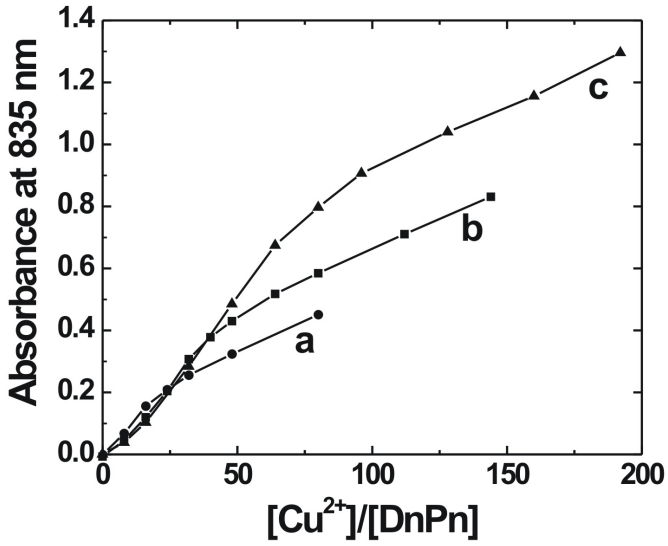

Figure 4.2. Spectrophotometric titration curves recorded at λ_{max} = 835 nm for differe ratios of [Cu^{2+}] and [DnPn] for (a) D16P16, (b) D32P32 and (c) D64P64. The initial concentration of each dendrimer was 0.050 mM. The optical path length was 1 cm, the temperature was 25 ± 2°C, and the solvent was $CHCl_3$:MeOH (4:1, v/v).

alkyl groups, there are only two types of nitrogens present: interior tertiary amines and amides. Accordingly, it doesn't seem likely that strong, specific interactions between Cu^{2+} and interior ligands are responsible for encapsulation. However, to test the importance of interactions between amides and Cu^{2+}, N,N'-hexamethylenebisacetamide was mixed with Cu^{2+} in $CHCl_3$:MeOH. No shift in λ_{max} was observed and addition of $NaBH_4$ caused immediate precipitation, which indicates little or no coordination of Cu^{2+} with the amide ligand. Additionally, the titration threshold numbers (D16P16: 20 ± 2, D32P32: 40 ± 3, and D64P64: 75 ± 5) are significantly larger than the number of tertiary amines within these dendrimers (14, 30, and 62, respectively). Finally, we have previously shown that coordination between Cu^{2+} and tertiary amines in PAMAM dendrimers is actually substoichiometric ($[Cu^{2+}]$/[tertiary amines] = 0.25 for hydroxyl-terminated G4 PAMAM dendrimers). On the basis of these arguments, we conclude that the high concentration of Cu^{2+} associated with DnPn dendrimers is primarily due to differential solubility of the metal ion in the dendrimer interior versus in the solvent.

A control experiment showed that in the absence of dendrimer, the extinction coefficient of $CuCl_2$ in $CHCl_3$:MeOH (4:1, v/v) ($\varepsilon \sim 130\ M^{-1}\ cm^{-1}$) is much larger than ε_2. That is, after the threshold is attained for Cu^{2+} encapsulation in DnPn, the excess metal does not exist as free Cu^{2+}. We also observed that the value of ε_2 is independent of dendrimer generation. We conclude that prior to the encapsulation threshold Cu^{2+} is strongly associated with the dendrimer and after the threshold it is still associated, but more weakly so. This difference in the association constants accounts for the difference in the numerical values of ε_1 and ε_2. This conclusion is supported by the finding that

reduction of solutions in which the $[Cu^{2+}]$/[DnPn] ratio is less than the threshold value results in soluble DEMNs, while ratios exceeding the threshold lead to immediate metal precipitation.

Similar experiments employing DnHn dendrimers yield nearly identical results. That is, the extinction coefficients for Cu^{2+} complexed with DnHn before the threshold is ~ 170 M^{-1} cm^{-1}, and the slope after the threshold is ~ 90 M^{-1} cm^{-1}. This indicates that the length of the alkyl chain (> 6 carbon atoms) appended to the periphery of PPI dendrimers does not substantially influence encapsulation of Cu^{2+}.

Although the exact nature and location of the loosely associated Cu^{2+} is unknown at this time, it is clear that a relatively large amount of Cu^{2+} is driven into the dendrimer by differential solubility below the threshold value and that it can be reduced to yield stable DEMNs.[27-30,89] Because of the aforementioned air oxidation of Cu, and because of their poor contrast in TEM, it was not possible to obtain good images of Cu DEMNs.

Dendrimer-encapsulated Pd nanoparticles can be synthesized using the approach just described for Cu DEMNs. These experiments were carried out by adding $Pd(OAc)_2$ to a $CHCl_3$:MeOH (2:1, v/v) solution of DnPn. Here, $CHCl_3$:MeOH (2:1, v/v) was used as the solvent, because a Pd precipitate was obtained when $NaBH_4$ was added to the D32P32/Pd^{2+} complex in 4:1 $CHCl_3$:MeOH. Prior to reduction this solution was yellow, but a clear golden brown solution was obtained following reduction by $NaBH_4$. The absorption spectra of D32P32$(Pd^{2+})_{20}$ and D32P32(Pd_{20}) (Figure 4.3) are consistent with formation of Pd DEMNs.[32] XPS analysis of the Pd DEMNs confirms the presence of Pd^0 (Figure 4.4). The Pd DEMNs were analyzed by HRTEM and found to have a size of

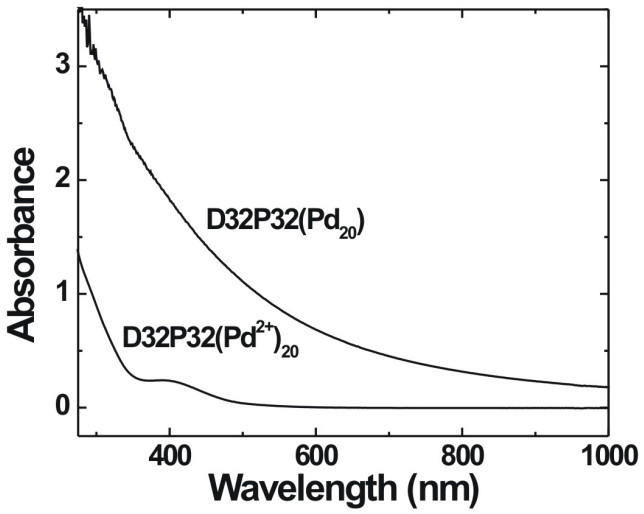

Figure 4.3. Absorption spectra of $CHCl_3$:MeOH (2:1, v/v) solutions of 5 x 10^{-5} M D32P32$(Pd^{2+})_{20}$ and D32P32(Pd_{20}). The optical path length was 0.1 cm, and temperature was 25 ± 2°C.

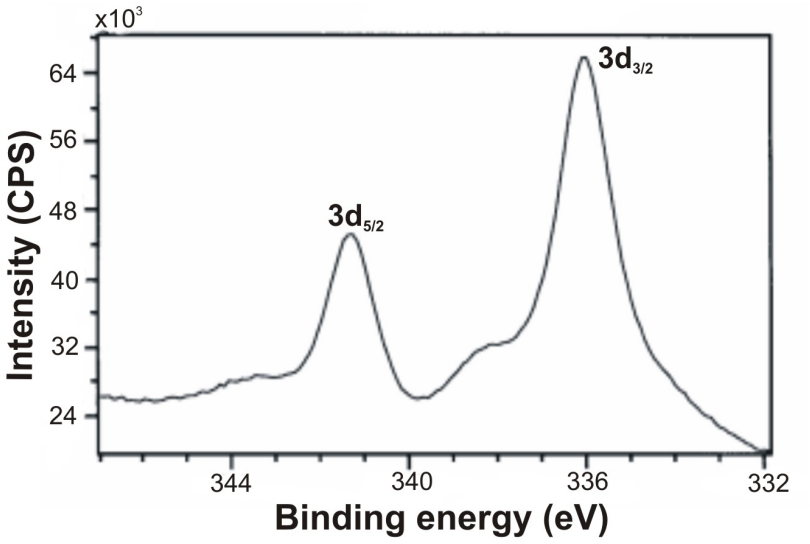

Figure 4.4. XPS spectrum of D32P32(Pd_{20}).

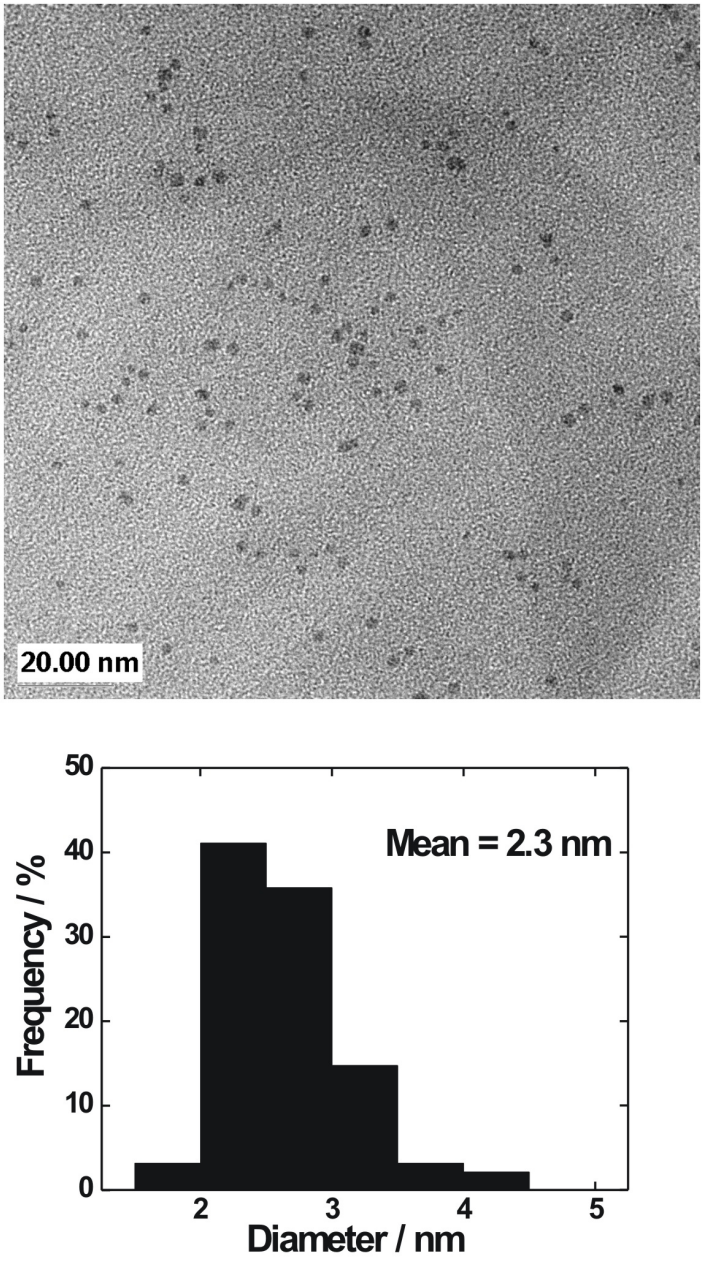

Figure 4.5. TEM images and particle size distributions of the D32P32(Pd_{20}).

2.3 ± 0.2 nm (Figure 4.5). Currently we don't understand why the sizes of these particles are larger than the value calculated for a 20–atom crystal (0.9 nm).[163] However, our group[5,26,32,33] and others[89,94] have previously observed larger-than-anticipated particle sizes for certain combinations of dendrimers and metals. We believe this difference may result from particles having complex shapes that are most easily accommodated by the restricted interior dendrimer volume.

Because these dendrimer-encapsulated Pd nanoparticles are hydrophobic, they can be used for catalysis in organic solvents. For example, the rate of hydrogenation for 1-hexene in the presence of the D32P32(Pd_{20}) catalyst was determined by H_2 uptake.[33] The initial turnover frequencies in $CHCl_3$:MeOH (2:1, v/v) for this substrate was 120 mol H_2(mol Pd)$^{-1}$ h^{-1}. This rate is about the same as that reported for polymer-supported Pd^0 catalysts.[164] However, in contrast to PAMAM-based DEMNs, the modified PPI dendrimer-encapsulated Pd nanoparticles are only stable for about 20 min under hydrogenation conditions.[26,32,33] The underlying reason for the poor stability is not understood at this time.

4.5. Summary and Conclusions

The important result of this study is that solubility differences between metal ions in solution and within dendrimers can be used to drive encapsulation. Although the dielectric constant of dendrimer interiors has not been definitively measured, we estimate the value is somewhat less than 23.[165] The estimated dielectric constant of the

mixed solvent systems is 10.[166] It is this difference in dielectric constant that we believe to be responsible for metal ion encapsulation under the conditions used in this study.

This approach complements our previous discovery that functional groups within dendrimers can be used as a metal-ion template for the formation of DEMNs.[5,75] The results of this study indicate that the main function of the alkyl groups on the modified PPI dendrimers is simply to solubilize the dendrimer. However, they may also weakly associate with the metal ions in a way that we do not understand at this time. This method is sufficiently versatile that both Pd and Cu DEMNs can be synthesized. Pd DEMNs prepared using this method are catalytically active, but they are far less stable than DEMNs prepared by other routes.

CHAPTER V

SIZE-SELECTIVE HYDROGENATION OF OLEFINS BY DENDRIMER-ENCAPSULATED PALLADIUM NANOPARTICLES*

5.1. Synopsis*

Nearly monodisperse (1.7 ± 0.2 nm) palladium nanoparticles were prepared within the interiors of three different generations of hydroxyl-terminated poly(amidoamine) (PAMAM) dendrimers. These dendrimer-encapsulated catalysts (DECs) were used to hydrogenate allyl alcohol and four α-substituted derivatives in a 4:1 methanol/water mixture. The results indicate that steric crowding on the dendrimer periphery, which increases with dendrimer generation or surface sterics, can act as an adjustable-mesh nanofilter. That is, by controlling the packing density on the dendrimer periphery, it is possible to control access of substrates to the encapsulated catalytic nanoparticle. In general, higher generation DECs or larger substrates resulted in lower turn-over frequencies (although some interesting exceptions were noted). Although the main products of the olefin hydrogenation reactions were the corresponding alkanes, ketones were also obtained when monosubstituted α-olefins were used as substrates. NMR spectroscopy was used to measure the size selectivity of DECs for the competitive hydrogenation of allyl alcohol and 3-methyl-1-penten-3-ol. The effect on catalytic rate as a function of nanoparticle size is also briefly discussed.

---

*Reprinted with permission from Niu, Y.; Yeung, L. K.; Crooks, R. M. *J. Am. Chem. Soc.* **2001**, 120, 6480-6468: copyright 2001 American Chemical Society.

5.2 Introduction

In this chapter we show that dendrimer-encapsulated catalysts (DECs), consisting of Pd nanoparticles contained within poly(amidoamine) (PAMAM) dendrimers,[5] are highly selective catalysts for hydrogenation reactions.[32] Specifically, we have examined the catalytic activity of a series of DECs towards hydrogenation of allyl alcohol and four α-substituted derivatives having different sizes and shapes. The interesting result is that by controlling the steric crowding on the dendrimer periphery it is possible to selectively control access of substrates to the encapsulated metal particle. Because selectivity is induced by the dendrimer, rather than by the intrinsically non-selective Pd catalyst, this approach should be generally applicable to any reaction that involves a catalyst that can be placed within the interior of a dendrimer or related nanoporous materials.

We have previously shown that metal[23-26,32] and semiconductor[31] nanoparticles of nearly monodisperse size can be prepared within dendritic hosts. These composite materials are easily prepared by mixing together solutions containing dendrimers and metal ions such as Pt^{2+}, Pd^{2+}, Au^{3+}, Cu^{2+}, Ni^{2+}.[5,28] In favorable cases the metal ions partition into the dendrimer where they are strongly complexed by interior tertiary amine groups. Subsequent chemical reduction of the dendrimer/metal ion composite yields a zero-valent metal nanoparticle that remains sterically trapped within the dendrimer. Because the dendrimers are nearly monodisperse in size and chemical composition they contain a nearly monodisperse number of interior tertiary amine groups. Because the maximum metal ion/dendrimer ratio is fixed for a particular metal ion, it follows that the maximum number of metal ions sorbed into the dendrimer is also nearly monodisperse

and that the resulting nanoparticles are, likewise, of similar size. That is, the nanoparticle replica is a good representation of the dendritic template from which it is prepared.

Dendrimers have been shown to be effective for enabling chemical separations based on the size, shape, and charge of the dendrimer or the species being separated, and they have also been used as stationary phases and additives for various liquid-phase separation methods such as capillary electrophoresis.[167,168] Composite materials having dendrimers incorporated into the structure have also been used to prepare selectively permeable electrode coatings,[169,170] xerogels,[171] and organic membranes for gas separations.[172] All of these separation processes are based on interactions between dendrimers and the much smaller analyte molecules. There are two classes of interactions between dendrimers and smaller molecules: those involving physical interactions, such as size and shape, and those involving electronic interactions, such as surface charge and polarity. For example, Meijer *et al*. demonstrated that dendrimers could selectively encapsulate analyte molecules based on shape.[61,62] Similarly, we have shown that by controlling the pH of a solution dendrimers can act as molecular-gates, admitting molecules based on overall charge.[32,169,170]

The selective nature of dendrimers can also be applied to problems in catalysis. Specifically, we envision that dendrimers encapsulating catalysts may act as selective gates that control the access of small molecules to the embedded catalytic moiety. In this regard, it is productive to think of the dendrimer as a nanofilter having a mesh that can be controlled by chemically altering the periphery. Indeed, others have previously

recognized that dendritic structures have the potential to function as selective moieties in catalytic processes. For example, dendrons grafted onto metalloporphyrins were shown to be selective for different-shaped ligands[173] as well as for epoxidation substrates.[174,175] Dendrimers containing metal ion cores and dendritic ligands have also been shown to affect both selectivity and reactivity for Ru(II)-catalyzed asymmetric hydrogenation[176] and Cu(II)-catalyzed Diels-Alder reactions.[177] These catalysts were composed of a catalytically active species surrounded by a dendritic shell designed to regulate both substrate selectivity and overall catalytic reactivity.

There are two characteristics of DECs that make them particularly attractive. First, solubility is controlled principally by the chemical composition of the dendrimer periphery.[5] Second, because the encapsulated particles are very small (typically 1-3 nm),[5] they have a high surface-area-to-volume ratio, which is important for high efficiency.[106,178] We have taken advantage of these properties to show that DECs are effective for the reduction of olefins in aqueous,[26,32] organic,[91] and fluorous[99] solvents. Additionally, synthetically more useful carbon-carbon bond forming reactions have been catalyzed by Pd(0) nanoparticles encapsulated in modified poly(propylene imine) (PPI) dendrimers in both hydrocarbon/fluorocarbon[24] and supercritical CO_2 solvent[23] systems.

Although some data in our previous reports suggested high levels of selectivity for either a particular substrate or a particular product,[5] no detailed study correlating dendrimer size and structure to a catalytic process has thus far been reported. Accordingly, this report is the first quantitative study correlating DEC structure to catalytic rate. Specifically, the catalytic efficiency of dendrimer encapsulated Pd

nanoparticles towards reduction of the double bond in differently shaped allylic alcohols (**1-5**) is reported. Three generations of PAMAM dendrimers were used as the template, while the size of the catalytic nanoparticle was kept constant by controlling the amount of Pd(II) salt used in the synthesis. The results show that the activity of DECs can be controlled by varying the generation of the dendrimer and that differently sized substrates have pronounced effects on the turn-over frequency (TOF) for a given catalytic reaction.

5.3. Experimental

Materials. Hydroxyl-terminated fourth-, sixth-, and eighth-generation (G4-OH, G6-OH, and G8-OH, respectively) poly(amidoamine) (PAMAM) dendrimers having an ethylenediamine core were obtained as 10-25% methanol solutions (Dendritech, Inc., Midland, MI). Prior to use, the methanol was removed under vacuum at room temperature. The unsaturated alcohols, methanol, deuterated solvents, and $NaBH_4$ were used as received from the Aldrich Chemical Co. (Milwaukee, WI). K_2PdCl_4 was purchased from Strem Chemicals, Inc. (Newburyport, MA) and used without further purification. 18 MΩ·cm Milli-Q water (Millipore, Bedford, MA) was used to prepare aqueous solutions. Cellulose dialysis sacks having a molecular weight cut-off of 12,000 were purchased from Sigma Diagnostics, Inc. (St. Louis, MO).

Instrumentation. ^{1}H and ^{13}C NMR spectra were recorded on a Unity p300 spectrometer at 300 MHz (75 MHz for ^{13}C). High-resolution transmission electron micrographs (HRTEM) were obtained with a JEOL-2010 transmission electron

microscope having a point-to-point resolution of 0.19 nm. Samples were prepared by placing a drop of solution on a holey-carbon-coated Cu TEM grid and allowing the solvent to evaporate in air. GC data were recorded on a HP 5890 GC system, equipped with J&W DB-FFAP columns (30 m length, 0.32 mm I.D., 0.25 μm film, column head pressure 14 psi) and a flame ionization detector. Helium was used as the carrier gas. The initial temperature was set at 32 ^{o}C and increased at a rate of 10 ^{o}C/min.

Preparation of Gn-OH/Pd(0) Catalysts. A 5×10^{-3} M aqueous solution of Gn-OH (n = 4, 6, 8) PAMAM dendrimer was prepared from dry Gn-OH. The Gn-OH/$Pd(II)_{40}$ complex was prepared by adding 50 μL of the Gn-OH solution into 9.75 mL of purified water, followed by 100 μL of a 0.1 M K_2PdCl_4 (aq) solution (40 eq) under vigorous stirring. A light yellow solution was obtained immediately. After stirring for 30 min, 100 μL of a 1 M $NaBH_4$ (aq) solution was added, which changed the color of the solution to golden brown. The solution was purified by overnight dialysis against water. 40 mL of methanol was then added to the solution to prepare the catalytic solution.

Hydrogenation Apparatus. Hydrogenation reactions were carried out in a 150 mL round-bottomed Schlenk flask with an adapter connected to the top of a buret filled with hydrogen gas. A three-way stopcock was used with one arm attached to a hydrogen gas cylinder, the second to the gas buret, and the third to the reaction flask. A dibutyl phthalate-filled reservoir was connected to the bottom of the buret and open to the atmosphere at the top. All the hydrogenation reactions were run at atmospheric pressure and room temperature (25 ± 2°C).

Hydrogenation Reactions. 50 mL of the catalytic solution and a magnetic stir bar were placed in a Schlenk flask. All the joints of the apparatus were sealed with silicone grease and checked for leaks before adding the substrate. The system was purged with H_2 for 15 min. To verify that H_2 was not consumed in the absence of substrate, the catalyst was stirred in solution over a known volume of H_2. The H_2 volume did not change over a period of hours. Experiments were carried out by adding 10 mmol of substrate by syringe under vigorous stirring conditions. The rate of stirring was maintained high and constant throughout all hydrogenation reactions. There was no evidence for Pd^0 aggregation during or after hydrogenation of the substrates in the MeOH-H_2O solvent system, indicating that the catalysts are stable on the time scale of the reactions.

NMR Characterization of Hydrogenation Reaction Products. The products of the hydrogenation reactions were identified by ^{1}H NMR by performing the catalytic reactions in deuterated solvents. When more than one product was observed ^{13}C NMR spectra were also obtained. The procedure was the same for all substrates and is illustrated using allyl alcohol as an example. 10 μL of a 5×10^{-4} M G4-OH aqueous solution was added to 170 μL of D_2O in a reaction vial, followed by 2 μL of 0.1 M K_2PdCl_4 (0.2 μmol) under vigorous stirring for 30 min. 1 mg of $NaBH_4$ (26 μmol) was then added with stirring. After 30 min, 682 μL of CD_3OD was added ($CD_3OD/D_2O = 4$) to aid in solubilizing the substrate, and then 136 μL of allyl alcohol (2.0 mmol) was added. A ^{1}H NMR spectrum of this solution was obtained just prior to the hydrogenation reaction. The hydrogenation reaction was then performed in a reaction

vial using the previously described apparatus. After 24 h the reaction mixture was analyzed by ^{1}H NMR to identify the reaction product(s) (48 h after hydrogenation of substrates **4** and **5**).

n-propanol (**1a**). ^{1}H NMR: δ 1.06 (t, CH_3, 3H), 1.69 (m, CH_2, 2H), 3.66 (t, CH_2, 2H), 4.81 (b, OH, 1H).

2-butanol (**2a**) and ethyl methyl ketone (**2b**) mixture. ^{1}H NMR: δ 0.90 (t, CH_3, 3H), 1.01 (t, CH_3, 3H), 1.14 (d, CH_3, 3H), 1.45 (m, CH_2, 2H), 2.16 (s, CH_3, 3H), 2.53 (q, CH_2, 2H), 3.66 (m, CH, 1H), 4.86 (b, OH, 1H); ^{13}C NMR: δ 8.56, 10.56, 22.97, 29.76, 32.72, 37.64, 70.13, 214.70.

3-pentanol (**3a**) and diethyl ketone (**3b**) mixture. ^{1}H NMR: δ 0.92 (t, CH_3, 6H), 1.02 (t, CH_3, 3H), 1.45 (m, CH_2, 4H), 2.49 (q, CH_2, 4H), 3.39 (m, CH, 1H), 4.63 (b, OH, 1H); ^{13}C NMR: δ 8.44, 10.56, 30.36, 36.32, 75.36, 216.55.

2-methyl-2-butanol (**4a**). ^{1}H NMR: δ 0.90 (t, CH_3, 3H), 1.17 (s, CH_3, 6H), 1.49 (q, CH_2, 2H), 4.65 (b, OH, 1H).

3-methyl-3-pentanol (**5a**). ^{1}H NMR: δ 0.88 (t, CH_3, 6H), 1.10 (s, CH_3, 3H), 1.47 (q, CH_2, 4H), 4.76 (b, OH, 1H).

NMR Study of G4-OH Substrate Selectivity. 10 μL of a 5×10^{-4} M aqueous solution of G4-OH was added to 149 μL of D_2O in a reaction vial followed by 4 μL of 0.05 M K_2PdCl_4 (0.2 μmol) under vigorous stirring for 30 min. 1 mg of $NaBH_4$ (26 μmol) was then added with stirring. After 30 min, 650 μL CD_3OD was added (CD_3OD/D_2O = 4) followed by 68 μL of allyl alcohol (**1**) (1.0 mmol) and 120 μL of 3-

methyl-1-penten-3-ol (**5**) (1.0 mmol). A ^{1}H NMR spectrum of this reaction mixture was obtained just prior to the treatment with hydrogen. The hydrogenation reaction was then carried out using the previously described apparatus. ^{1}H NMR spectra were obtained after 2.5, 5.0, 20, and 42 h to determine the product distribution.

Molecular Modeling. Molecular models were created using the Cerius^2 (version 4.0) software package (Molecular Simulations, Inc., San Diego, CA). The free volume and dimensions of the substrates (**1**-**5**) were measured based on their optimized structures obtained using MOPAC calculations.

Transmission Electron Microscopy (TEM). Carbon-coated gold grids (400 mesh) were treated for 25s in a glow-discharge chamber in partial vacuum to impart hydrophilic character to the carbon substrate. Specimens were prepared by depositing the sample solutions on the grid and allowed to dry in air. TEM images were taken at 200 kV with JOEL 2010 at a magnification of 200,000x. For statining TEM, 2% mass fraction of phosphotungstic acid was prepared in H_2O and a filtration was applied to remove any residue. Stained specimens were prepared by depositing the sample solutions on the grid and floating the grip on a drop of staining solution. The grid was then blotted on filter paper and air-dried. TEM image was then obtained at 100 kV with JOEL 2010 at a magnification of 40,000x.

5.4. Results and Dicussion

We previously showed that hydroxyl-terminated PAMAM dendrimers (Gn-OH) can be used as templates for the encapsulation of Pd^0 and Pt^0 nanoparticles in aqueous

solution.[26,32] The size of the entrapped metal nanoparticles can be controlled either by using different dendrimer generations and/or manipulating the dendrimer/metal-ion ratio.[26,32,75] For the present study, we are interested in probing the extent of substrate selectivity imparted to the DEC by the surrounding dendrimer "nanofilter". The hypothesis is that dendrimer generation can be used to select substrates based on their size, because higher generation dendrimers have more crowded surfaces which limit access of the substrate to the encapsulated nanoparticle (Figure 5.1). To test this hypothesis, we prepared dendrimer-encapsulated nanoparticles containing an average of 40 Pd atoms within the interior of Gn-OH dendrimers (n = 4, 6, 8, where n corresponds to different PAMAM generations). This results in a homologous series of DECs in which only the porosity of the dendrimer and their diameter vary. The hydrogenation rates of chemically similar, but structurally different, olefins were then measured to test the aforementioned hypothesis. A decrease in turnover frequency (TOF) is anticipated as the substrate size increases (Figure 5.1).

Because allyl alcohol (**1**) is the simplest unsaturated alcohol and was used as a substrate in a prior study,[32] it was a natural starting point for this work. The following structurally related materials were also studied: 3-buten-2-ol (**2**), 1-penten-3-ol (**3**), 2-methyl-3-buten-2-ol (**4**), and 3-methyl-1-penten-3-ol (**5**). Because hydrogenation of C3-C6 unsaturated alcohols with Pd/C catalyst showed no significant difference in reaction rate at room temperature and atmospheric pressure,[26] the chemical structural effect by these substrates on the catalytic rate by DEC can be neglect. The structures of all five substrates are provided in Table 5.1. Because the solubility of substituted alcohols in

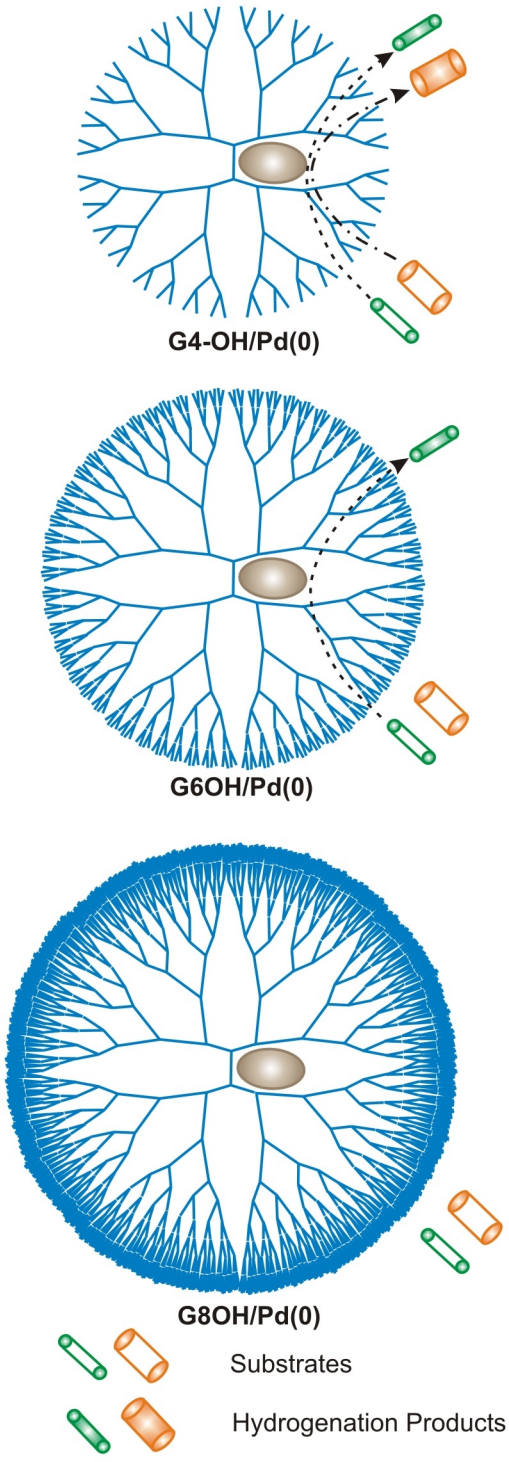

Figure 5.1. Schematic representation of size-selective hydrogenation by DEMNs prepared within different generation dendrimers.

H_2O is not as great as in MeOH, a MeOH-H_2O (4:1, v/v) mixed solvent system was chosen to maintain a homogeneous reaction mixture.

The composite catalysts used in this study are composed of Pd(0) nanoclusters encapsulated within G4-OH, G6-OH, and G8-OH PAMAM dendrimers. In each case the DEC was prepared using a Pd(II)-to-dendrimer ratio of 40. We expected, and transmission electron microscopy confirms, that following reduction the average Pd(0) cluster size was independent of dendrimer generation (Figure 5.2 and 5.3). Specifically, the encapsulated Pd(0) nanoparticles had an average diameter and dispersity of 1.7 ± 0.2 nm regardless of the dendrimer generation. Staining TEM technique has also been used. However because relatively low Z value of Pd compared to tungsten stain the constrast of the images is not god. However, the data suggest that each dendrimer contains one Pd nanoparticle and the particles are located in each dendrimer. The calculated sizes of G4OH, G6OH and G8OH by staining TEM are 6.3 ± 0.2 nm, 7.0 ± 0.2 nm, and 9.7 ± 0.2 nm, respectively. These sizes are relatively larger than the reported value.[36] Some aggregation of dendrimers (dimers and trimers) can be observed.

The rate of hydrogenation for the five allylic alcohol substrates (**1**-**5**) in the presence of the three catalysts was determined by H_2 uptake (Table 5.1). Turnover frequencies (TOFs, mol of H_2 per mol of Pd(0) per hour) in the mixed solvent ranges from 50 to 480 depending on the dendrimer generation and substrate. Qualitatively, Table 1 indicates that for a particular catalyst (dendrimer generation) the TOFs generally decrease as the substrates become bulkier. For example, the maximum TOF for the G4-

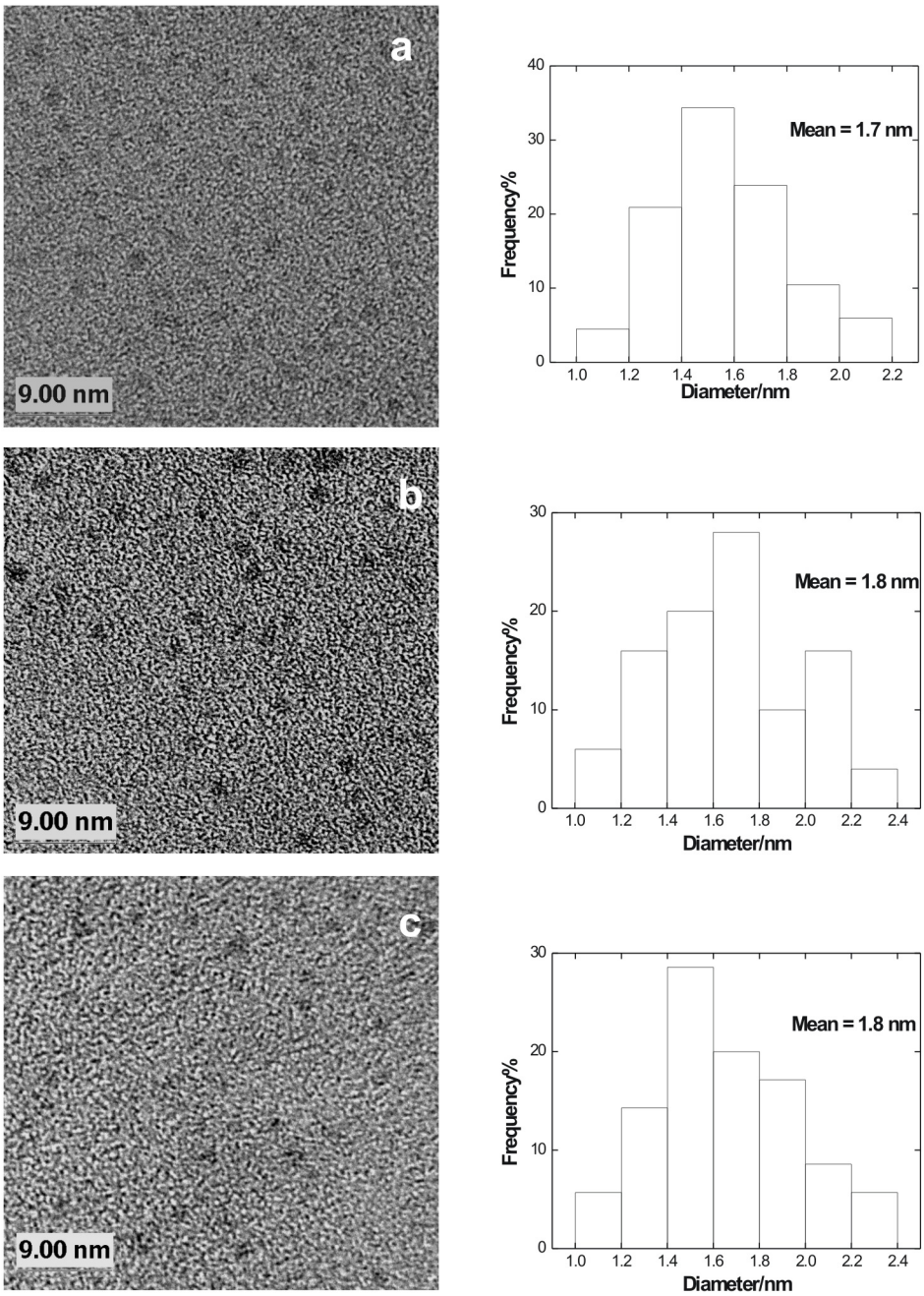

Figure 5.2. TEM images and particle size distributions of the GnOH/Pd(0)40 catalysts before use in the hydrogenation reactions (a) G4OH/Pd(0)40, (b) G6OH/Pd(0)40, (c) G8OH/Pd(0)40.

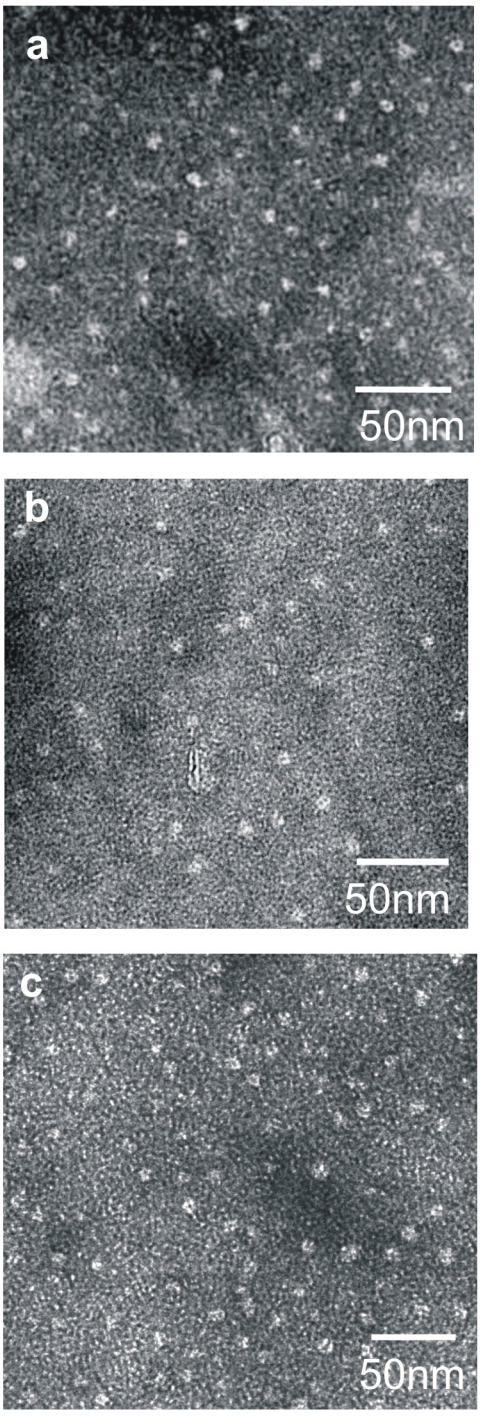

Figure 5.3. Staining TEM images of the GnOH/Pd(0)40 catalysts before use in the hydrogenation reactions (a) G4OH/Pd(0)40, (b) G6OH/Pd(0)40, (c) G8OH/Pd(0)40. The stain used here is phosphotungstic acid (PTA) at pH = 7.

Table 5.1. Hydrogenation reaction rates using Gn-OH/Pd(0)40 catalysts for structurally related allyl alcohol and allylic alcohols.

Substrates	TOF[mol H_2(mol Pd)$^{-1}$ h^{-1}]		
	G4-OH(Pd40)	G6-OH/Pd(0)40	G8-OH/Pd(0)40
(**1**) 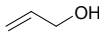	480/470[2]	450/460[2]	120
(**1**) 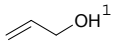 [1]	220[1]	200[1]	130[1]
(**2**) 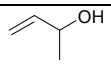	450/460[2]	380	93
(**3**) 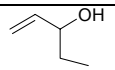	260	280	68
(**4**) 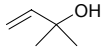	150	75	62
(**5**) 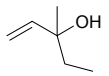	100	40	50

Hydrogenation reactions were carried out at 25 ± 2 ^{o}C using 2 × 10^{-4} M Pd(0) composite catalysts in MeOH-H_2O (4:1, v/v) mixtures. The turnover frequency (TOF) was calculated based on H_2 uptake (mol H_2 (mol Pd(0) h)$^{-1}$).

[1]Hydrogenation reactions were carried out at 25 ± 2 ^{o}C using 2 × 10^{-4} M Pd(0) composite catalysts in water only (no methanol).

[2]Duplicate measurements were performed to illustrate the level of run-to-run reproducibility.

OH/Pd(0)40 catalyst for the hydrogenation of allyl alcohol (**1**) was 480 mol H_2(mol Pd)$^{-1}$ h^{-1}. This reaction rate is comparable to that obtained using polymer-supported Pd(0) catalysts in methanol (565 mol H_2(mol Pd)$^{-1}$ h^{-1})[164] and PAMAM encapsulated Pd(0) in fluorous-phase solvent (400 mol H_2(mol Pd)$^{-1}$ h^{-1}).[99] A substrate having one α methyl group, 3-buten-2-ol (**2**), yielded a slightly lower TOF. When the methyl group was changed to ethyl (**3**), the reaction rate decreased further to 260 mol H_2(mol Pd)$^{-1}$ h^{-1}. This trend continues when two methyl groups are present at the α position (**4**) and when both a methyl and an ethyl group are present at the α position of the substrate (5). Overall, the TOF for the bulkiest substrate (**5**) was five times lower than the smallest (**1**). The same trend was found for the G6-OH/Pd(0)40 and G8-OH/Pd(0)40 catalysts.

It is possible to correlate these experimental data to a semi-quantitative structural model of the dendrimer. That is, if we make the following five assumptions, then the distance between adjacent terminal groups for the different generation dendrimers can be calculated using appropriate molecular models (see Experimental Section): (1) the dendrimers are spheroidal in shape;[36] (2) all the terminal groups are locate at the surface of the dendrimer;[36,179] (3) the terminal C-O bonds are perpendicular to the dendrimer surface with equal distances among adjacent oxygen atoms; (4) the diameters of the G4-OH, G6-OH and G8-OH dendrimers are 4.5 nm, 6.7 nm, and 9.7 nm, respectively,[180] and (5) the number of terminal hydroxyl groups for G4-OH, G6-OH, and G8-OH are 64, 256, and 1024, respectively. Using these assumptions, the calculated average edge to edge distance between two O-H end groups (based on the van der Waals surface of the outermost O atoms) in G4-OH is 8.2 Å, while the distance decreases to 5.4 Å for G6-

OH, and further to 3.2 Å for G8-OH. These data confirm that the "mesh size" of the dendrimer "nanofilter" depends very sensitively on generation.

Molecular modeling was also used to calculate the free volumes of the five substrates, which are as follows: (1) 60.7, (2) 75.4, (3) 96.1, (4) 89.7, and (5) 103 $Å^3$. It seems reasonable that the substrates first penetrate into the dendrimer through their hydroxyl groups, and therefore a good measure of substrate size is the largest linear dimension perpendicular to the O-H bond direction. For substrates **1**-**5**, these values are 5.5, 7.0, 7.5, 7.0, and 8.0 Å, respectively. The results of the molecular modeling parameters (substrate size and dendrimer pore size) correlate well to the experimental data for all three dendrimer generations (Table 5.1), except for substrate **4**, which is smaller than **3** and has a smaller TOF. This suggests that the model described by Figure 5.1, which is based solely on stationary steric considerations, is fairly good but does not predict all of the experimental data correctly. Apparently there are chemical and more complex structural aspects of the substrate that must be taken into account to fully resolve this issue, and therefore additional experiments are underway to further refine the model proposed here.

It is interesting to compare hydrogenation rates for the same substrate when different generation dendrimers encapsulate the Pd(0) nanoparticle. Table 5.1 shows that there is a clear trend in this regard: the lower generation DECs, with just two exceptions, result in the highest TOFs. In addition, for substrates **1**-**3** there is a much larger decrease in TOF when the generation changes from G6 to G8 than for the change between G4 and G6. These observations correlate well with the average distance

between terminal groups of the dendrimers (*vide supra*: G4-OH, 8.2 Å; G6-OH, 5.4 Å; G8-OH, 3.2 Å). That is, when the dendrimer generation increases to 8, the average distance between terminal groups (3.2 Å) is significantly less than the critical dimension of the substrates (range: 5.5 – 8.0 Å, *vide supra*). Thus, because the dendrimer porosity can be controlled by varying either the generation, as in this study, or the bulkiness of the peripheral functional groups, it is possible to prepare selective catalysts using as a first approximation the very simple concept of steric crowding on the dendrimer surface.

We previously reported TOF values for **1** in water-only (Table 5.1),[32] and these rates are generally smaller than in the mixed MeOH-H_2O solvent used here. Unfortunately, it was not possible to perform a thorough comparison of the reaction rates of all five substrates in both solvent systems due to the limited solubility of most of the substrates and products in pure water. However, allyl alcohol (**1**) and the hydrogenation product are both appreciably soluble in H_2O. The TOFs of G4-OH/Pd(0)40, G6-OH/Pd(0)40, and G8-OH/Pd(0)40 for the hydrogenation of allyl alcohol in water are 220, 200, and 130 mol H_2(mol Pd)$^{-1}$ h^{-1}, respectively. In contrast, we found the maximum TOFs for allyl alcohol hydrogenation in the mixed MeOH-H_2O solvent to be greater by about a factor of two for G4-OH/Pd(0)40 and G6-OH/Pd(0)40, but nearly the same for G8-OH/Pd(0)40. This result is consistent with previous findings that solvent plays an important role in determining hydrogenation reaction rate at colloidal nanoparticles.[181,182] For example, the hydrogenation of the ethyl ester of mandelic acid in ethanol is much faster than in water.[183] Other studies have shown that trace amounts of water are very beneficial for increasing the hydrogenation rate in ketonic solvent[184] or

methyl acetate.[185] At this time we do not fully understand why there are such large changes in TOF as a function of solvent for identical dendrimer-encapsulated catalysts, but it seems likely that this finding results from either changes in the surface chemistry of the encapsulated Pd nanoparticles, structural changes of the dendrimer template driven by differences in solvent polarity, or enhanced partitioning of the substrate into the dendrimer in the mixed solvent.[115,116]

The size of dendrimer-encapsulated nanoparticles can also be used to tune the rate of chemical reactions. Specifically, preliminary results indicate that increasing the size of a Pd nanoparticle leads to a rate enhancement for the hydrogenation reaction. For example, it is possible to hold the ratio of Pd(0) to tertiary amines constant for all three generations of dendrimers. That is, encapsulated Pd(0) clusters containing 40, 164, and 659 atoms can be prepared within G4-OH, G6-OH, and G8-OH, respectively. The allyl alcohol hydrogenation reaction rates measured for the DECs containing large metal particles were extremely fast compared with the data presented thus far: 1000 and 2500 mol H_2(mol Pd)$^{-1}$ h^{-1} TOF for G6-OH/Pd(0)$_{164}$ and G8-OH/Pd(0)$_{659}$, respectively. Interestingly, neither of these larger catalysts was stable on the timescale of the reactions. One possible explanation for this result is that the distance between the dendrimer periphery and the Pd surface is related to the TOF. That is, as shown in Figure 5.1, once a substrate enters a dendrimer it must diffuse further to reach the encapsulated nanoparticle as the generation increases. This hypothesis provides a direction for refining our existing model.

The hydrogenation products were identified by NMR spectroscopy. The NMR spectra of reaction mixtures of 5×10^{-6} M G4-OH/Pd(0)$_{40}$ and 2.0 M unsaturated alcohols in CD_3OD-D_2O (4:1, v/v) before and after treatment with H_2 are shown in Figure 5.4 and Figure 5.5. Characterization of the reaction mixture is simplified because the concentration of G4-OH/Pd(0) catalyst is below the NMR detection limit. Before the start of each reaction, the spectra of the reaction mixtures showed the characteristic peaks of the vinylic protons (5-6 ppm). After exposure to H_2, the disappearance of the double bond peaks indicated that the reaction went to completion. Substrates **1**, **4**, and **5** were cleanly hydrogenated yielding only the saturated alkyl alcohols without isomerization or any other by-products (Figure 5.4).

Hydrogenation of substrates **2** and **3**, both of which contain an α hydrogen, generated not only the anticipated hydrogenation products, but also a small amount of unexpected byproducts (Figure 5.5). In the case of 1-penten-3-ol (**3**), in addition to the expected product (3-pentanol, **3a**), which has peaks at 3.39 ppm (m), 1.45 ppm (m) and 0.92 ppm (t) in the ^{1}H NMR spectrum, there are two extra sets of peaks at 2.49 ppm (q) and 1.02 ppm (t) that correspond to 3-pentanone (**3b**). The characteristic chemical shift at 216.55 ppm in ^{13}C NMR spectrum further confirmed the presence of ketone. Integration of the ^{1}H NMR spectrum indicated that the ratio of the expected 3-pentanol (**3a**) to the ketone byproduct is 4.7:1. Similarly, hydrogenation of 3-buten-2-ol (**2**) yielded the anticipated alcohol (**2a**) and a 2-butanone (**2b**) as a byproduct in a 6.7:1 ratio. GC measurements for both reaction mixtures were made to confirm the NMR data. The

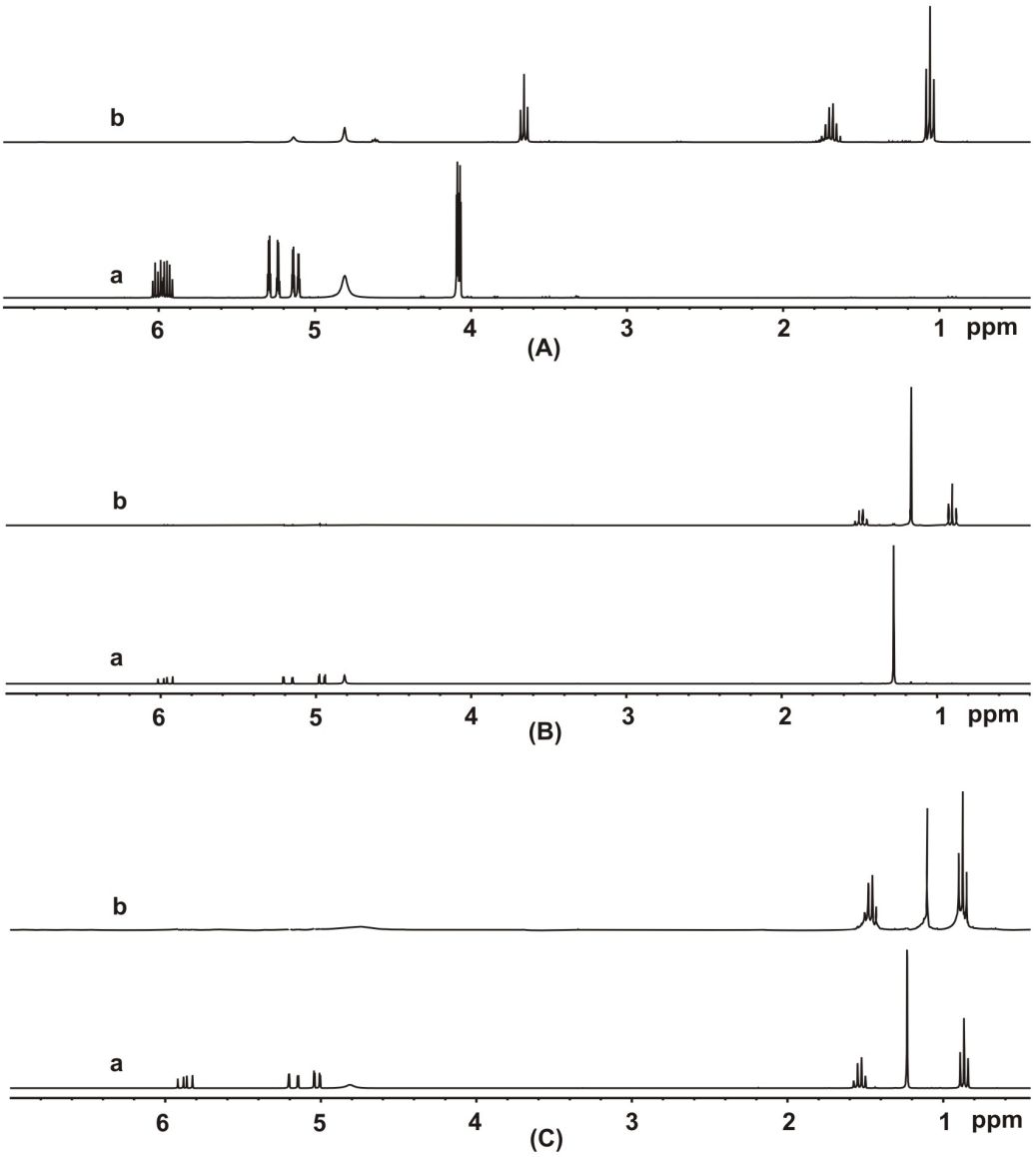

Figure 5.4. ^{1}H NMR spectra of reaction mixtures of 5 x 10^{-6} M G4OH/$Pd(0)_{40}$, and 2 M unsaturated alcohols (A) allyl alcohol (**1**), (B) 2-methyl-3-buten-2-ol (**4**), (C) 3-methyl-1-penten-3-ol (**5**) respectively, before (a) and after (b) treatment with H_2, in CD_3OD-D_2O (4:1, v/v).

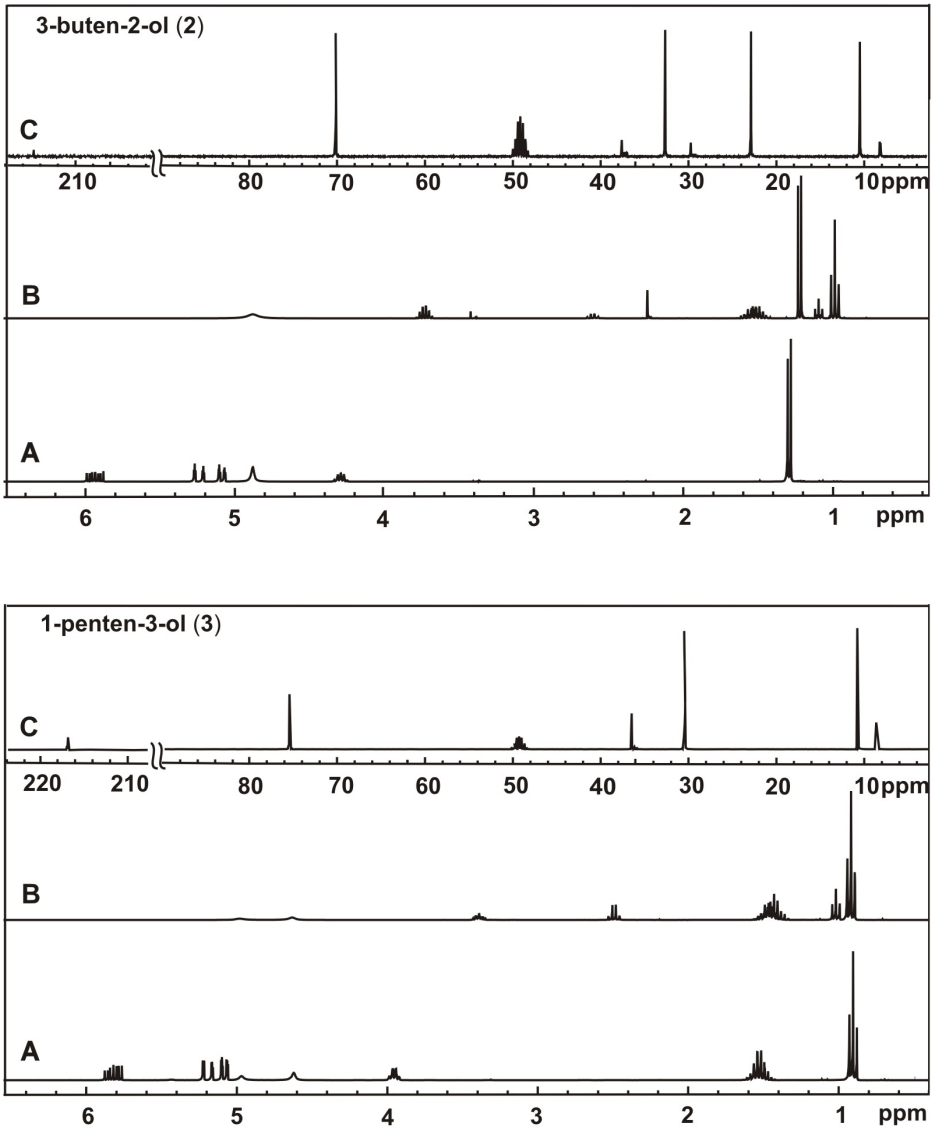

Figure 5.5. ^{1}H NMR spectra of reaction mixtures containing 5 x 10^{-6} M G4OH/Pd(0)40 and 2 M unsaturated 3-buten-2-ol (2) or 1-penten-3-ol (3) before (A) and after (B) reaction with H_2 in CD_3OD-D_2O (4:1 v/v). The data shown in parts C are the ^{13}C NMR spectra of the reaction mixture after hydrogenation.

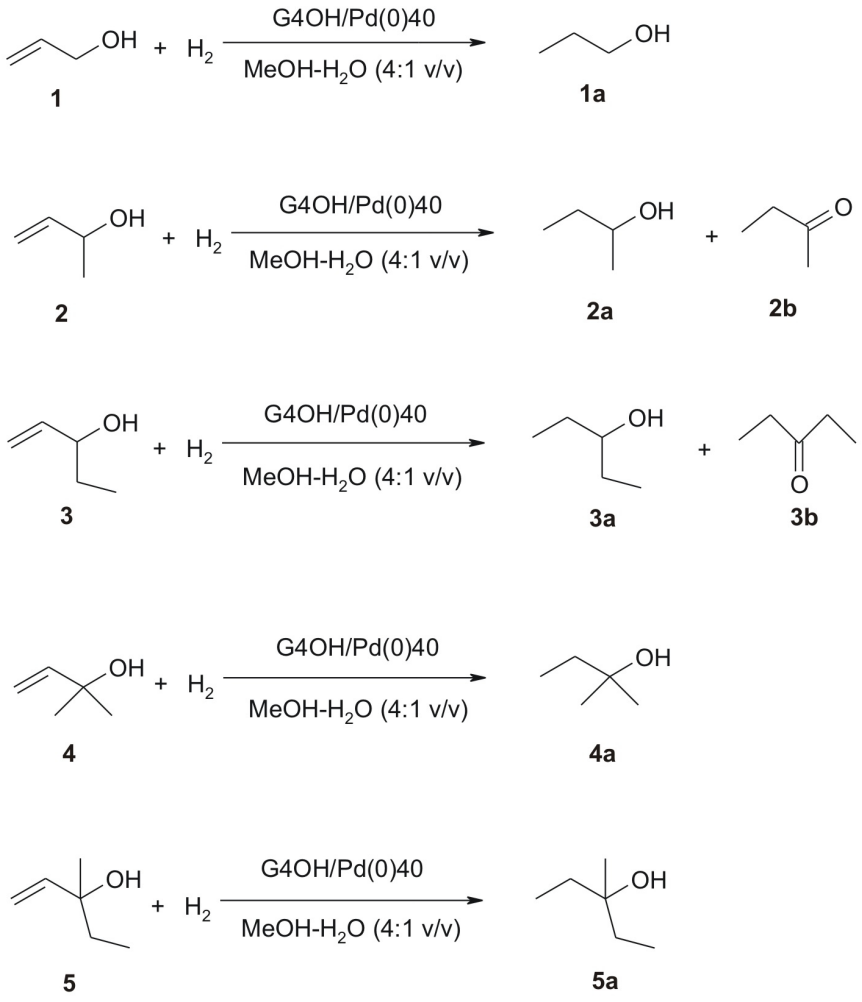

Figure 5.6. Hydrogenation reaction schemes of substrates (**1**-**5**) catalyzed by DECs.

reactions of all 5 substrates with H_2 are given in Figure 5.6. The formation of byproduct ketones is known to involve a double bond migration in **2** and **3**, respectively, to generate the corresponding enol isomers, which then slowly tautomerize to ketones.[38] The important point is that reactions occurring *within* DECs do not always yield the expected products. Once understood, this finding is likely to be of great value in designing product-selective DECs.

Having characterized the catalytic properties of the DECs in single-substrate solvents, we endeavored to demonstrate their selective nature by performing a competitive hydrogenation reaction. Allyl alcohol (**1**) and 3-methyl-1-penten-3-ol (**5**) were used for this study because the reaction does not yield byproducts and because they have very different TOFs (Table 5.1). Because **1** is a more linear molecule than **5**, we expected that it would have an easier time navigating through the dendrimer branches than **5**. ^{1}H NMR spectra of the reaction mixture of **1** and **5** (1:1 mol eq) before and after treatment with H_2 were recorded as a function of time using G4-OH/Pd(0)40 as the catalyst (Figure 5.7). After 2.5 h of hydrogenation, 50% of the allyl alcohol (**1**) was reduced to *n*-propanol (**1a**), while only 1.6% 3-methyl-3-pentanol (**5a**) was generated. After an additional 2.5 h, 100% of **1** is converted to **1a**, but only 11% **5** was converted to **5a**. After a total reaction time of 20 h, a third of the 3-methyl-1-penten-3-ol was still unconverted to product, but the conversion was finally complete after 42 h. These results correlate well to the single-substrate data in Table 5.1, and they provide additional support for the model embodied by Figure 5.1.

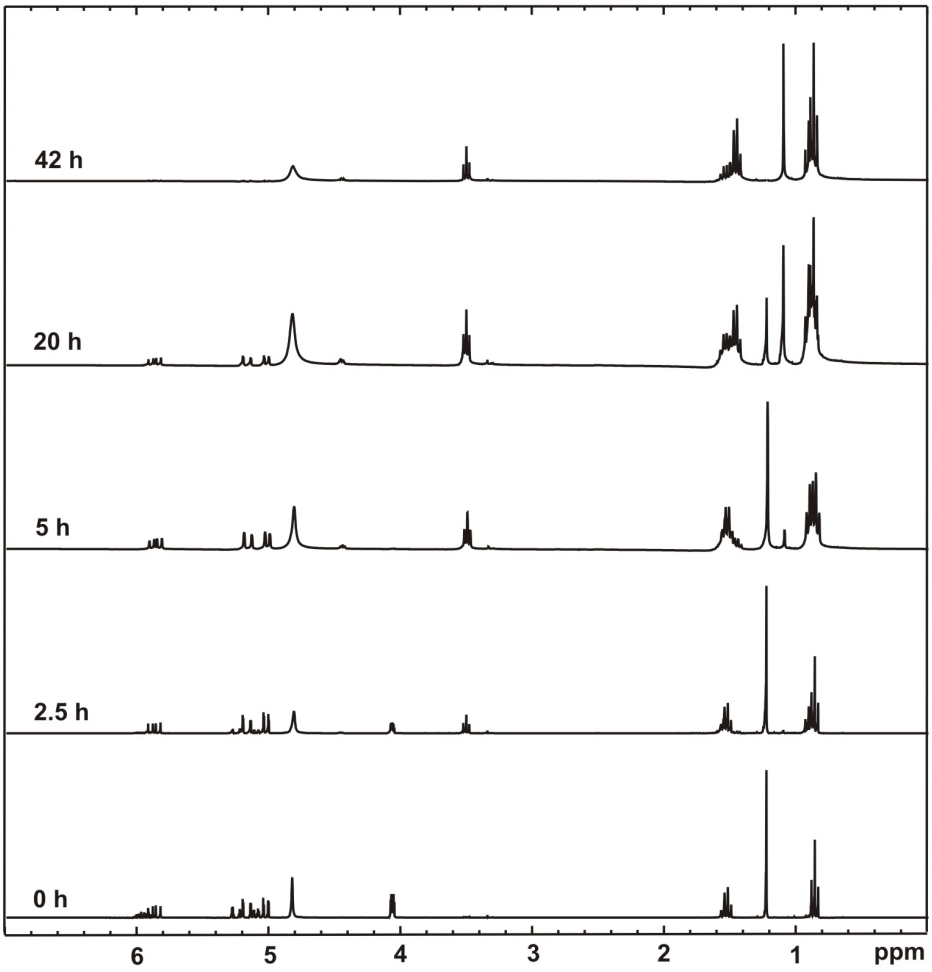

Figure 5.7. ^{1}H NMR spectra of a reaction mixture containing 5 x 10^{-6} M G4OH/Pd(0)40, 1 M allyl alcohol (**1**), and 1 M 3-methyl-1-penten-3-ol (**5**), before reaction with H_2 and at various time increments after the hydrogenation reaction commenced (solvent: CD_3OD-D_2O, 4:1 v/v).

To further investigate if this concept can be applied to a broader field, we investigated whether an increase in the surface density of dendrimer periphery caused by surface functional groups results in a decrease in hydrogation reaction turn-over frequency, as shown in Figure 5.8.

Various PAMAM dendrimers with α-aminoalcohol end groups were designed and synthesized for this study (G4-EPn, n = 1-3) by the reactions between the 4th generation amine terminated PAMAM dendrimer (G4-NH_2) and epoxides (glycidol, (s)-2-methylglycidol, and t-butyl glycidol ether) (Figure 5.9). ^{1}H NMR, ^{13}C NMR and MALDI-MS studies confirmed the formation the expected dendrimers. These dendrimers were used as templates for the formation of palladium nanoparticles. TEM measurement showed the average diameter of Pd particles is 1.7 ± 0.2 nm (Figure 5.10).

These dendrimer-encapsulated catalysts are then used to hydrogenate allyl alcohol and α-allyllic alcohols while monitoring the reaction rate (Table 5.2). Kinetic studies showed a clear trend of decreasing TOF of allyl alcohol and allylic alcohol reduction with the increasing of the surface density from G4OH, G4-EP1, G4-EP2 to G4-EP3. And for a particular catalyst the reaction TOFs decrease as the substrate becomes bulkier. Thus, it is also possible to control access of substrates to the interior of dendrimer of different sterics.

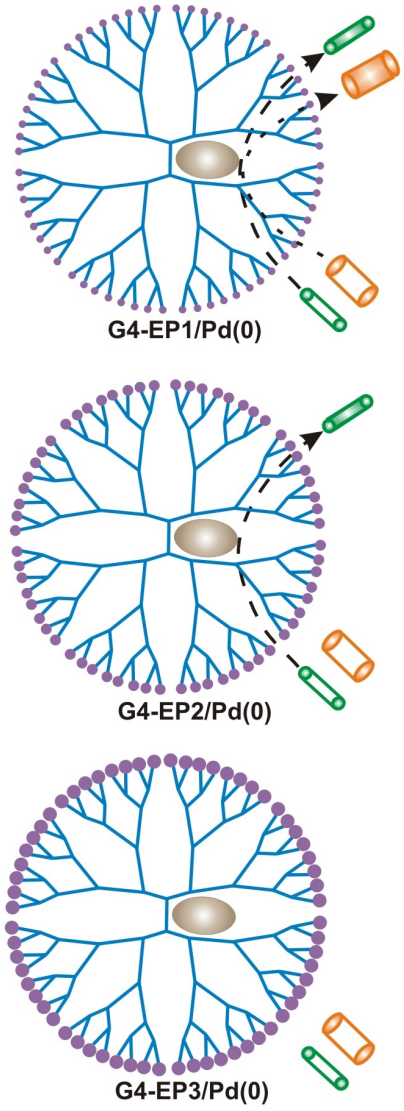

Figure 5.8. Schematic representation of size-selective hydrogenation by DEMNs prepared within dendrimers with different surface sterics.

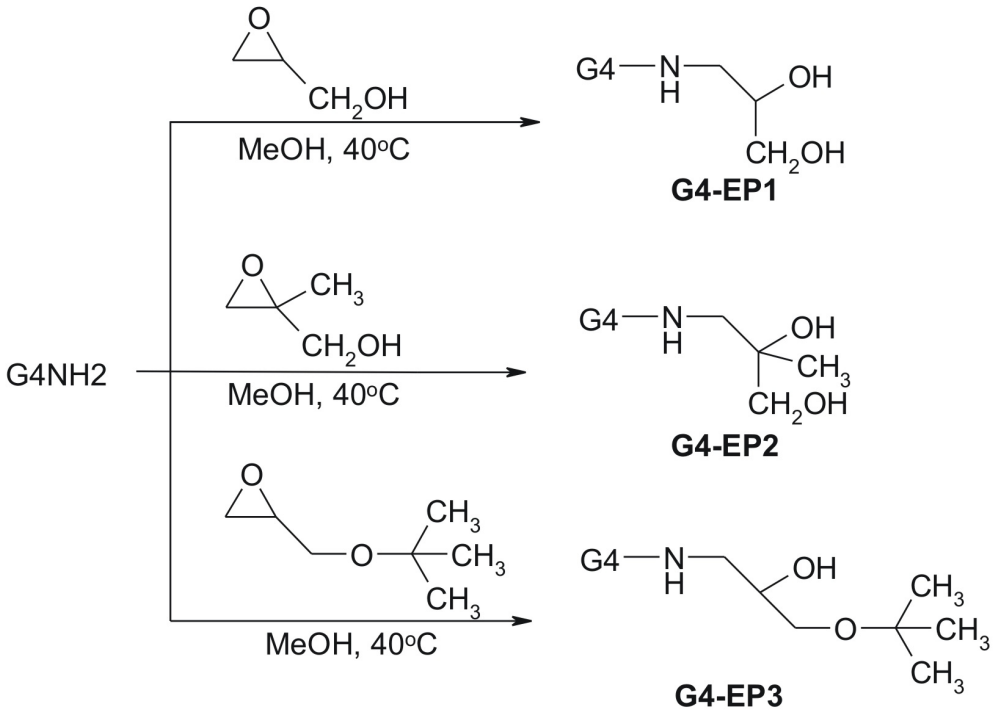

Figure 5.9. Synthetic approach for covalently linking α-aminoalcohol groups to the periphery of G4-NH_2 PAMAM dendrimers.

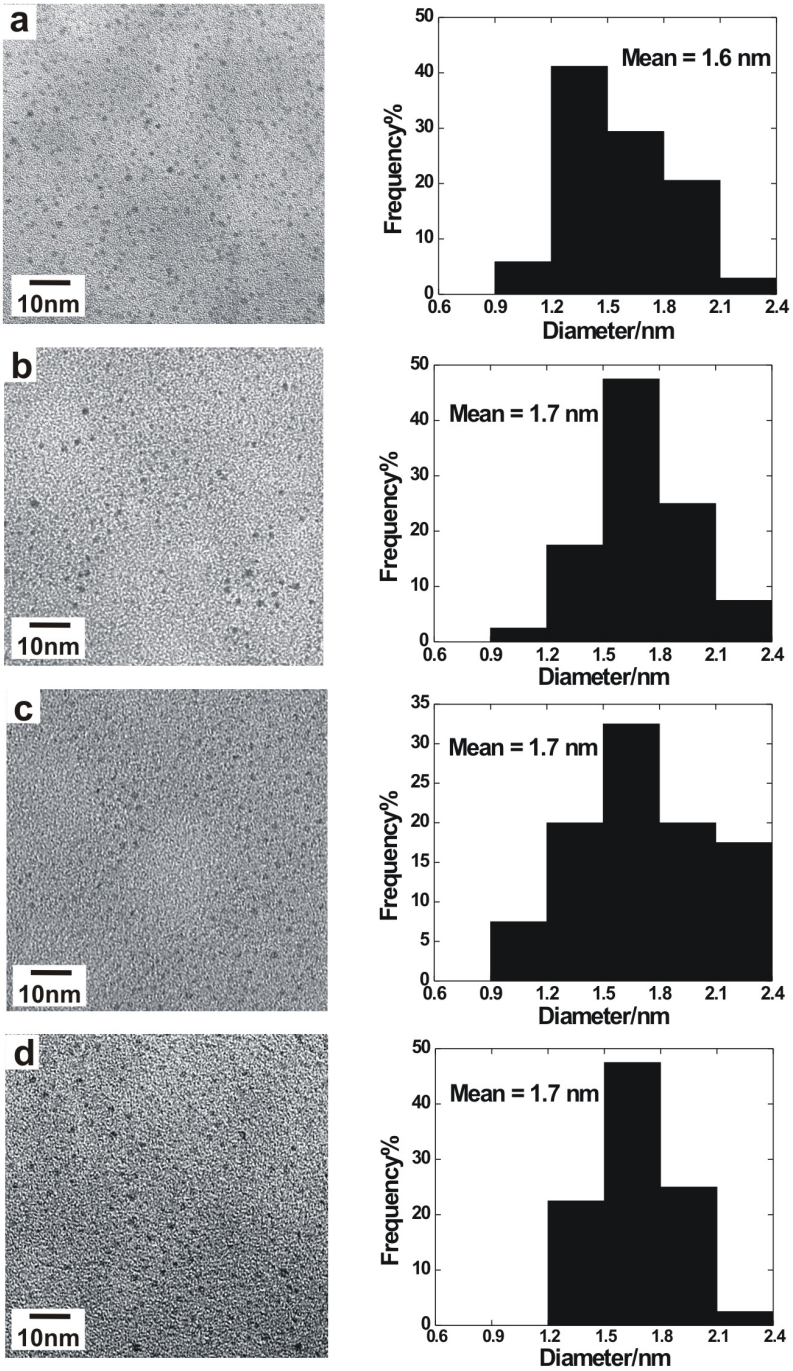

Figure 5.10. TEM images and particle size distributions for (a) G4-OH/Pd(0)40; (b) G4-EP1/Pd(0)40; (c) G4-EP2/Pd(0)40; and (d) G4-EP3/Pd(0)40 catalysts.

Table 5.2. Hydrogenation reaction rates using Gn-OH/Pd(0)40 and G4-EPn/Pd40 catalysts for structurally related allyl alcohol and allylic alcohols.

Substrates	TOF[mol H_2(mol Pd)$^{-1}$ h^{-1}]			
	G4-OH/Pd40	G4-EP1/Pd40	G4-EP2/Pd40	G4-EP3/Pd40
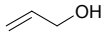	125	83	62	43
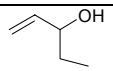	105	62	60	53
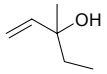	50	55	43	31

5.5. Summary and Conclusions

Dendrimers In this study we have described a general approach for rendering intrinsically unselective catalysts selective. This strategy involves encapsulation of the nonselective catalyst (the Pd nanoparticle) within a nanoporous cage (the dendrimer). As we have shown, selective nanoreactors that can distinguish between two substrates that differ only slightly in chemical structure. On the basis of the experimental data and molecular modeling results, we have proposed a model (Figure 5.1 and Figure 5.8) that attributes selectivity principally to steric interactions between substrates and functional groups on the dendrimer periphery. Yet to be examined thoroughly are the effects of different solvents and peripheral groups on reaction rates; those issues are being addressed at the present time and will be reported in due course. The important point, however, is that by simply changing dendrimer generation reaction rates can be varied by nearly a factor of five in favorable cases.

Other issues that merit investigation include the effect of the *intradendrimer* reaction medium on product yields. Specifically, is it possible to develop a reasonable model to correlate the interior structure of the dendrimer (which is undoubtedly a strong function of solvent) to product distribution, and subsequently design DECs that are both substrate and product selective? Finally, we reported a few tantalizing initial results that correlate TOF to nanoparticle size. Heterogeneous catalysis studies have previously shown that either quantum electronic or structural effects can have a dramatic influence on reaction rates.[105] DECs are ideally suited for studying such effects for dispersed catalysts.

CHAPTER VI

MOLECULAR RULERS AS *IN-SITU* PROBES OF CATALYTICALLY ACTIVE DENDRIMER-ENCAPSULATED PALLADIUM NANOPARTICLES

6.1 Synopsis

Here we report an *in-situ* method for determining the average distance between the surface of dendrimer-encapsulated palladium nanoparticles and the surface of their fourth-generation, hydroxyl-terminated poly(amidoamine) dendrimer hosts. The measurements were made using molecular rulers consisting of three parts: a catalytically active probe at the distal terminus that may undergo a hydrogenation reaction upon contact with the encapsulated catalyst; a large molecular "stopper" at the proximal end that is unable to enter the host; and intervening alkyl chains having different lengths that tether the probe to the stopper and which therefore define the maximum extension of the ruler (Figure 5.1). The time necessary to hydrogenate these molecular rulers was monitored by ^{1}H NMR, and then used to estimate the average location of the encapsulated Pd nanoparticles. The results showed that the shortest ruler, mono-6-deoxy-6-(allylamino)cyclodextrin (0.5 nm in length), had the slowest reaction rate while the two longer rulers (0.9 and 1.3 nm) reacted substantially faster. The data indicate that the surface of the encapsulated nanoparticle is situated 0.7 ± 0.2 nm from the surface of the dendrimer.

6.2 Introduction

We[5,75] and others[27-30] have previously reported the synthesis of dendrimer-encapsulated metal and semiconductor[31] nanoparticles. The approach relies on the use of dendrimers as templates that sequester metal ions within their interior. Subsequent reduction results in formation of metal nanoparticles whose size reflects the chemical and physical properties of the dendrimeric template. We have shown that the dendrimer serves three additional functions: it is a stabilizer that prevents metal agglomeration; chemical functionalization of the periphery provides a means for solubilizing nanoparticles in solvents ranging from water to supercritical carbon dioxide;[23] and the dendrimer can be used as a permselective filter that controls access of small molecules to the interior on the basis of size[33] or charge.[186] These properties make DEMNs an intriguing platform for studying catalysis.[5,23,24,26,32,33]

A key question raised in these previous studies concerns the size, shape, and location of the encapsulated nanoparticles. To begin addressing these questions, Gröhn and coworkers used transmission electron microscopy (TEM) and scattering methods to place Au nanoparticles somewhat offset from the center of generation 6 – 9 (G6-G9) poly(amidoamine) (PAMAM) dendrimers.[28] However, interpretation of data from these methods, and correlation of the results to the conformation of solution-phase dendrimers, is complex and model dependent. For example, TEM imaging necessitates that the dendrimers be stained and placed under vacuum or in frozen solutions,[187] all of which distort the shape of the dendrimer.[188,189] Likewise, scattering data for DEMNs have been interpreted by assuming that the encapsulated nanoparticles are spherical,[28] but this

assumption is approximate. For example, we have found that TEM over-estimates the size of DEMNs by more than 50%.[5,32] This, along with the high degree of steric crowding within the dendrimer interior, suggests that encapsulated nanoparticles have complex shapes.

6.3 Experimental

Materials. Fourth-generation, hydroxyl-terminated fourth-generation poly(amidoamine) (PAMAM) dendrimers (G4-OH) having an ethylenediamine core was obtained as 24.89% methanol solutions (Dendritech, Inc., Midland, MI). Prior to use, methanol was removed under vacuum at room temperature. β-cyclodextrin was obtained from Cerestar USA, Inc. (Hammond, IN). Allyl amine was received from the Aldrich Chemical Co. (Milwaukee, WI) and dried over CaH_2 for 2 days and filtered just before use. 7-bromo-1-heptene, potassium phthalimide, methanol, hydrazine, and $NaBH_4$ were used as received from the Aldrich Chemical Co. (Milwaukee, WI). 11-bromo-undecene was purchased from Pfaltz and Bauer (Waterbury, CT) and used without further purification. K_2PdCl_4 and 5% Pd on carbon was purchased from Strem Chemicals, Inc. (Newburyport, MA) and used without further purification. Deuterium Oxide (99.9%) was purchased from Cambridge Isotope Laboratories.

TLC plates were silica gel 60 F 254 having a 0.2 mm layer thickness (Riedel-de Haën AG, Seelze, Germany). The eluant used for TLC was 7:7:5 EtOAc/2-propanol/H_2O. TLC spots were visualized with an indicator prepared by mixing 26.25 g

of 2-naphtol with 315 mL of EtOH, 105 mL H_2SO_4, and 66 mL of Milli-Q water. After drying at 70 ^oC for 10 min, cyclodextrin derivatives gave a dark red color.

Instrumentation. ^1H and ^{13}C NMR spectra were recorded on a Unity spectrometer at 500 MHz (126 MHz for ^{13}C).

Synthesis of mono-6-deoxy-(*p*-Tolylsulfonyl)-β-Cyclodextrin (2). Preparation of **2** (Supporting Material Scheme 1) followed a literature procedure[190] with minor modifications. β-cyclodextrin (**1**) (120.0 g, 115.9 mmol) was suspended in 1 L of water. A solution containing 232 mmol of NaOH in 40 mL H_2O was added dropwise over 10 min. The white suspension became homogeneous and slightly yellow before the addition was complete. *p*-Tolylsulfonyl chloride (20.16 g, 115.9 mmol) in 60 mL acetonitrile was added dropwise over 8 min, causing immediate formation of a white precipitate. After stirring at r.t. for 2 h the precipitate was removed by suction filtration and the filtrate was refrigerated for 2 days at 10 ^oC. The resulting white precipitate was recovered by suction filtration. After drying under vacuum for 5 h, a white solid was obtained (8.55 g). ^1H NMR, ^{13}C NMR, and ESI-MS data agree with the literature values.[19]

Synthesis of mono-6-deoxy-6-(Allylamino)-β-Cyclodextrin (R1). Mono-6-deoxy-(*p*-tolylsulfonyl)-β-cyclodextrin (1.200 g, 0.932 mmol) was dissolved in 8.0 mL dry allyl amine. The mixture was refluxed at 55 ^oC for 48 h. Excess allyl amine was removed by vacuum and a yellow solid was obtained. The crude product was dissolved in H_2O and run through a pack of Amberjet-4200Cl (12 cm) 3 times. Rota-evaporation gave 1.140 g of yellow solid (95% yield). TLC (SiO_2) R_f 0.25; ^1H NMR (500 MHz,

D_2O) δ 3.00 (br, m, 2H), 3.25 (br, 2H), 3.48 (br, m, 14H), 3.76 (br, m, 25H), 3.93 (t, 1H), 4.94 (m, 7H), 5.28 (m, 2H), 5.77 (m, 1H); ^{13}C NMR (126 MHz, CD_3OD) δ 61.87 (m), 74.12 (m), 83.00 (m), 103.82 (m), 121.38 (s), 144.62 (s); m/z calcd for $C_{45}H_{75}O_{34}N$ (M – Cl) 1174.07, ESI-TOF-MS measured 1174.43, MALDI-TOF-MS measured 1174.31.

Synthesis of mono-6-deoxy-6-(6-Hepten-1-amino)-β-Cyclodextrin (R5). A suspension obtained as mono-6-deoxy-(*p*-tolylsulfonyl)-β-cyclodextrin (1.005 mg, 0.780 mmol) was introduced to 7.5 mL 7-amino-1-heptene.[191] A clear solution was obtained when the mixture was heated to 50 ^oC. The mixture was stirred at 90 ^oC for 40 h. Excess 7-amino-1-heptene was removed by vacuum and a yellow solid was obtained. The crude product was dissolved in H_2O and run through a pack of Amberjet-4200Cl (12 cm) 3 times. Rota-evaporation gave 0.865 mg yellow solid (86% yield). TLC (SiO_2) Rf 0.20; ^1H NMR (500 MHz, D_2O) δ 1.13 and 1.24 (br, m, 4H), 1.47 (m, 2H), 1.97 (m, 2H), 2.67 (m, 1H), 2.97 (m, 3H), 3.20 (m, 1H), 3.48 (br, m, 19H), 3.74 (br, m, 19H), 3.90 (t, 1H), 4.97 (m, 9H), 5.77 (m, 1H); ^{13}C NMR (126 MHz, CD_3OD) δ 26.88 (m), 28.44 (s), 29.41 (s), 29.49 (s), 34.48 (s), 40.69 (s), 61.99 (m), 74.19 (m), 82.97 (m), 103.90 (m), 115.41 (s), 139.53 (s); m/z calcd for $C_{49}H_{83}O_{34}N$ (M – Cl) 1230.18, ESI-TOF-MS measured 1230.53.

Synthesis of mono-6-deoxy-6-(10-Undecen-1-amino)-β-Cyclodextrin (R9). A suspension obtained as mono-6-deoxy-(*p*-tolylsulfonyl)-β-cyclodextrin (1.270 mg, 0.986 mmol) was introduced to 8.0 mL 11-amino-1-undecene.[191] A clear solution was obtained when the mixture was heated to 90 ^oC. The mixture was stirred at 110 ^oC for

48 h. Excess 11-amino-1-undecene was removed by vacuum at 120 ^{o}C and a yellow solid was obtained. The crude product was dissolved in H_2O and run through a pack of Amberjet-4200Cl (12 cm) for 3 times. TLC (SiO_2) Rf 0.20; ^{1}H NMR (500 MHz, D_2O) δ 1.21 (br, 10H), 1.39 (br, m, 2H), 1.50 (br, m, 2H), 2.05(q, 2H), 2.98 (m, 4H), 3.23 (m, 1H), 3.51 (br, m, 19H), 3.73 (br, m, 20H), 4.96 (m, 9H), 5.81 (m, 1H); ^{13}C NMR (126 MHz, CD_3OD) δ 27.62 (m), 30.05(s), 30.08 (s), 30.35 (s), 30.39 (s), 34.95 (s), 40.85 (s), 61.82 (m), 74.18 (m), 83.17 (m), 85.59 (s), 103.79 (m), 114.92 (s), 140.09 (s); m/z calcd for $C_{53}H_{91}O_{34}N$ (M – Cl)1285.75, ESI-TOF-MS measured ($C_{53}H_{91}O_{34}N$) 1286.60.

Preparation of G4-OH(Pd_{40}) Catalysts. The G4-OH(Pd^{2+})$_{40}$ complex was prepared by adding 125 μL of 5 × 10^{-4} M G4-OH (in D_2O) to 1.250 mL of D_2O, followed by 250 μL of a 0.01 M K_2PdCl_4 solution (in D_2O, 40 eq) under vigorous stirring. A light yellow solution was obtained immediately. After stirring for 30 min, 100 μL of a 0.5 M $NaBH_4$ (aq) solution was added, which changed the color of the solution to golden brown.

Hydrogenation Reactions. Hydrogenation reactions were carried out in a 10 mL reaction vial fitted with a magnetic stir bar. The substrate and catalyst solutions were bubbled with H_2 separately for 10 min. Experiments were carried out by adding the catalyst to the substrate solution under H_2 with vigorous stirring. There was no evidence for Pd(0) aggregation during or after hydrogenation of the substrates, indicating that the catalysts are stable on the time scale of the reactions. All hydrogenation reactions were run at atmospheric pressure and room temperature (25 ± 2°C). A ^{1}H NMR spectrum of this solution was obtained just prior to the hydrogenation

reaction. A 0.6 mL aliquot of the reaction mixture was removed every 5 or 10 min using a syringe and analyzed by ^{1}H NMR immediately (3 min before obtaining the spectrum) to monitor the progress of the reaction. A control experiment showed that once the reaction mixture was transferred to the NMR tube, there was no measurable change in the NMR integration of the sample mixture after 4 min, indicating no change in mixture composition during the NMR measurement.

6.4 Results and Discussion

We chose to study the distance between the periphery of fourth-generation, hydroxyl-terminated PAMAM dendrimers (G4-OH), and the surface of encapsulated 40-atom Pd nanoparticles ($D_{Pd\text{-}D}$, Figure 6.1). By measuring the periphery-to-surface distance, we avoid having to make assumptions about the nanoparticle size and shape. The three molecular rulers were configured with a monosubstituted β-cyclodextrin (β-CD) stopper, which is too large to penetrate the dendrimer periphery,[192] at one end and an alkene functional group at the other. We have previously shown that water-soluble *n*-alkene derivatives easily penetrate G4-OH dendrimers and undergo hydrogenation if a Pd nanoparticle is present within.[32,33] The ends of the three rulers, **R1**, **R5**, and **R9**, were separated by alkyl chains containing 1, 5, or 9 methylene groups, yielding ruler lengths of 0.5, 0.9, and 1.3 nm, respectively (Figure 6.2).[193,190,191]

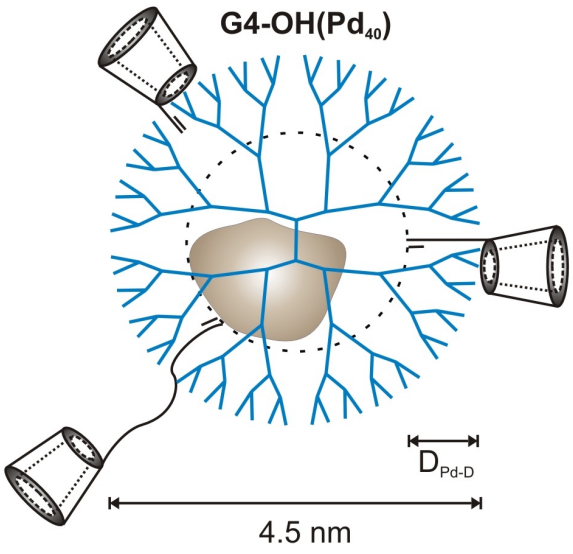

Figure 6.1. Schematic representation of the use of molecular rulers to probe the structure of G4-OH(Pd_{40}) DEMNs.

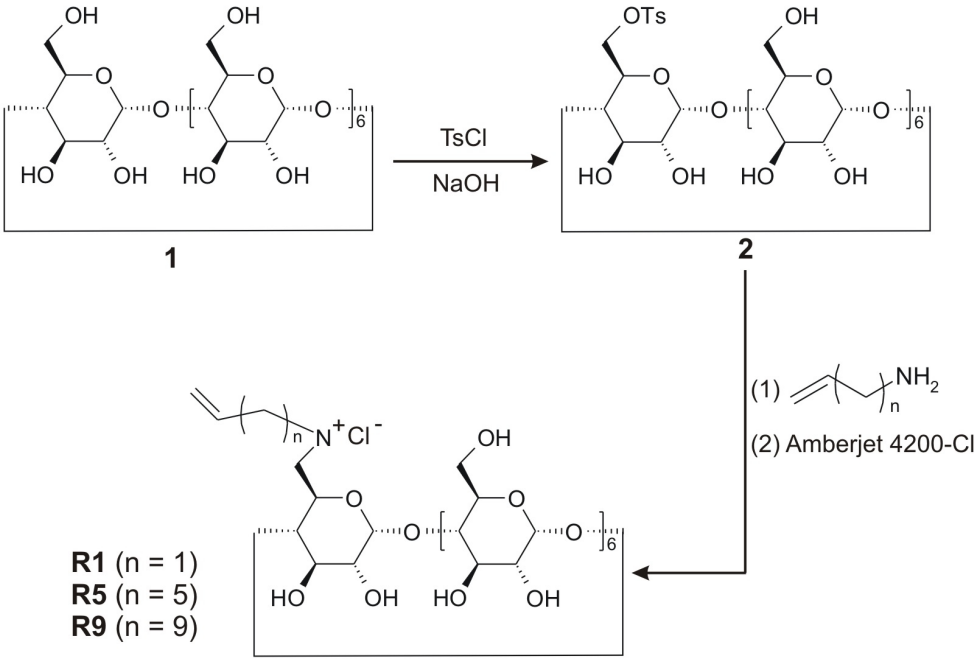

Figure 6.2. Synthesis of molecular rulers.

Prior to determining hydrogenation times using DEMNs we measured the time necessary to hydrogenate each ruler using intrinsically nonselective carbon-supported Pd (Pd/C) catalysts. These experiments were carried out to ensure that differences between reaction rates were attributable to the catalyst rather than to the ruler itself. All reaction times were measured by observing the disappearance of the alkene functional groups by NMR spectroscopy (representative spectra, Figure 6.3). Surprisingly, the results showed that the longest ruler (**R9**) reacted more slowly on Pd/C than the shorter ones (Figure 6.4a). This is likely a consequence of the propensity of alkyl chains to form inclusion complexes with β-CD, which in turn reduce the hydrogenation rate.[194] It was possible to avoid this unintended consequence of using β-CD as the stopper by adding 1-adamantanol to the reaction solution. 1-Adamantanol forms a complex with β-CD (log K ~ 4), and thus reduces the effect of intra- and/or intermolecular complexation between the alkyl chains and β-CD (log K ~ 1 to 3).[194] The time required to hydrogenate the longest ruler before (**R9**) and after (**R9A**) addition of 1-adamantanol dropped from 120 to 50 min. The latter time is within the range (30-60 min) found for hydrogenation of the shorter rulers on Pd/C in the absence (Figure 6.4a) or presence (Figure 6.4b) of 1-adamantanol, and we therefore conclude that this inclusion bias can be avoided.

The dendrimer-based catalyst used in this study consisted of G4-OH containing, on average, 40-atom Pd nanoparticles (G4-OH(Pd_{40})).[5,32,33] It is possible to bracket $D_{Pd\text{-}D}$ by comparing the reaction times for the three rulers. The experimental results show that in the absence (Figure 6.4c) or presence (Figure 6.4d) of 1-adamantanol, the time

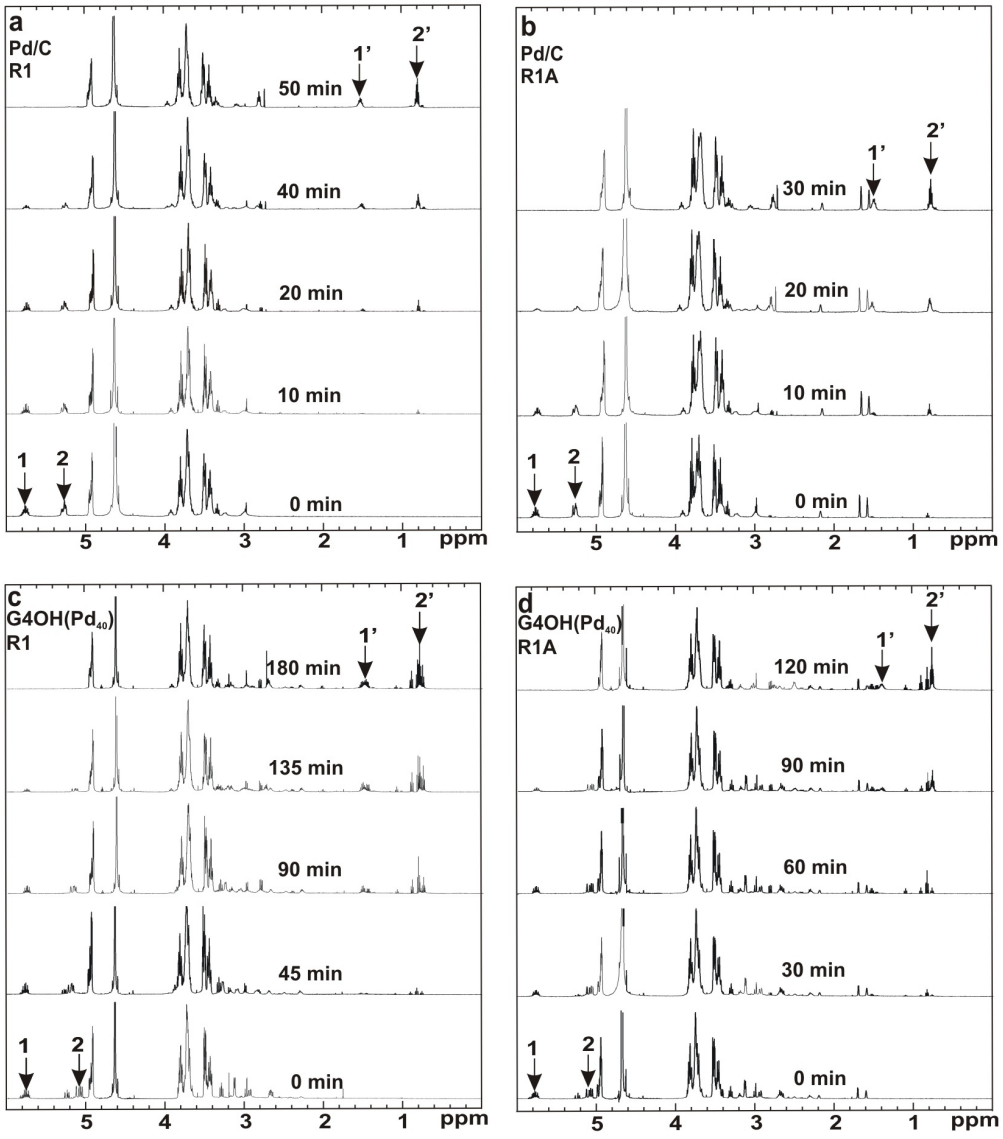

Figure 6.3. ^{1}H NMR spectra of hydrogenation mixtures containing 5 mM molecular ruler in the presence (**R1A**) and absence **(R1**) of 1-adamantanol at various time increments after the hydrogenation reaction commenced (solvent: D_2O). The catalysts were (a) and (b) Pd supported on carbon (5% Pd/C), (c) and (d) G4-OH(Pd_{40}). The substrate/Pd ratio was 10. Chemical shifts of proton(s) on CH= and CH_2= are labeled as **1** and **2**, respectively, while corresponding chemical shifts of those proton(s) after hydrogenation reaction are marked as **1**' and **2**'.

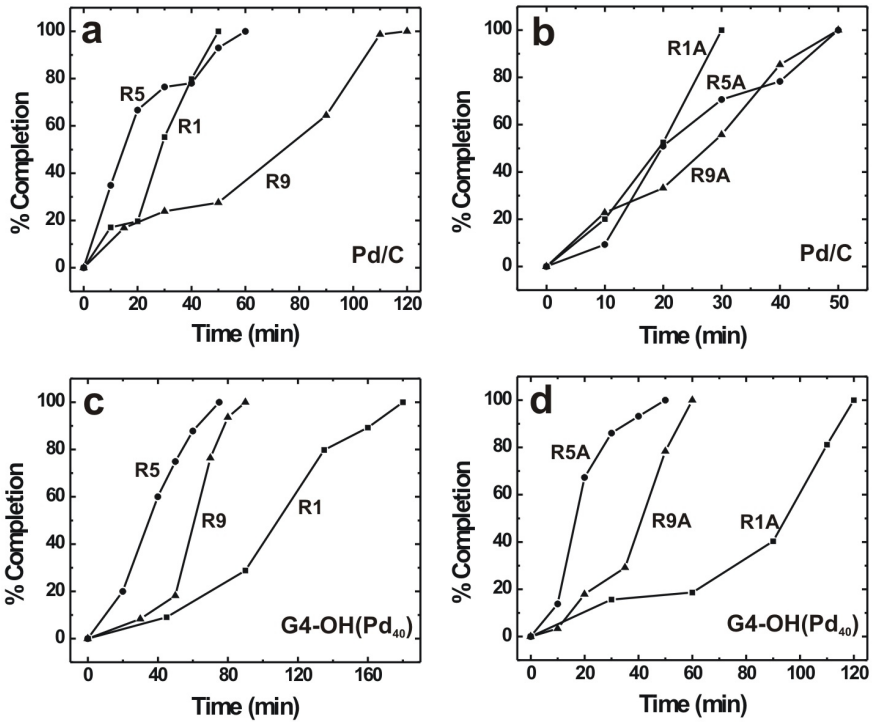

Figure 6.4. Plots of the percentage completion of the hydrogenation reactions as a function of time for aqueous (D_2O) solutions containing 5 mM molecular rulers in the absence (**R1**, **R5**, and **R9**) and presence (**R1A**, **R5A**, and **R9A**) of 1-adamantanol. The catalysts were: (a) and (b) Pd supported on carbon (5% Pd/C); (c) and (d) G4-OH(Pd_{40}). The substrate/Pd ratio was 10. Data were obtained by measuring the disappearance of alkene protons by NMR spectroscopy. The results shown in the figure are the average of two or three independent measurements. The estimated run-to-run variation in the percent completion is ±5%, and the estimated variation in the measurement times is ±5 min.

required to complete the hydrogenation of **R1** (**R1A)** is more than twice that required for **R5** (**R5A**) or **R9** (**R9A**), but the times for **R5** (**R5A**) and **R9** (**R9A**) are very similar. Note also that hydrogenation times for all the rulers are about one-third shorter when they are hydrogenated in the presence of 1-adamantanol.

Because the only difference between the rulers is their length, the results described in the previous paragraph indicate that access of the alkene group of R1 (0.5 nm) to the surface of the encapsulated nanoparticle is hindered compared to R5 (0.9 nm) or R9 (1.3 nm). We conclude that $D_{Pd\text{-}D}$ is between 0.5 nm and 0.9 nm. There are two reasonable explanations for the finding that the hydrogenation of R1 can eventually be completed: (1) the dendrimer and/or the β-CD structures are sufficiently flexible that the rigid model illustrated in Scheme 1 is imperfect; (2) there is a significant distribution in the size, shape, or location of the encapsulated Pd nanoparticles. Both of these explanations are likely to be relevant.

6.5 Summary and Conclusions

In conclusion, we have shown that molecular rulers can be used to estimate the distance between the surface of a dendrimer and the surface of an encapsulated nanoparticle under catalytic conditions. The results show that the surface of the Pd nanoparticles resides, on average, 0.5 – 0.9 nm from the dendrimer surface; that is, $D_{Pd\text{-}D} = 0.7 \pm 0.2$ nm. If we imagine that the Pd nanoparticles are spherical in shape and contain 40 atoms, then they would be 1.1 nm in diameter.[32] To meet the condition that $D_{Pd\text{-}D} = 0.7 \pm 0.2$ nm, the center of the Pd nanoparticle would be displaced 1.0 ± 0.2 nm

from the center of the dendrimer. Because both the dendrimers and nanoparticles used in our study differ substantially from those used in previously reported scattering studies,[28] it is difficult to directly compare results. Nevertheless, both experimental approaches do indicate that the nanoparticles are offset from the center of the dendrimer. However, it is important to remember that the true shape of the nanoparticles is not yet known, and that our experiment is designed primarily to probe the catalytically relevant distance $D_{Pd\text{-}D}$.

The above molecular ruler approach to probe the structure of DEMNs do have a few limitations and the followings are some suggestions on improving the experiment in the future. 1) Monitoring the reaction in a more precise manner. The curves in Figure 6.4 show a lot of variation, which may due to the experimental procedure of using NMR to detect the reaction. Accurate detections can be done via hydrogen uptake, GC or HPLC. 2) Study of higher dendrimer generation (G6 or G8) would be very helpful to support the concept. In this study we found that even the shortest ruler can be catalyzed given enough time. This may due to the relatively more open and flexible structure of smaller generation dendrimer. Because the surface of higher generation dendrimer is more crowded, the difference in reactivity of rulers could be more pronounce.

CHAPTER VII

SUMMARY AND CONCLUSIONS

In this dissertation the synthesis and application of dendrimer-encapsulated metalnanoparticles to catalysis has been investigated. The interactions between dendrimers and charged probe molecules have revealed the special properties of dendrimers. Independent of the type or generation of dendrimer template in which they are synthesized, DEMNs are among the most monodisperse 1-4 nm metal particles thus far reported. These materials have proven to be highly effective homogeneous catalysts for reactions ranging from simple hydrogenations to more sophisticated Heck and Suzuki reactions. One of the most promising aspects of DEMNs is that the dendrimer fraction of the composite can be tailored to induce substrate or product selectivity. Likewise, the periphery of the dendrimer can be configured to render DEMNs soluble in solvents ranging from water to supercritical CO_2, or to attach the dendrimers to surfaces for applications to heterogeneous catalysis. Specificly, our new findings regarding dendrimers can be summaried as follows.

First, the effect of solution pH on the protonation of the dendrimers has been investigated. Specifically, a good correlation of a theoretical calculation based on a multishell model to experimental spectroscopic pH titrations of G4-OH, G4-NH_2 dendrimers has been demonstrated. Such an analysis yields two binding parameters: the intrinsic proton binding constant and a constant that characterizes the strength of electrostatic interactions among occupied binding sites. The significant finding is that

these two factors are greatly modulated by the unique and hydrophobic microenvironment in the dendrimer interior. A key finding is that the intrinsic binding constant (or pK) is reduced by more than 1 pK unit and the strength of electrostatic interactions is reduced by nearly an order of magnitude. Both are attributed to specific ion pairing between bound charges and counter ions.

To prepare metal nanoclusters within amphiphilic dendrimers in organic solution hydrophilic PPI dendrimers were modified with various hydrophobic alkyl chains through an amide linkage. The modified dendrimers were then used as templates for preparing intradendrimer copper nanoclusters by first sorbing Cu^{2+} into the dendrimer interior and then reducing the composite. We found the main driving force for encapsulating metal-ions is the differences in metal-ion solubility between the solvent and the interior of the dendrimer. This method has also been allpied to the preparation of dendrimer/Pd nanoparticles.

Nanometer-sized metal particles are synthesized and encapsulated into the interior of dendrimers by first mixing together the dendrimer and metal ion solution and then reducing the composite chemically, and the resulting dendrimer-encapsulated metal nanoparticles can then be used as homogenous catalysts. The investigation of the size selectively of these DEMNs indicates that by controlling the packing density on the dendrimer periphery by using either different dendrimer generations or dendrimer surface functionalities, it is possible to control access of substrates to the encapsulated catalytic nanoparticle. That is, a non selective catalyst can be rendered with selectivity by simply changing its dendrimer template.

An *in-situ* method was developed to determine the average distance between the surface of dendrimer-encapsulated palladium nanoparticles and the periphery of their fourth-generation, hydroxyl-terminated PAMAM dendrimer hosts. The advantage of measuring the periphery-to-surface distance *in-situ*, is that we avoid having to make assumptions about the nanoparticle size and shape. The measurements were made using molecular rulers consisting of three parts: a catalytically active probe at the distal terminus that may undergo a hydrogenation reaction upon contact with the encapsulated catalyst; a large molecular "stopper" at the proximal end that is unable to enter the host; and intervening alkyl chains having different lengths that tether the probe to the stopper and which therefore define the maximum extension of the ruler. Three molecular rulers were configured with a monosubstituted β-cyclodextrin (β-CD) stopper, which is too large to penetrate the dendrimer periphery, at one end and an alkene functional group at the other. The time necessary to hydrogenate these molecular rulers was monitored by ^{1}H NMR, and this information was then used to estimate the average location of the encapsulated Pd nanoparticles. The data indicate that the surface of the encapsulated nanoparticle is situated 0.7 ± 0.2 nm from the surface of the dendrimer. However, because the limitation of the system and detection method, the results here are very rough and need a more careful study.

Although dendrimers are relatively expensive compared with other commercial catalysts, we have shown that they can be easily recovered and recycled which perhaps makes it possible to consider the use of DEMNs for some real-world applications. An alternative is to use DEMNs as model systems to study structure-function relationships,

and then devise methods to incorporate the same functions into nanoparticles encapsulated within inexpensive star or hyperbranched polymers.

Because of the unique and easily tunable properties of DEMNs, and because of their high degree of uniformity, DEMNs may find applications beyond catalysis. For example, they could be used as tags for bioassays, as active components in nanoelectronics, and as magnetic materials for data storage. For example, Dickson et al. have shown that DEMNs containing just a few Ag atoms are highly fluorescent,[30] and Dai *et al.* have demonstrated that single-walled carbon nanotubes having very narrow diameter distributions can be templated by DEMNs.[195]

REFERENCES

(1) Buhleier, E.; Wehner, W.; Vögtle, F. "Cascade"- and "Nonskid-Chain-Like" Syntheses of Molecular Cavity Topologies. *Synthesis* **1978**, 155-158.

(2) Tomalia, D. A.; Baker, H.; Dewald, J.; Hall, M.; Kallos, G.; Martin, S.; Roeck, J.; Ryder, J.; Smith, P. A New Class of Polymers: Starburst-Dendritic Macromolecules. *Polym. J.* **1985**, *17*, 117-32.

(3) Astruc, D.; Chardac, F. Dendritic Catalysts and Dendrimers in Catalysis. *Chem. Rev.* **2001**, *101*, 2991-3023.

(4) Bosman, A. W.; Jansen, R. A. J. J.; Meijer, E. W. About Dendrimers: Structure, Physical Properties, and Applications. *Chem. Rev.* **1999**, *99*, 1665-1688.

(5) Crooks, R. M.; Zhao, M.; Sun, L.; Chechik, V.; Yeung, L. K. Dendrimer-Encapsulated Nanoparticles: Synthesis, Characterization, and Applications to Catalysis. *Acc. Chem. Res.* **2001**, *34*, 181-190.

(6) Fréchet, J. M. J. Dendrimers and Supramolecular Chemistry. *Proc. Natl. Acad. Sci. USA* **2002**, *99*, 4782-4787.

(7) Newkome, G. R.; Moorefield, C. N.; Vögtle, F. *Dendritic Macromolecules: Concepts, Synthesis, Perspectives*; Wiley-VCH: Weinheim, Germany, 1996.

(8) van Heerbeek, R.; Kamer, P. C. J.; van Leeuwen, P. W. N. M.; Reek, J. N. H. Dendrimers as Support for Recoverable Catalysts and Reagents. *Chem. Rev.* **2002**, *102*, 3717-3756.

(9) Vögtle, F.; Gestermann, S.; Hesse, R.; Schwierz, H.; Windisch, B. Functional Dendrimers. *Prog. Polym. Sci.* **2000**, *25*, 987-1041.

(10) Zimmerman, S. C.; Lawless, L. J. Supramolecular Chemistry of Dendrimers. *Top. Curr. Chem.* **2001**, *217*, 95-120.

(11) Zeng, F.; Zimmerman, S. C. Dendrimers in Supramolecular Chemistry: From Molecular Recognition to Self-Assembly. *Chem. Rev.* **1997**, *97*, 1681-1712.

(12) Kojima, C.; Kono, K.; Maruyama, K.; Takagishi, T. Synthesis of Polyamidoamine Dendrimers Having Poly(Ethylene Glycol) Grafts and their Ability to Encapsulate Anticancer Drugs. *Bioconjugate Chem.* **2000**, *11*, 910-917.

(13) Patri, A. K.; Majoros, I. J.; Baker, J. R., Jr. Dendritic Polymer Macromolecular Carriers for Drug Delivery. *Curr. Opin. Chem. Biol.* **2002**, *6*, 466-471.

(14) Adronov, A.; Fréchet, J. M. J. Light-Harvesting Dendrimers. *Chem. Commun.* **2000**, *18*, 1701-1710.

(15) Adronov, A.; Gilat, S. L.; Fréchet, J. M. J.; Ohta, K.; Neuwahl, F. V. R.; Fleming, G. R. Light Harvesting and Energy Transfer in Laser-Dye-Labeled Poly(Aryl Ether) Dendrimers. *J. Am. Chem. Soc.* **2000**, *122*, 1175-1185.

(16) Swallen, S. F.; Zhu, Z. G.; Moore, J. S.; Kopelman, R. Correlated Excimer Formation and Molecular Rotational Dynamics in Phenylacetylene Dendrimers. *J. Phys. Chem. B* **2000**, *104*, 3988-3995.

(17) Baars, M. W. P. L.; Meijer, E. W. Host-Guest Chemistry of Dendritic Molecules. *Top. Curr. Chem.* **2000**, *210*, 131-182.

(18) Chen, W.; Tomalia, D. A.; Thomas, J. L. Unusual pH-Dependent Polarity Changes in PAMAM Dendrimers: Evidence for pH-Responsive Conformational Changes. *Macromolecules* **2000**, *33*, 9169-9172.

(19) Koper, G. J. M.; van Genderen, M. H. P.; Elissen-Roman, C.; Baars, M. W. P. L.; Meijer, E. W.; Borkovec, M. Protonation Mechanism of Poly(propylene imine) Dendrimers and Some Associated Oligo Amines. *J. Am. Chem. Soc.* **1997**, *119*, 6512-6521.

(20) Sun, L.; Crooks, R. M. Interactions between Dendrimers and Charged Probe Molecules. 1. Theoretical Methods for Simulating Proton and Metal Ion Binding to Symmetric Polydentate Ligands. *J. Phys. Chem. B* **2002**, *106*, 5864-5872.

(21) Niu, Y.; Sun, L.; Crooks, R. M. Interactions between Dendrimers and Charged Probe Molecules: 2. Determination of Intrinsic Proton Binding Constants via Potentiometric pH Titration. *submitted to Macromolecules*.

(22) Crooks, R. M.; Lemon, B. I., III; Sun, L.; Yeung, L. K.; Zhao, M. Dendrimer-Encapsulated Metals and Semiconductors: Synthesis, Characterization, and Applications. *Top. Curr. Chem.* **2001**, *212*, 81-135.

(23) Yeung, L. K.; Lee, C. J., Jr.; Johnston, K. P.; Crooks, R. M. Heck Catalysis in Supercritical CO_2 using Palladium Nanoparticles Encapsulated in Dendrimer Nanoreactors. *Chem. Commun.* **2001**, 2290-2291.

(24) Yeung, L. K.; Crooks, R. M. Heck Heterocoupling within a Dendritic Nanoreactor. *Nano Lett.* **2001**, *1*, 14-17.

(25) Zhao, M.; Sun, L.; Crooks, R. M. Preparation of Cu Nanoclusters within Dendrimer Templates. *J. Am. Chem. Soc.* **1998**, *120*, 4877-4878.

(26) Zhao, M.; Crooks, R. M. Dendrimer-Encapsulated Pt Nanoparticles: Synthesis, Characterization, and Applications to Catalysis. *Adv. Mater.* **1999**, *11*, 217.

(27) Esumi, K.; Suzuki, A.; Yamahira, A.; Torigoe, K. Role of Poly(amidoamine) Dendrimers for Preparing Nanoparticles of Gold, Platinum, and Silver. *Langmuir* **2000**, *16*, 2604-2608.

(28) Gröhn, F.; Bauer, B. J.; Akpalu, Y. A.; Jackson, C. L.; Amis, E. J. Dendrimer Templates for the Formation of Gold Nanoclusters. *Macromolecules* **2000**, *33*, 6042-6050.

(29) Varnavski, O.; Ispasoiu, R. G.; Balogh, L.; Tomalia, D.; Goodson, T., III. Ultrafast Time-Resolved Photoluminescence from Novel Metal-Dendrimer Nanocomposites. *J. Chem. Phys.* **2001**, *114*, 1962-1965.

(30) Zheng, J.; Dickson, R. M. Individual Water-Soluble Dendrimer-Encapsulated Silver Nanodot Fluorescence. *J. Am. Chem. Soc.* **2002**, *124*, 13982-13983.

(31) Lemon, B. I., III; Crooks, R. M. Preparation and Characterization of Dendrimer-Encapsulated CdS Semiconductor Quantum Dots. *J. Am. Chem. Soc.* **2000**, *122*, 12886-12887.

(32) Zhao, M.; Crooks, R. M. Homogeneous Hydrogenation Catalysis with Monodisperse, Dendrimer-Encapsulated Pd and Pt Nanoparticles. *Angew. Chem. Int. Ed.* **1999**, *38*, 364-366.

(33) Niu, Y.; Yeung, L. K.; Crooks, R. M. Size-Selective Hydrogenation of Olefins by Dendrimer-Encapsulated Palladium Nanoparticles. *J. Am. Chem. Soc.* **2001**, *123*, 6840-6846.

(34) Niu, Y.; Alvarez, J.; Crooks, R. M. Molecular Nanorulers as *in-situ* Reporter of Palladium Nanoparticle Encapsulated in Dendrimer. *in preparation*.

(35) Fréchet, J. M. J. Functional Polymers and Dendrimers - Reactivity, Molecular Architecture, and Interfacial Energy. *Science* **1994**, *263*, 1710-1715.

(36) Tomalia, D. A.; Naylor, A. M.; Goddard III, W. A. Starburst Dendrimers: Molecular-Level Control of Size, Shape, Surface Chemistry, Topology, and Flexibility from Atoms to Macroscopic Matter. *Angew. Chem., Int. Ed. Engl.* **1990**, *29*, 138-175.

(37) *Advances in Dendritic Macromolecules*; Newkome, G. R., Ed.; JAI Press: Greenwich, Conn., 1994; Vol. 1.

(38) de Brabander-van den Berg, E. M. M.; Meijer, E. W. Poly(propylenimine) Dendrimers: Large-Scale Synthesis via Heterogeneously Catalyzed Hydrogenation. *Angew. Chem., Int. Ed. Engl.* **1993**, *32*, 1308-1311.

(39) Naylor, A. M.; Goddard III, W. A.; Kaifer, G. E.; Tomalia, D. A. Starburst Dendrimers. 5. Molecular Shape Control. *J. Am. Chem. Soc.* **1989**, *111*, 2339-2341.

(40) Vögtle, F.; Gestermann, S.; Hesse, R.; Schwierz, H.; Windisch, B. Functional Dendrimers. *Prog. Polym. Sci.* **2000**, *25*, 987-1041.

(41) Moors, R.; Vögtle, F. Dendrimeric Polyamines. *Chem. Ber.* **1993**, *126*, 2133-2135.

(42) Moszner, N.; Volkel, T.; Rheinberger, V. Synthesis, Characterization and Polymerization of Dendrimers with Methacrylic End Groups. *Macromol. Chem. Phys.* **1996**, *197*, 621-631.

(43) Baars, M. W. P. L.; Froehling, P. E.; Meijer, E. W. Liquid-Liquid Extractions Using Poly(Propyleneimine) Dendrimers with an Apolar Periphery. *Chem. Commun.* **1997**, 1959-1960.

(44) Archut, A.; Vögtle, F.; De Cola, L.; Azzellini, G. C.; Balzani, V.; Ramanujam, P. S.; Berg, R. H. Azobenzene-Functionalized Cascade Molecules: Photoswitchable Supramolecular Systems. *Chem. Eur. J.* **1998**, *4*, 699-706.

(45) Schenning, A. P. H. J.; Elissen-Roman, C.; Weener, J.-W.; Baars, M. W. P. L.; van der Gaast, S. J.; Meijer, E. W. Amphiphilic Dendrimers as Building Blocks in Supermolecular Assemblies. *J. Am. Chem. Soc.* **1998**, *120*, 8199-8208.

(46) Stevelmans, S.; van Hest, J. C. M.; Jansen, J. F. G. A.; van Boxtel, D. A. F. J.; van den Berg, E. M. M. D.; Meijer, E. W. Synthesis, Characterization, and Guest-Host Properties of Inverted Unimolecular Dendritic Micelles. *J. Am. Chem. Soc.* **1996**, *118*, 7398-7399.

(47) Cooper, A. I.; Londono, J. D.; Wignall, G.; McClain, J. B.; Samulski, E. T.; Lin, J. S.; Dobrynin, A.; Rubinstein, M.; Burke, A. L. C.; Fréchet, J. M. J.; DeSimone, J. M. Extraction of a Hydrophilic Compound from Water into Liquid CO_2 Using Dendritic Surfactants. *Nature* **1997**, *389*, 368-371.

(48) Sandershovens, M. S. T. H.; Jansen, J. F. G. A.; Vekemans, J. A. J. M.; Meijer, E. W. Dendrimers as Chiral Catalysts - a Critical Note. *Polym. Mater. Sci. Eng.* **1995**, *73*, 338-339.

(49) Wiener, E. C.; Auteri, F. P.; Chen, J. W.; Brechbiel, M. W.; Gansow, O. A.; Schneider, D. S.; Belford, R. L.; Clarkson, R. B.; Lauterbur, P. C. Molecular Dynamics of Ion-Chelate Complexes Attached to Dendrimers. *J. Am. Chem. Soc.* **1996**, *118*, 7774-7782.

(50) Pillai, O.; Panchagnula, R. Polymers in Drug Delivery. *Curr. Opin. Chem. Biol.* **2001**, *5*, 447-451.

(51) Esfand, R.; Tomalia, D. A. Poly(Amidoamine) (PAMAM) Dendrimers: From Biomimicry to Drug Delivery and Biomedical Applications. *Drug Discovery To.* **2001**, *6*, 427-436.

(52) Liu, M.; Fréchet, J. M. J. Designing Dendrimers for Drug Delivery. *Pharm. Sci. Technol. To.* **1999**, *1*, 393-401.

(53) Baker, J. R., Jr.; Quintana, A.; Piehler, L.; Banazak-Holl, M.; Tomalia, D.; Raczka, E. The Synthesis and Testing of Anti-Cancer Therapeutic Nanodevices. *Biomedical Microdevices* **2001**, *3*, 61-69.

(54) Konda, S. D.; Aref, M.; Wang, S.; Brechbiel, M.; Wiener, E. C. Specific Targeting of Folate-Dendrimer MRI Contrast Agents to the High Affinity Folate Receptor Expressed in Ovarian Tumor Xenografts. *Magn. Reson. Mater. Phys. Biol. Med.* **2001**, *12*, 104-113.

(55) Wiener, E. C.; Brechbiel, M. W.; Brothers, H.; Magin, R. L.; Gansow, O. A.; Tomalia, D. A.; Lauterbur, P. C. Dendrimer-Based Metal Chelates: A New Class of Magnetic Resonance Imaging Contrast Agents. *Magn. Reson. Med.* **1994**, *31*, 1-8.

(56) Sideratou, Z.; Tsiourvas, D.; Paleos, C. M. Quaternized Poly(Propylene Imine) Dendrimers as Novel pH-Sensitive Controlled-Release Systems. *Langmuir* **2000**, *16*, 1766-1769.

(57) Liu, M.; Kono, K.; Fréchet, J. M. J. Water-Soluble Dendritic Unimolecular Micelles: Their Potential as Drug Delivery Agents. *J. Controlled Release* **2000**, *65*, 121–131.

(58) Liu, M.; Kono, K.; Fréchet, J. M. J. Water-Soluble Dendrimer-Poly(Ethylene Glycol) Starlike Conjugates as Potential Drug Carriers. *J. Polym. Sci. A* **1999**, *37*, 3492–3503.

(59) Roberts, J. C.; Adams, Y. E.; Tomalia, D.; Mercer-Smith, J. A.; Lavallee, D. K. Using Starburst Dendrimers as Linker Molecules to Radiolabel Antibodies. *Bioconjugate Chem.* **1990**, *1*, 305-308.

(60) Fréchet, J. M. J. Functional Polymers and Dendrimers - Reactivity, Molecualr Architechture, and Interfacial Energy. *Science* **1994**, *263*, 1710-1715.

(61) Jansen, J. F. G. A.; de Brabander-van den Berg, E. M. M.; Meijer, E. W. Encapsulation of Guest Molecules into a Dendritic Box. *Science* **1994**, *266*, 1226-1229.

(62) Jansen, J. F. G. A.; de Brabander-van den Berg, E. M. M.; Meijer, E. W. The Dendritic Box: Shape Selective Liberation of Encapsulated Guests. *J. Am. Chem. Soc.* **1995**, *117*, 4417-4418.

(63) Jansen, J. F. G. A.; Peerlings, H. W. I.; de Brabander-Van den Berg, E. M. M.; Meijer, E. W. Optical Activity of Chiral Dendritic Surfaces. *Angew. Chem., Int. Ed. Engl.* **1995**, *34*, 1206-1209.

(64) Jansen, J. F. G. A.; de Brabander - Van Den Berg, E. M. M.; Meijer, E. W., in *New Macromolecular Architecture and Functions, Proceedings of the OUMS'95*, Springer, Toyonaka, Japan, **1995**.

(65) Wallimann, P.; Mattei, S.; Seiler, P.; Diederich, F. New Cyclophanes as Initiator Cores for the Construction of Dendritic Receptors. Host-Guest Complexation in Aqueous Solutions and Structures of Solid-State Inclusion Compounds. *Helv. Chim. Acta* **1997**, *80*, 2368-2390.

(66) Wallimann, P.; Seiler, P.; Diederich, F. Dendrophanes: Novel Steroid-Recognizing Dendritic Receptors. *Helv. Chim. Acta* **1996**, *79*, 779-788.

(67) Mattei, S.; Seiler, P.; Diederich, F.; Gramlich, V. Dendrophanes: Water-Soluble Dendritic Receptors. *Helv. Chim. Acta* **1995**, *78*, 1904-1912.

(68) Castro, R.; Cuadrado, I.; Alonso, B.; Casado, C. M.; Moran, M.; Kaifer, A. E. Multisite Inclusion Complexation of Redox Active Dendrimer Guests. *J. Am. Chem. Soc.* **1997**, *119*, 5760-5761.

(69) Bar-Haim, A.; Klafter, J. Geometric versus Energetic Competition in Light Harvesting by Dendrimers. *J. Phys. Chem. B* **1998**, *102*, 1662-1664.

(70) Bar-Haim, A.; Klafter, J. Dendrimers as Light Harvesting Antennae. *J. Lumin.* **1998**, *76&77*, 197-200.

(71) Shortreed, M. R.; Swallen, S. F.; Shi, Z.-Y.; Tan, W.; Xu, Z.; Devadoss, C.; Moore, J. S.; Kopelman, R. Directed Energy Transfer Funnels in Dendrimeric Antenna Supermolecules. *J. Phys. Chem. B* **1997**, *101*, 6318-6322.

(72) Gilat, S. L.; Adronov, A.; Fréchet, J. M. J. Modular Approach to the Accelerated Convergent Growth of Laser Dye-Labeled Poly(Aryl Ether) Dendrimers Using a Novel Hypermonomer. *J. Org. Chem.* **1999**, *64*, 7474-7484.

(73) Gilat, S. L.; Adronov, A.; Fréchet, J. M. J. Light Harvesting and Energy Transfer in Novel Convergently Constructed Dendrimers. *Angew. Chem., Int. Ed. Engl.* **1999**, *38*, 1422-1427.

(74) Schenning, A. P. H. J.; Peeters, E.; Meijer, E. W. Energy Transfer in Supramolecular Assemblies of Oligo(p-phenylene vinylene)s Terminated Poly(propylene imine) Dendrimers. *J. Am. Chem. Soc.* **2000**, *122*, 4489-4495.

(75) Zhao, M.; Sun, L.; Crooks, R. M. Preparation of Cu Nanoclusters within Dendrimer Templates. *J. Am. Chem. Soc.* **1998**, *120*, 4877.

(76) Scott, R. W. J.; Datye, A. K.; Crooks, R. M. Bimetallic Palladium-Platinum Dendrimer-Encapsulated Catalysts. *J. Am. Chem. Soc.* **2003**, in press.

(77) Twyman, L. J.; King, A. S. H. Catalysis Using Peripherally Functionalized Dendrimers. *J. Chem. Res. -S* **2002**, *2*, 43-59.

(78) Reetz, M. T.; Lohmer, G.; Schwickardi, R. Synthesis and Catalytic Activity of Dendritic Diphosphane Metal Complexes. *Angew. Chem., Int. Ed. Engl.* **1997**, *36*, 1526-1529.

(79) Adams, R. D.; Cotton, F. A. *Catalysis by di- and Polynuclear Metal Cluster Complexes*; Wiley-VCH: New York, 1998.

(80) Kleij, A. W.; Gossage, R. A.; Jastrzebski, J. T. B. H.; Boersma, J.; van Koten, G. The "Dendritic Effect" in Homogeneous Catalysis with Carbosilane-Supported Arylnickel (II) Catalysts: Observation of Active-Site Proximity Effects in Atom-Transfer Radical Addition. *Angew. Chem. Int. Ed.* **2000**, *39*, 176-178.

(81) Twyman, L. J.; King, A. S. H.; Martin, I. K. Catalysis inside Dendrimers. *Chem. Soc. Rev.* **2002**, *31*, 69-82.

(82) Oosterom, G. E.; Reek, J. N. H.; Kamer, P. C. J.; Van Leeuwen, P. W. N. M. Transition Metal Catalysis Using Functionalized Dendrimers. *Angew. Chem. Int. Ed.* **2001**, *40*, 1828-1849.

(83) Kreiter, R.; Kleij, A. W.; Gebbink, R. J. M. K.; van Koten, G. Dendritic Catalysts. *Top. Curr. Chem.* **2001**, *217*, 163-199.

(84) Oosterom, G. E.; van Haaren, R. J.; Reek, J. N. H.; Kamer, P. C. J.; van Leeuwen, P. W. N. M. Catalysis in the Core of a Carbosilane Dendrimer. *Chem. Commun.* **1999**, 1119-1120.

(85) Both dendrimer can be purchased from Aldrich Chemical Co. (Milwaukee, WI). PAMAM dendrimers are produced by Dendritech, Inc. (Midland, MI). PPI dendrimers are prodiuced by DSM Fine Chemicals (The Netherlands).

(86) Ottaviani, M. F.; Montalti, F.; Romanelli, M.; Turro, N. J.; Tomalia, D. A. Characterization of Starburst Dendrimers by EPR. 4. Mn(II) as a Probe of Interphase Properties. *J. Phys. Chem.* **1996**, *100*, 11033-11042.

(87) Zhao, M.; Crooks, R. M. Intradendrimer Exchange of Metal Nanoparticles. *Chem. Mater.* **1999**, *11*, 3379-3385.

(88) Bosman, A. W.; Schenning, A. P. H. J.; Janssen, R. A. J. J.; Meijer, E. W. Well-Defined Metallodendrimers by Site-Specific Complexation. *Chem. Ber./Recueil* **1997**, *130*, 725-728.

(89) Floriano, P. N.; Noble, C. O.; Schoonmaker, J. M.; Poliakoff, E. D.; McCarley, R. L. Cu(0) Nanoclusters Derived from Poly(propylene imine) Dendrimer Complexes of Cu(II). *J. Am. Chem. Soc.* **2001**, *123*, 10545-10553.

(90) Zhou, L.; Russell, D. H.; Zhao, M.; Crooks, R. M. Characterization of Poly(amidoamine) Dendrimers and Their Complexes with Cu^{2+} by Matrix Assisted Laser Desorption Ionization Mass Spectrometry. *Macromolecules* **2001**, *34*, 3567-3573.

(91) Chechik, V.; Zhao, M.; Crooks, R. M. Self-Assembled Inverted Micelles Prepared from a Dendrimer Template: Phase Transfer of Encapsulated Guests. *J. Am. Chem. Soc.* **1999**, *121*, 4910-4911.

(92) Curtis, A. C.; Duff, D. G.; Edwards, P. P.; Jefferson, D. A.; Johnson, B. F. G.; Kirkland, A. I.; Wallace, A. S. A. A Morphology-Selective Copper Organosol. *Angew. Chem., Int. Ed. Engl.* **1988**, *27*, 1530-1533.

(93) Lisiecki, I.; Pileni, M. P. Synthesis of Copper Metallic Clusters Using Reverse Micelles as Microreactors. *J. Am. Chem. Soc.* **1993**, *115*, 3887-3896.

(94) Li, Y.; El-Sayed, M. A. The Effect of Stabilizers on the Catalytic Activity and Stability of Pd Colloidal Nanoparticles in the Suzuki Reactions in Aqueous Solution. *J. Phys. Chem. B* **2001**, *105*, 8938-8943.

(95) Oh, S.-K.; Niu, Y.; Crooks, R. M., *in preparation*.

(96) *Clusters and Nanomaterials: Theory and Experiment*; Kawazoe, Y.; Kondow, T.; Ohno, K., Eds.; Springer: Berlin, 2002.

(97) *Clusters and Colloides: From Theory to Applications*; Schmid, G., Ed.; VCH: Weinheim, Germany, 1994.

(98) Häeberlen, O. D.; Chung, S.-C.; Stener, M.; Röesch, N. From Clusters to Bulk: A Relativistic Density Functional Investigation on a Series of Gold Clusters Au_n, n = 6,...,147. *J. Chem. Phys.* **1997**, *106*, 5189-5201.

(99) Chechik, V.; Crooks, R. M. Dendrimer-Encapsulated Pd Nanoparticles as Fluorous Phase-Soluble Catalysts. *J. Am. Chem. Soc.* **2000**, *122*, 1243.

(100) Sayed-Sweet, Y.; Hedstrand, D. M.; Spinder, R.; Tomalia, D. A. Hydrophobically Modified Poly(amidoamine) (PAMAM) Dendrimers: Their Properties at the Air-Water Interface and Use as Nanoscopic Container Molecules. *J. Mater. Chem.* **1997**, *7*, 1199-1205.

(101) Esumi, K.; Hosoya, T.; Suzuki, A.; Torigoe, K. Preparation of Hydrophobically Modified Poly(amidoamine) Dendrimer-Encapsulated Gold Nanoparticles in Organic Solvents. *J. Colloid Interf. Sci.* **2000**, *229*, 303-306.

(102) Esumi, K.; Nakamura, R.; Suzuki, A.; Torigoe, K. Preparation of Platinum Nanoparticles in Ethyl Acetate in the Presence of Poly(amidoamine) Dendrimers with a Methyl Ester Terminal Group. *Langmuir* **2000**, *16*, 7842-7846.

(103) Niu, Y.; Crooks, R. M. Preparation of Dendrimer-Encapsulated Metal Nanoparticles using Organic Solvents. *in preparation*.

(104) Gates, B. C. Supported Metal Clusters: Synthesis, Structure, and Catalysis. *Chem. Rev.* **1995**, *95*, 511-522.

(105) Valden, M.; Lai, X.; Goodman, D. W. Onset of Catalytic Activity of Gold Clusters on Titania with the Appearance of Nonmetallic Properties. *Science* **1998**, *281*, 1647-1650.

(106) Hirai, H. Formation and Catalytic Functionality of Synthetic Polymer-Noble Metal Colloid. *J. Macromol. Sci.-Chem.* **1979**, *A13*, 633-649.

(107) Kiwi, J.; Graetzel, M. Projection, Size Factors, and Reaction Dynamics of Colloidal Redox Catalysts Mediating Light Induced Hydrogen Evolution from Water. *J. Am. Chem. Soc.* **1979**, *101*, 7214-7217.

(108) Templeton, A. C.; Wuelfing, W. P.; Murray, R. W. Monolayer-Protected Cluster Molecules. *Acc. Chem. Res.* **2000**, *33*, 27-36.

(109) Brust, M.; Fink, J.; Bethell, D.; Schiffrin, D. J.; Kiely, C. Synthesis and Reactions of Functionalized Gold Nanoparticles. *Chem. Commun.* **1995**, *16*, 1655-1656.

(110) Pileni, M. P. Colloidal Self-Assemblies Used as Templates to Control Size, Shape and Self-organization of Nanoparticles. *Supramol. Sci.* **1998**, *5*, 321-329.

(111) Králik, M.; Biffis, A. Catalysis by Metal Nanoparticles Supported on Functional Organic Polymers. *J. Mol. Catal. A-Chem.* **2001**, *177*, 113-138.

(112) Mayer, A. B. R. Colloidal Metal Nanoparticles Dispersed in Amphiphilic Polymers. *Polym. Adv. Technol.* **2001**, *12*, 96-106.

(113) Rylander, P. N. *Catalytic Hydrogenation in Organic Syntheses*; Academic Press: New York, 1979.

(114) Rylander, P. N. *Catalysis in Organic Syntheses*; Academic Press: New York, 1980.

(115) Chai, M.; Niu, Y.; Youngs, W. J.; Rinaldi, P. L. Structure and Conformation of DAB Dendrimers in Solution via Multidimensional NMR Techniques. *J. Am. Chem. Soc.* **2001**, *123*, 4670-4678.

(116) Murat, M.; Grest, G. S. Molecular Dynamics Study of Dendrimer Molecules in Solvents of Varying Quality. *Macromolecules* **1996**, *29*, 1278-1285.

(117) Jessop, P. G.; Ikariya, T.; Noyori, R. Homogeneous Catalysis in Supercritical Fluids. *Chem. Rev.* **1999**, *99*, 475.

(118) Horváth, I. T.; Raba, J. Facile Catalyst Separation without Water: Fluorous Biphasic Hydroformylation of Olefins. *Science* **1994**, *266*, 72-75.

(119) Richter, B.; Spek, A. L.; van Koten, G.; Deelman, B.-J. Fluorous Versions of Wilkinson's Catalyst. Activity in Fluorous Hydrogenation of 1-Alkenes and Recycling by Fluorous Biphasic Separation. *J. Am. Chem. Soc.* **2000**, *122*, 3945-3951.

(120) Kendall, J. L.; Canelas, D. A.; Young, J. L.; DeSimone, J. M. Polymerizations in Supercritical Carbon Dioxide. *Chem. Rev.* **1999**, *99*, 543-564.

(121) Darr, J. A.; Poliakoff, M. New Directions in Inorganic and Metal-Organic Coordination Chemistry in Supercritical Fluids. *Chem. Rev.* **1999**, *99*, 495-542.

(122) Dijkstra, H. P.; van Klink, G. P. M.; van Koten, G. The Use of Ultra- and Nanofiltration Techniques in Homogeneous Catalyst Recycling. *Acc. Chem. Res.* **2002**, *35*, 798-810.

(123) Inoue, K. Functional Dendrimers, Hyperbranched and Star Polymers. *Prog. Polym. Sci.* **2000**, *25*, 453-571.

(124) Sun, L.; Crooks, R. M. Dendrimer-Mediated Immobilization of Catalytic Nanoparticles on Flat, Solid Supports. *Langmuir* **2002**, *18*, 8231-8236.

(125) Ruckenstein, E.; Yin, W. SiO_2-Poly(amidoamine) Dendrimer Inorganic/Organic Hybrids. *J. Polym. Sci. Part A: Polym. Chem.* **2000**, *38*, 1443-1449.

(126) Kreibig, U.; Vollmer, M. *Optical Properties of Metal Clusters*; Springer-Verlag: Berlin, 1995.

(127) Kreibig, U.; Genzel, L. Optical Absorption of Small Metallic Particles. *Surf. Sci.* **1985**, *156*, 678-700.

(128) Bozzola, J. J.; Russell, L. D. *Electron Microscopy: Principles and Techniques for Biologists*; 2nd ed.; Jones and Bartlett: Sudbury, Mass., 1999.

(129) Watt, I. M. *The Principles and Practice of Electron Microscopy*; 2nd ed.; Cambridge University Press: Cambridge; New York, 1997.

(130) Hayat, M. A. *Positive Staining for Electron Microscopy*; Van Nostrand Reinhold Co.: New York, 1975.

(131) Hayat, M. A. *Stains and Cytochemical Methods*; Plenum Press: New York, 1993.

(132) *Practical Surface Analysis*; 2nd ed.; Briggs, D.; Seah, M. P., Eds.; John Wiley & Sons Ltd.: Chichester ; New York, 1990; Vol. 1.

(133) Borkovec, M.; Koper, G. J. M. Ising Models of Polyprotic Acids and Bases. *J. Phys. Chem.* **1994**, *98*, 6038-6045.

(134) This is the ionic strength at the end of a titration, where the initial HCl is completely converted to NaCl. At the beginning of the titration, the majority of HCl binds with dendrimer, and the ionic strength is somewhat undefined. For example, the ionic strength is lower than the value quoted here if we exclude the contribution from the molecules being studied: i.e. charged dendrimer molecules and their associated counter ions. Otherwise, a higher value will be obtained because a highly charged dendrimer molecule contributes more to ionic strength than a simple 1:1 salt.

(135) *Lange's Handbook of Chemistry*; 13 ed.; Dean, J. A.; Lange, N. A., Eds.; McGraw-Hill: New York, 1985.

(136) Diameters used here are literature values measured using either size-exclusion chromatography or small-angle neutron scattering: see, for example, Crooks, R. M.; Lemon III, B. I.; Sun, L.; Yeung, L. K.; Zhao, M. Dendrimer-Encapsulated Metals and Semiconductors: Synthesis, Characterization, and Applications. in *Top. Cur. Chem.*, Vol. 212; Springer-Verlag: Berlin, 2001; pp. 81-135.

(137) Eq 3.4 has exactly the same form as a well-known theory for analyzing protonation of colloids and polymers. In fact, $G(\bar{h})$ has already been used to model protonation of a cascade dendrimer: see, for example, Zhang, H.; Dubin, P. L.; Kaplan, J.; Moorefield, C. N.; Newkome, G. R. Dissociation of Carboxyl-Terminated Cascade Polymers: Comparison with Theory. *J. Phys. Chem. B* **1997**, *101*, 3494-3497.

(138) Tanford, C. *Physical Chemistry of Macromolecules*; Wiley: New York, 1961.

(139) Pistolis, G.; Malliaris, A.; Paleos, C. M.; Tsiourvas, D. Study of Poly(amidoamine)Starburst Dendrimers by Fluorescence Probing. *Langmuir* **1997**, *13*, 5870-5875.

(140) The dielectric constant was estimated using a peak ratio method. Unfortunately, the value quoted here is for a G2-NH2 PAMAM dendrimer. An alternative probe has also been used to study the PAMAM interior up to G8 generation, but the interior dielectric constant is not quantified: Richter-Egger, D. L.; Landry, J. C.; Tesfai, A.; Tucker, S. A. Spectroscopic Investigations of Polyamodo Amine Starburst Dendrimers Using the Solvatochromic Probe Phenol Blue. *J. Phys. Chem. A* **2001**, *105*, 6826-6833.

(141) This is the value for a PAMAM dendrimer with an ammonia core (3 branches) whereas the dendrimer we used has an ethylene diamine core (4 branches). Thus, the value quoted here might be an upper limit because we expect a smaller electrolyte volume for the 4-branch core.

(142) Nisato, G.; Ivkov, R.; Amis, E. J. Size Invariance of Polyelectrolyte Dendrimers. *Macromolecules* **2000**, *33*, 4172-4176.

(143) Newkome, G. R.; Young, J. K.; Baker, G. R.; Potter, R. L.; Audoly, L.; Cooper, D.; Weis, C. D.; Morris, K.; Johnson, C. S., Jr. Cascade Polymers. pH Denpendence of Hydrodynamic Radii of Acid Terminated Dendrimers. *Macromolecules* **1993**, *26*, 2394-2396.

(144) Martell, A. E.; Smith, R. M.; Motekaitis, R. J. NIST Critically Selected Stability Constants of Metal Complexes. **2000**, *Database 46, Version 6*.

(145) This expression gives the electric potential energy around an ion according to Debye-Hückel's theory of electrolyte. The size of counter ions has been set to zero, as it is also assumed in our shell model.

(146) Only a rough estimate of r_{AVG} is used here: the average dynamic distance between two terminal amines is estimated to be 0.4 nm using established C-N and C-C bond lengths and the root-mean-square formula described in reference 17 (only applicable when the intervening C-N and C-C bonds have complete translational and rotational freedom). As expected, this value is comparable to the average radius difference (0.35 nm to 0.45 nm) between two neighboring shells of a PAMAM dendrimer because these shells are separated by roughly the same number of covalent bonds. Other implied assumptions in eq 8 are (a) only mobile ion distribution around one of the amine sites is considered whereas (b) the other site is treated as a non-perturbing test charge.

(147) Vieux, A. S.; Rutagengwa, N. Organic Phase Species in the Extraction of Hydrochloric Acid by Triisootylamine in Various Organic Diluents. *J. Phys. Chem.* **1976**, *80*, 1283-1291.

(148) Mayer, U. Solvent Effects on Ion-Pair Equilibria. *Coord. Chem. Rev.* **1976**, *21*, 159-179.

(149) Huang, Q. R.; Dubin, P. L.; Moorefield, C. N.; Newkome, G. R. Counterion Binding on Charged Spheres: Effect of pH and Ionic Strength on the Mobility of Carboxyl-Terminated Dendrimers. *J. Phys. Chem. B* **2000**, *104*, 898-904.

(150) The activity coefficient for proton *H* has already been included because the pH meter directly measures activity. Thus, a *K* determined from Figure 2A is equal to a binding constant (at infinite dilution) times γ_{HA}/γ_A, where γ_{HA} and γ_A are activity coefficients. For a neutral binding ligand *A* (i.e., the amine), *HA* would be positively charged: so γ_{HA} is expected to be smaller than γ_A, and the ratio γ_{HA}/γ_A will decrease as ionic strength increases. As a result, *pK* will increase as ionic strength increases.

(151) The compound, denoted as M1 in the following reference, contains a tertiary amine connected to two amide bonds through ethylene linkers: Barbucci, R.; Casolaro, M.; Danzo, N.; Beni, M. C.; Barone, V.; Ferruti, P. Thermodynamics of Protonation and Complex Formation of Multifunctional Polymers. *Gazz. Chim. Ital.* **1982**, *112*, 105-113.

(152) Mehler, E. L.; Fuxreiter, M.; Simon, I.; B., G.-M. E. The Role of Hydrophobic Microenvironments in Modulating pKa Shifts in Proteins. *Proteins* **2002**, *48*, 283-292.

(153) We have been careful to not overspecify the number of adjustable parameters. Here, only two scaling factors are chosen: one for the charges on the outmost shell and the other for charges in all the inner shells. These factors can be determined reliably from the two sets of titration data for G4-OH and for G4-NH_2. However, this might not be the case if more scaling factors (e.g., one for each shell) were used.

(154) The compound we selected is N-acetylethylenediamine: a primary amine linked to one amide bond through an ethylene linker. Its pK is 9.28: see Hall, H. K., Jr. Field and Inductive Effects on the Base Strengths of Amines. *J. Am. Chem. Soc.* **1956**, *78*, 2570-2572.

(155) Emrick, T.; Fréchet, J. M. J. Self-Assembly of Dendritic Structures. *Curr. Opin. Colloid Interface Sci.* **1999**, *4*, 457.

(156) Fischer, M.; Vögtle, F. Dendrimers: From Design to Application - A Progress Report. *Angew. Chem. Int. Ed.* **1999**, *38*, 885-905.

(157) Walker, C. H.; St. John, J. V.; Wisian-Neilson, P. Synthesis and Size Control of Gold Nanoparticles Stabilized by Poly(methylphenylphosphazene). *J. Am. Chem. Soc.* **2001**, *123*, 3846-3847.

(158) Brown, L. O.; Hutchison, J. E. Convenient Preparation of Stable, Narrow-Dispersity, Gold Nanocrystals by Ligand Exchange Reactions. *J. Am. Chem. Soc.* **1997**, *119*, 12384-12385.

(159) Brown, L. O.; Hutchison, J. E. Controlled Growth of Gold Nanoparticles during Ligand Exchange. *J. Am. Chem. Soc.* **1999**, *121*, 882-883.

(160) Stevelmans, S.; vanHest, J. C. M.; Jansen, J. F. G. A.; van Boxtel, D. A. F. J.; de Brabander-van den Berg, E. M. M.; Meijer, E. W. Synthesis, Characterization, and Guest-Host Properties of Inverted Unimolecular Dendritic Micelles. *J. Am. Chem. Soc.* **1996**, *118*, 7398-7399.

(161) Liu, M.; Fréchet, J. M. J. Preparation, MALDI-TOF Analysis, and Micelle-like Behavior of Alkyl-Modified Poly(propylene imine) Dendrimers. *Polym. Bull.* **1999**, *43*, 379-386.

(162) $Cu(OAc)_2$ and related complexes were avoided in this study, because their d-d transitions are too close to where the Cu-N d-d transition occurs.

(163) The size of a spheroidal particle containing 20 close-packed Pd atoms should be 0.9 nm in diameter.

(164) Selvaraj, P. C.; Mahadevan, V. Polymer-Supported Palladium and Rhodium Species as Hydrogenation Catalysts. *J. Polym. Sci. Part A: Polym. Chem.* **1997**, *35*, 105.

(165) Because no reference is available for the dielectric constant value of poly(propylene imine) dendrimer, the value quoted here is for a G2-NH_2 PAMAM dendrimer using a fluorescent pyrene probe: Pistolis, G.; Malliaris, A.;

Paleos, C. M.; Tsiourvas, D. Langmuir 1997, 13, 5870-5875. An estimated value of 23 can be inferred from their data. An alternative probe has also been used to study the PAMAM interior up to G8 generation, but the interior dielectric constant is not quantified: Richter-Egger, D. L.; Landry, J. C.; Tesfai, A.; Tucker, S. A. J. Phys. Chem. A 2001, 105, 6826-6833.

(166) Sanchez, C.; de Soler-Illia, G. J.; Ribot, F.; Lalot, T.; Mayer, C. R.; Cabuil, V. Designed Hybrid Organic-Inorganic Nanocomposites from Functional Nanobuilding Blocks. *Chem. Mater.* **2001**, *13*, 3061-3083.

(167) Gao, H. Y.; Carlson, J.; Stalcup, A. M.; Heineman, W. R. Separation of Aromatic Acids, DOPA, and Methyl-DOPA by Capillary Electrophoresis with Dendrimers as Buffer Additives. *J. Chromatogr. Sci.* **1998**, *36*, 146-154.

(168) Gray, A. L.; Hsu, J. T. Novel Sulfonic Acid-Modified Starburst Dendrimer Used as a Pseudostationary Phase in Electrokinetic Chromatography. *J. Chromatogr. A* **1998**, *824*, 119-124.

(169) Dermody, D. L.; Peez, R. F.; Bergbreiter, D. E.; Crooks, R. M. Chemically Grafted Polymeric Filters for Chemical Sensors: Hyperbranched Poly(acrylic acid) Films Incorporating beta-Cyclodextrin Receptors and Amine-Functionalized Filter Layers. *Langmuir* **1999**, *15*, 885-890.

(170) Liu, Y.; Zhao, M.; Bergbreiter, D. E.; Crooks, R. M. pH-Switchable, Ultrathin Permselective Membranes Prepared from Multilayer Polymer Composites. *J. Am. Chem. Soc.* **1997**, *119*, 8720-8721.

(171) Kriesel, J. W.; Tilley, T. D. Dendrimers as Building Blocks for Nanostructured Materials: Micro- and Mesoporosity in Dendrimer-Based Xerogels. *Chem. Mater.* **1999**, *11*, 1190.

(172) Kovvali, A. S.; Chen, H.; Sirkar, K. K. Dendrimer Membranes: A CO_2-Selective Molecular Gate. *J. Am. Chem. Soc.* **2000**, *22*, 7594-7595.

(173) Bhyrappa, P.; Vaijayanthimala, G.; Suslick, K. S. Shape-Selective Ligation to Dendrimer-Metalloporphyrins. *J. Am. Chem. Soc.* **1999**, *121*, 262-263.

(174) Bhyrappa, P.; Young, J. K.; Moore, J. S.; Suslick, K. S. Dendrimer-Metalloporphyrins: Synthesis and Catalysis. *J. Am. Chem. Soc.* **1996**, *118*, 5708-5711.

(175) Bhyrappa, P.; Young, J. K.; Moore, J. S.; Suslick, K. S. Shape Selective Epoxidation of Alkenes by Metalloporphyrin-Dendrimers. *J. Mol. Catal. A-Chem.* **1996**, *113*, 109-116.

(176) Fan, Q. H.; Chen, Y. M.; Chen, X. M.; Jiang, D. Z.; Xi, F.; Chan, A. S. C. Highly Effective and Recyclable Dendritic BINAP Ligands for Asymmetric Hydrogenation. *Chem. Commun.* **2000**, *9*, 789-790.

(177) Chow, H. F.; Mak, C. C. Dendritic Bis(oxazoline)copper(II) Catalysts .2. Synthesis, Reactivity, and Substrate Selectivity. *J. Org. Chem.* **1997**, *62*, 5116-5127.

(178) Lewis, L. N. Chemical Catalysis by Colloids and Clusters. *Chem. Rev.* **1993**, *93*, 2693-2730.

(179) Topp, A.; Bauer, B. J.; Klimash, J. W.; Spindler, R.; Tomalia, D. A.; Amis, E. J. Probing the Location of the Terminal Groups of Dendrimers in Dilute Solution. *Macromolecules* **1999**, *32*, 7226-7231.

(180) Information provided by Dendritech Inc.; Midland; MI.

(181) Sulman, E.; Bodrova, Y.; Matveeva, V.; Semagina, N.; Cerveny, L.; Kurtc, V.; Bronstein, L.; Platonova, O.; Valetsky, P. Hydrogenation of Dehydrolinalool with Novel Catalyst Derived from Pd Colloids Stabilized in Micelle Cores of Polystyrene-Poly-4-Vinylpyridine Block Copolymers. *Applied Catalysis A-General* **1999**, *176*, 75-81.

(182) Augustine, R. L.; Warner, R. W.; Melnick, M. J. Heterogeneous Catalysis in Organic-Chemistry. 3. Competitive Adsorption of Solvents During Alkene Hydrogenations. *J. Org. Chem.* **1984**, *49*, 4853-4856.

(183) Ronchina, L.; Tonioloa, L.; Cavinato, G. Hydrogenation of Mandelic Acid Derivatives to the Corresponding Phenyl Acetic Acid Derivative Catalysed by Pd/C. A Kinetic Study. *Appl. Catal. A* **1997**, *165*, 133-145.

(184) Collier, P. J.; Iggo, J. A.; Whyman, R. Preparation and Characterisation of Solvent-Stabilised Nanoparticulate Platinum and Palladium and their Catalytic Behaviour towards the Enantioselective Hydrogenation of Ethyl Pyruvate. *J. Mol. Catal. A-Chem.* **1999**, *146*, 149-157.

(185) Augustine, R. L.; Tanielyan, S. K.; Doyle, L. K. Enantioselective Heterogeneous Catalysis. 1. A Working Model for the Catalyst-Modifier-Substrate Interactions in Chiral Pyruvate Hydrogenations. *Tetrahedron-Asymmetry* **1993**, *4*, 1803-1827.

(186) Zhao, M.; Tokuhisa, H.; Crooks, R. M. Interactions Between Organized, Surface-Confined Monolayers and Liquid-Phase Probe Molecules. 5. Molecule-Sized Gates Based on Surface-Confined Dendrimers. *Angew. Chem. Int. Ed. Engl.* **1997**, *36*, 2596-2598.

(187) Jackson, C. L.; Chanzy, H. D.; Booy, F. P.; Drake, B. J.; Tomalia, D. A.; Bauer, B. J.; Amis, E. J. Visualization of Dendrimer Molecules by Transmission Electron Microscopy (TEM): Staining Methods and Cryo-TEM of Vitrified Solutions. *Macromolecules* **1998**, *31*, 6259-6265.

(188) Hierlemann, A.; Campbell, J. K.; Baker, L. A.; Crooks, R. M.; Ricco, A. J. Structural Distortion of Dendrimers on Gold Surfaces: A Tapping-Mode AFM Investigation. *J. Am. Chem. Soc.* **1998**, *120*, 5323-5324.

(189) Tokuhisa, H.; Zhao, M.; Baker, L. A.; Phan, V. T.; Dermody, D. L.; Garcia, M. E.; Peez, R. F.; Crooks, R. M.; Mayer, T. M. Preparation and Characterization of Dendrimer Monolayers and Dendrimer-Alkanethiol Mixed Monolayers Adsorbed to Gold. *J. Am. Chem. Soc.* **1998**, *120*, 4492-4501.

(190) Petter, R. C.; Salek, J. S.; Sikorski, C. T.; Kumaravel, G.; Lin, F.-T. Cooperative Binding by Aggregated Mono-6-(alkylamino)-β-Cyclodextrins. *J. Am. Chem. Soc.* **1990**, *112*, 3860-3868.

(191) Graham, R. L.; Bain, C. D.; Biebuyck, H. A.; Laibinis, P. E.; Whitesides, G. M. Damage to CF_3CONH-Terminated Organic Self-Assembled Monolayers (SAMs) on Al, Ti, Cu, and Au by Al Kα X-Rays Is Due Principally to Electrons. *J. Phys. Chem.* **1993**, *97*, 9456-9464.

(192) The dimensions of β-CD is (1.54 ± 0.04 nm, diameter of outer periphery) × (0.79 ± 0.01 nm, height of torus). See: J. Szejtli, *Chem. Rev.* **1998**, *98*, 1743-1753. The calculated edge-to-edge distance between two O-H end groups in G4-OH dendrimer is 0.82 nm, based on the van der waals surface of the outermost O atoms with the assumptions mentioned in Y. Niu, L. K. Yeung, R. M. Crooks, *J. Am. Chem. Soc.* **2001**, *123*, 6840-6846.

(193) This distance is based on the distance between the nuclei of the internal carbon atom on the double bond and the carbon atom on β-CD which connects the linker and stopper, assuming an all-trans conformation, using the Cerius2 (version 4) software package (Molecular Simulations, Inc., San Diego, CA).

(194) Support for this contention comes from previous studies that have shown that alkyl chains (C3 to C9) complex with β-CD; for example, log K = 2.34 for 1-hexanol and log K = 1.22 for 1-butanol. See: M. V. Rekharsky, Y. Inoue, Complexation Thermodynamics of Cyclodextrins. *Chem. Rev.* **1998**, *98*, 1875-1918.

(195) Choi, H. C.; Kim, W.; Wang, D.; Dai, H. Delivery of Catalytic Metal Species onto Surfaces with Dendrimer Carriers for the Synthesis of Carbon Nanotubes with Narrow Diameter Distribution. *J. Phys. Chem. B* **2002**, *106*, 12361-12365.

VITA

Yanhui Niu received her B.S. degree in organic chemistry from Zhengzhou University (Zhengzhou, China) in July of 1994, a M.S. in polymer chemistry and physics from The Institute of Chemistry, Chinese Academy of Sciences (Beijing, China) in May of 1997, and a M.S. in chemistry from The University of Akron (Akron, Ohio) in May of 1999. She received her Ph.D. from Texas A&M University (College Station, Texas) in May of 2003 under the guidance of Dr. Richard M. Crooks. Her permanent address is Hebi Professional Technology College, Building 2, #2, Henan 458030, China.